

**The Effect of Electrical Stimulation on Neuronal Outgrowth and
the Development of a New Method for
Chronic Long-Term Stimulation and Recording
from Groups of Neurons in Culture.**

**Thesis by
Tina Kramer Garyantes**

**In Partial Fulfillment of the Requirements
for the Degree of
Doctor of Philosophy**

**California Institute of Technology
Pasadena, California
1992
(Submitted 9-17-91)**

Acknowledgments

First, I must thank my thesis advisor, Jerry Pine, whose support has been instrumental in shaping both this thesis and, I suspect, my career. Henry Lester has provided support throughout my tenure as a graduate student: all of Jerry's graduate students have benefited from his efforts to include us in the lab. I would also like to thank Wade Regehr for teaching me to use the IC fabrication lab and collaborating with me on the calcium measuring experiments. Thanks also go to David Tank for allowing me to perform these experiments at AT&T. Chi-Bin Chien and John Gilbert were invaluable for helping me learn neurophysiology and electronics and mostly for supporting me through some rather anxious times. I would not have done this without them. Becky Tanamachi and Annie Gouin also deserve thanks for teaching and helping me with cell culture.

I also would like to thank my earlier scientific advisors; Howard Berg, Mel Simon, John Balderschweiler, Scott Emr, Ken Foster, Anne Marie Weber, Don Schultz, and Frank Kelly; who have all been most supportive and encouraged me by word and example to continue in science. They will probably never know what a great influence they have been. In these labs I have had the privilege of working with some wonderful fellow scientists, notably, Dave Blair, Steve Block, Pat Connelly, Joe Falke, Jeff Gelles, Tracy Handel, Kathy Kanen, Graham Lowe, Markus Meister, Paul Meyer, Joel Morgan, Kenji Oosawa, Jeff Segall, Paula Watnick, and Paul West. Thanks also to my committee members, Henry Lester, Carver Mead, Paul Patterson, Jerry Pine, and David Van Essen.

Just as important to me, are the friends I have made throughout my time at Caltech. Prufrock has been a constant support throughout the last eight years and I would like to thank its members through the years, they were really the ones that initiated me into graduate life. I would also like to thank my friends, only some of whom I can possibly list here. Thank-you, Brenda Baker, Jim Barry, Rosie Benzanelli, Chi-Bin Chien, Sam Coker, Lane Dailey, Pam Derry, Elaine Gese, Hardin Gilbert, John Gilbert, Danny Jones, Bill Healy, Bill and Beth Katz, Sue Larson, Kath Mixter-Mayne, Joel Morgan, Mark Muldoon, Nalini and Larry Murdter, Margaret Rankin, Pat Renfranz, Joe Rushanan, Roy Smith, Steve Warwick, Paula Watnick, Elizabeth Williams, and Lei Yu.

Most importantly, I want to thank my parents family for everything they have done for me since my birth. They are extremely important to me and I hope to be closer in the near future. I am extremely fortunately to also have a loving family in-law, who are grateful that I'm finally out of school but could not have been more supportive while I was still there, and two of the best friends in the world, Bev and Greg Matthews. Thank-you for your support so far. I hope I will always have you around me.

Mike; thank-you! (You're stuck)

Abstract

In this dissertation, I shall examine the response of neurite outgrowth from cultured rat superior cervical ganglion (SCG) neurons to electrical stimulation and to changes in cytoplasmic calcium. Previous studies have shown that suprathreshold electrical stimulation arrests axonal growth from mouse dorsal root ganglion (DRG) and *Helisoma* neurons (Fields et al., 1990; Cohan and Kater, 1986). Cohan and collaborators (1987) have attributed the arrest of neurite outgrowth from *Helisoma* neurons to a rise in the growth-cone calcium concentration, $[Ca]_{GC}$. In the experiments presented in this dissertation, neurite outgrowth from neonatal rat SCG neurons continued unabated during continuous suprathreshold electrical stimulation at 10 Hz for up to one hour. As in previous studies, the internal calcium concentration rose during stimulation. Fura-2 measurements showed that growth cone calcium levels rose from about 100 nM to greater than 500 nM, before settling at about 350 nM during stimulation. Despite this increase, neurite outgrowth continued. My results suggest that electrical activity is not a universal signal for neurons to stop growing and that a rise in internal calcium does not always arrest the migration of growth cones.

I was also able to record from and stimulate rat SCG neurons using a new device that allows maintained two-way communication between neurons and electronic circuitry. The new device or "neuron well array" holds individual neurons in surface micromachined holes. A self-supporting overhanging grillwork restrains the neurons in the holes. Each hole has an electrical contact which allows recording from and stimulation of the cell trapped therein. Neurons that grow in the holes appeared to suffer no observable ill effects of entrapment. Future neuronal development studies are planned with the wells.

References

- Cohan C.S., Connor J.A., and Kater S.B. (1987). Electrically and chemically mediated increases in intracellular calcium in neuronal growth cones. *J. Neurosci.*, 7:3588-3599.
- Cohan C.S. and Kater S.B. (1986). Suppression of neurite elongation and growth cone motility by electrical activity. *Science* 232:1638-1640.
- Fields R.D., Neale E.A., and Nelson P.G. (1990). Effects of patterned electrical activity on neurite outgrowth from mouse neurons. *J. Neurosci.* 10:2950-2964.

Acknowledgements	ii
Abstract	iii
Table of Contents	v
<u>Part A: The Activity Dependence of Neuronal Outgrowth</u>	1
Chapter 1: The Effects of Electrical Activity on Cell Growth	2
1.1 Evidence that Electrical Activity Affects Neuronal Development	2
1.1.1 Synapse Regulation by Electrical Activity	3
1.1.2 Electrical Activity Regulates Process Segregation and Pruning	4
1.2 Evidence that Electrical Activity Regulates Neuronal Morphology	7
1.2.1 Assessing Neurite Outgrowth During Electrical Stimulation	7
1.2.2 Neurotransmitter Application Affects Neurite Outgrowth	8
1.2.3 Changes in Membrane Polarization May Regulate Neurite Outgrowth	11
1.3 Summary	12
References	13
Chapter 2: The Effects of Intracellular Calcium on Outgrowth	18
2.1 Stimulation, $[Ca]_i$, and Neuron Outgrowth	18
2.2 Calcium Alone May Regulate Neurite Outgrowth	22
2.3 Correlation of Growth Cone Calcium Concentrations with Growth	24
2.4 Summary	26
References	27
Chapter 3: Electrical Stimulation and Changes in $[Ca]_i$ Affect Neurite Elongation from Sympathetic Neurons I	31
3.1 The Choice of Neonatal Rat SCG Neurons	32
3.2 Methods	34
3.2.1 Cell Culture	34
3.2.2 Media	34
3.2.3 Substrate	35
3.2.4 Stimulation	35
3.2.5 Outgrowth Experiments	37
3.2.6 Calcium Measurements	38
3.3 Reliability of Measurements	43
3.3.1 Reliability of Outgrowth Measurements	43
3.3.2 Reliability of Calcium Measurements	46
References	49

Chapter 4: Effects of Electrical Stimulation and Changes in $[Ca]_i$ on Outgrowth from SCG Neurons II	51
4.1 Results	51
4.1.1 Possible Reasons Why Neurite Outgrowth Slows	58
4.1.2 Stimulation	61
4.1.3 Outgrowth During Stimulation	62
4.1.4 Growth-Cone Calcium and Neurite Outgrowth	67
4.2 Discussion	71
4.2.1 Electrical Activity and Neurite Outgrowth?	71
4.2.2 $[Ca]_i$ and Outgrowth	73
4.2.3 Different Responses from SCG Neurons	75
4.2.4 in Vitro Results Relate to Growth in Vivo	76
4.2.5 Conclusions	77
References	77
<u>Part II: Wells: Devices for Chronic Recording and Stimulation of Cultured Neurons</u>	82
Chapter 5: Chronic Electrode to Neuron Interfaces	83
5.1 Introduction	83
5.2 Comparison of Recording and Stimulation Techniques	84
5.2.1 Glass-Pipette Electrodes	85
5.2.2 Multi-Electrode Culture-Dish Arrays	87
5.2.3 Diving Boards	89
5.2.4 Well Electrodes	90
5.3 Stimulation and Recording with Well Electrodes: The Theory	91
5.3.1 Stimulation	92
5.3.2 Recording	94
5.3.2a Noise	95
5.3.2b Interference	97
5.4 Design Criterion for the Well Electrodes	97
References	100
Chapter 6: Fabrication of the Well Electrodes	101
6.1 Fabrication: Introduction	101
6.2 Fabrication	105
6.3 Fabrication Techniques Developed Specifically for the Wells	114
6.4 Preparation of the Wells for Experiments	116
6.5 Platinization	118
6.6 Protein Coating	120
6.7 Plating Cells	121
6.8 Moving Cells	121
6.9 Survival in Wells	122

Chapter 7: Experimental Results	126
7.1 Stimulation and Recording with Wells: the Electronics	126
7.2 Stimulation and recording with wells: success	130
7.2.1 Stimulation	130
7.2.2 Recording	130
7.2.3 Simultaneous Stimulation and Recording	135
7.3 Solutions	136
7.3.1 Zero Residual Charge	136
7.3.2 Impractical Methods to Achieve Simultaneous Stimulation and Recording	138
7.3.3 Digital Subtraction :the Method of Choice	139
7.4 Summary of Attempt to Record an Action Potential Elicited with a Well Electrode.	139
References	140
Chapter 8: The Future for Well Electrodes	141
8.1 Solutions: Easy Loading Designs	142
8.1.1 Two-Piece Wells	142
8.1.2 Ratcheted Wells	144
8.2 Neural Probes	145
8.3 Summary	146
References	146
Appendix A: Step by Step Instructions to Microfabricate the Well Electrodes	147
Appendix B: Reconstitution of Signaling in Bacterial Chemotaxis	151

Part A

The Activity Dependence of Neuronal Outgrowth

The mammalian nervous system develops from billions of individual neurons. In the first part of this dissertation, I shall examine the possibility that electrical activity or changes in intracellular-calcium concentration ($[Ca]_i$), regulate a portion of this development—neurite elongation. Specifically, I will report the result of experiments that investigate the effect of electrical activity on neurite elongation from cultured neurons of the neonatal rat superior cervical ganglion (SCG).

In Chapters 1 and 2, I shall discuss what is known or postulated about the roles played by electrical activity and $[Ca]_i$ in neuronal development. In Chapter 3, I shall begin to describe experiments in which I test the universality of the hypothesis that electrical activity and the accompanying increase in $[Ca]_i$ regulate neurite outgrowth. In Chapter 4, I shall present the results of these experiments; I shall discuss what effects these two stimuli have on neurite outgrowth from neonatal rat SCG neurons and I shall relate these findings to those of previous studies.

Chapter 1

The Effects of Electrical Activity on Cell Growth

In an attempt to understand the roles that electrical activity or changes in $[Ca]_i$ may play in process outgrowth and elongation from neurons, I will review effects that these stimuli have on neuronal morphological development in general. I present evidence suggesting that electrical activity affects the development of some parts of the nervous system, emphasizing data that relate to the experiments presented in Chapters 3 and 4, which are studies of the effect of electrical activity and the accompanying increase in $[Ca]_i$ on process elongation from SCG neurons. In Section 1.1, I discuss evidence that electrical activity regulates neuronal morphology *in vivo*. I then review, in Section 1.2, evidence that electrical activity regulates neuronal morphology in culture. In Section 1.3, I summarize these findings and relate them to the experiments described in the subsequent chapters.

1.1 Evidence that Electrical Activity Affects Neuronal Development

Electrical activity may regulate many developmental decisions. It is easy to imagine that electrically active cells such as neurons could receive developmental instructions from pre- or postsynaptic activity. These instructions might regulate synapse formation and efficacy, or neurite outgrowth and structure. *In vivo* studies provide evidence that electrical activity regulates both synapse formation and strength, and neurite segregation and structure. In contrast, electrical activity probably does not affect neurite elongation.

1.1.1 Synapse Regulation by Electrical Activity

Electrical activity influences the strength and number of synapses in both the central nervous system (CNS) and the neuromuscular junction (NMJ). Nelson and associates (1989), have shown, for instance, that in cultures of mouse CNS neurons both the number and the efficacy of synaptic connections increase with electrical stimulation. When two cultured populations of dorsal root-ganglion (DRG) neurons synapse on neurons from the ventral horn, those synapses from the population stimulated with chronic phasic stimulation increased in number and efficacy whereas those from the unstimulated population remained unaffected (Nelson et al., 1989; 1990). In contrast, the rate of growth of the stimulated population toward the ventral horn is indistinguishable from that of the unstimulated population. This finding suggests that stimulation regulates synapse formation in, but not outgrowth from, at least some CNS neurons.

Electrical activity has also been implicated in the regulation of synapse formation and elimination at the neuromuscular junction (NMJ). Muscle fibers initially receive innervation from many neurons, but activity-dependent competition among the convergent neurons normally leads to the elimination of all synapses except those from a single afferent neuron (for reviews, see Jansen and Fladby, 1990; Van Essen et al., 1990; Thompson, 1985). In studies designed to evaluate the effect of electrical activity on synapse elimination, muscle cells preferentially retained their innervation from inactive neurons during the period of synapse elimination (Callaway et al., 1987; 1989; Callaway and Van Essen, 1989). In contrast, active motor neurons had a net advantage in the number of synapses formed and retained during reinnervation experiments (Ribchester and Tøxt, 1983; 1984; Ribchester et al., 1988). We can explain this discrepancy by postulating that, although inactive synapses are retained preferentially, inactivity reduces the capacity of neurons to form new synapses (Callaway et al., 1989). Inactivity may also reduce the rate of axonal regeneration or the ability to respond to sprouting cues (Callaway et al., 1989).

As in the DRG neurons discussed previously, motoneuron outgrowth continues during, and may even be enhanced by, normal electrical activity (Ribchester and Tait, 1983; 1984; Ribchester, 1988).

Dahm and Landmesser (1988; 1991) studied the effect of electrical activity on the development of the chick lumbosacral neuromuscular junction. As in the DRG and NMJ systems described in the last paragraph, electrical activity appears to regulate motoneuron development in the chick. Chronic neuromuscular blockade prevented cell death, apparently by increasing synapse formation. The blockade also increased nerve fasciculation and the peak rate of synapse formation.

Changes in synaptic morphology have also been found following activity-induced learning. In sensitized *Aplysia* sensory neurons, brief trains of electrical activity paired with the stimuli potentiate the inhibition of activity caused by sensitization (Small et al., 1989). The application of serotonin mimics this effect (Glanzman et al., 1990). Anatomical changes occur at the synapse in *Aplysia* neurons following sensitization or habituation (Bailey and Chen, 1983; 1988). There is an increase in number, size, and vesicle complement of the active zones and synaptic varicosities followed long-term sensitization *in vivo*. A complementary decrease follows long-term habituation. The time course of these synaptic changes correlates with the time course of memory formation, suggesting that the alterations may contribute to long-term sensitization (Bailey and Chen, 1989). Learning has also been correlated with synaptic changes in vertebrates (see Chang and Greenough, 1984, Burd and Nottebohm, 1985 and Greenough 1984).

1.1.2 Electrical Activity Regulates Process Segregation and Pruning

Evidence from the visual system also supports the hypothesis that electrical activity plays a role in regulating synaptic arrangement, particularly axonal and dendritic

segregation and pruning, though not neurite elongation. During retinal ganglion cell outgrowth to the amphibian tectum, activity at least partially regulates axonal segregation, since blockade of normal electrical activity results in improper tectal map formation. For example, the implantation of a third eye into frog embryos can lead to a dually innervated tectum. Normally, the retinal projections initially cover the tectum in a continuum. Later they segregate into eye-specific stripes. TTX-induced blockade of retinal ganglion cell activity can prevent this segregation (Reh and Constantine-Paton, 1985).

Electrical activity is also important for the proper retinal-tectal map formation in goldfish (Schmidt and Edwards, 1983). Blockade of electrical activity with TTX impairs the proper segregation of retinal-ganglion cell growth cones and neurites once they have reached the goldfish tectum (Schmidt and Edwards, 1983). Yet, bulk growth is seemingly unaffected since the receptive field of individual ganglion cells is not enlarged, and the cells' ability to grow to the tectum is not impaired. Schmidt (1989) showed that activity sharpened the retinal-tectal map during the regeneration of retinotectal projections. What seems to be most important is the lack of synchrony of signals from both eyes, because raising fish under a stroboscopic light that synchronizes the activity of the retinal ganglion cells from both eyes effectively prevents the reordering of the initially disorganized retinal tectal map (Schmidt and Eisele, 1985). From these studies one can conclude that proper segregation and pruning, but not growth, of the retinal-ganglion cell processes to the tectum requires electrical activity.

Axonal segregation in the cat lateral geniculate nucleus (LGN) is also activity dependent (Sretavan et al., 1988). As in the tectum, retinal axons are initially intermixed in the LGN, but by birth the axons have segregated into eye-specific layers. As with the retinal-ganglion cells above, a TTX blockade of cat retinal-ganglion cells during normal segregation prevents the neurons from segregating at their target but does not impede outgrowth (Sretavan et al., 1988).

Pruning by cell death has also been shown to be at least partially regulated by activity in studies of the rat retinal-collicular system. Rat retinal-ganglion cell axons initially innervate both the ipsilateral and the contralateral superior colliculus. Later, an inverted map of the retina forms by the elimination of the ipsilateral connections and the refinement of the contralateral projections. TTX blockade of one eye during the period of normal retinal-ganglion cell death results in the persistence of an extensive ipsilateral projection from the other active eye (Fawcett et al., 1984).

Activity probably also regulates axonal pruning in the primary visual cortex. Ocular dominance columns or strips that receive input from only one eye divide Layer IV of the primary visual cortex. As in the tectum, LGN, and colliculus, initially the inputs to the two eyes intermingle. TTX activity blockade of both eyes of a cat (Sretavan et al., 1988) or darkness induced activity reduction in kittens (Swindale, 1981) prevents or delays the segregation of the inputs into ocular dominance columns. Likewise, when two nerves fire synchronously the inputs remain overlapping whereas when the stimulation is asynchronous the input segregates into columns (Stryker and Strickland, 1984).

Evidence from the visual system thus demonstrates that electrical activity plays a role in regulating both axonal segregation and pruning. In contrast, there is no evidence that activity inhibits or stimulates neurite outgrowth or elongation. This result seems to hold across species and areas of the visual system.

1.2 Evidence that Electrical Activity Regulates Neuronal Morphology

The best evidence that electrical activity affects neurite elongation comes from culture experiments. I shall discuss the most direct assessment of the effect of electrical activity on growth from two cell types in Section 1.2.1. I shall discuss less direct studies of the effect of electrical activity such as the effect of neurotransmitter application or growth

in depolarizing or activity inhibiting media in Sections 1.2.2 and 1.2.3, respectively. All these experiments suggest that electrical activity regulates neurite outgrowth. I shall discuss the stimulation experiments first because they address the question of whether electrical activity regulates neuronal outgrowth most directly.

1.2.1 Assessing Neurite Outgrowth During Electrical Stimulation.

Electrical activity has been shown to impair neurite outgrowth from mouse DRG neurons (Fields et al. 1990) and *Helisoma* buccal-ganglion neurons (Cohan and Kater, 1986) in culture. Fields and associates (1990) have shown that DRG neurons reversibly stop growing when stimulated above threshold by a strong electrical field. Stimulation was achieved by the application of an electrical potential between two chambers of a culture dish: one chamber contained the cell bodies and proximal processes and the other contained the distal processes. A third unstimulated chamber that contained distal processes acted as a control. The magnitude of the response varied with the frequency of the stimulation. The experiments employed four stimulus paradigms: phasic¹ stimulation and chronic stimulation at 2.5, 5, and 10 Hz. All four stimulation paradigms caused the DRG neurons to retract their filopodia and lamellipodia, but only phasic stimulation caused essentially all of the neurites to retract. In response to 10 Hz chronic stimulation, for instance, only 75% of the neurites retracted. Interestingly, after 24 hours of stimulation numerous neurons apparently accommodated to the stimulus and resumed outgrowth. Furthermore, after 72 hours of continuous stimulation there was no significant difference between the number of neurons growing in the stimulated and non stimulated compartments.

¹Phasic stimulation is stimulation consisting of bursts of electrical pulses followed by quiescent periods. The phasic stimulation used here has an equal number of pulses per unit time as 2.5 Hz steady chronic stimulation (Nelson et al., 1989).

Growth cones from identified neurons in the *Helisoma* buccal-ganglion also stop growing when electrically stimulated. Electrical stimulation of the soma of B19 and B5 neurons, using cell-attached patches, causes the growth cones to reversibly stop advancing (Cohan and Kater, 1986). Chronic stimulation at four hertz inhibited outgrowth from 92% of B19 growth cones; 50% stopped growing completely or retracted.

1.2.2 Neurotransmitter Application Affects Neurite Outgrowth

Another way to investigate if activity affects neurite outgrowth is to stimulate neurons by adding excitatory neurotransmitters. These experiments assume that since neurotransmitters open ion channels to depolarize the membrane, the neurotransmitters stimulate the cell above threshold. However, the stimulation is seldom measured directly. The addition of neurotransmitters does, however, often affect neurite outgrowth. If mechanisms common to electrical stimulation mediate the effects of neurotransmitter application, then the response of neurons to neurotransmitter application will mimic their response to electrical stimulation.

Glutamate stimulates outgrowth from *Helisoma* and rat cerebellar granule cells in culture while inhibiting outgrowth from hippocampal neurons. Glutamate application inhibits bursting activity by *Helisoma* neuron B5 as well as neurite outgrowth. The relationship between these two phenomena is consistent with glutamate-induced (Jones et al., 1986) and stimulation-induced (Cohan and Kater, 1986) growth inhibition sharing a common mechanism. Likewise, neurite outgrowth from rat cerebellar granule cells in culture requires glutamate, since enzymatic removal of endogenous glutamate inhibits neurite outgrowth (Pearce et al., 1987). It is not known whether electrical activity affects outgrowth from these cells. In contrast, glutamate application inhibits hippocampal dendritic (but not axonal) outgrowth (Mattson et al., 1988a), while TTX application

stimulates dendritic outgrowth (Mattson et al., 1988b). The inhibitory effect of glutamate is thought to be due to the opening of voltage-dependent calcium channels (Mattson et al., 1988a), as would occur with electrical stimulation. These results are consistent with electrical activity and glutamate application affecting outgrowth by a common mechanism. In all three cell types, neurite outgrowth responds to glutamate application the same way as outgrowth responds to electrical stimulation, regardless of whether stimulation induces or inhibits outgrowth.

Glutamate also induces filopodial extensions of several microns from hippocampal neurons (S. Smith and C. Jahr, personal communication). These extensions are dependent upon the continued presence of glutamate source, retracting upon removal of the glutamate-filled pipette.

The addition of serotonin to the culture medium stopped outgrowth from the serotonin-sensitive B19 neurons but not the serotonin-insensitive *Helisoma* B5 neurons (Haydon et al., 1987; Haydon et al., 1984). Murrain et al., (1990) extended these findings to show that serotonin inhibits outgrowth from *Helisoma* B19 but not B15 neurons in the dissected intact ganglia. Both dopamine and serotonin inhibit growth cone motility from adult *Helisoma* neurons, most likely by regulating membrane voltage (McCobb and Kater, 1988). There are three types of evidence that support this hypothesis. First, neurons that stop growing in response to serotonin or dopamine also show evidence of sustained electrical excitation. Second, the magnitude of electrical response and growth inhibition correlate. Lastly, the injection of a hyperpolarizing current pulse prevents the transmitters from both inhibiting outgrowth and electrically exciting the cells (McCobb and Kater, 1988).

Acetylcholine also inhibits outgrowth from certain neurons, including in cultures rat retinal ganglion cells that endogenously produce acetylcholine (Lipton et al., 1988). The blockade of the ganglion cell's nicotinic receptors induces sprouting possibly by blocking

depolarization or acetylcholine-induced calcium entry into the cells. Dopamine inhibits outgrowth from chick retinal neurons (Lankford et al., 1987) although, because forskolin mimics this effect, the outgrowth inhibition is probably cAMP-dependent, not calcium-dependent.

This behavior appears to be somewhat age dependent since, in cultures of embryonic *Helisoma* neurons, serotonin can both stop growing neurons and initiate growth for others (Goldberg et al., 1991). Goldberg and Kater, (1989), have also looked at the effect of serotonin *in vivo* where transient perturbations in the endogenous serotonin levels during embryogenesis alters neuronal morphology, dye coupling, and the strength of synaptic connections. These phenomena are not necessarily seen in culture.

Glutamate, acetylcholine, serotonin and dopamine; all appear to regulate the rate of neurite outgrowth from cultured neurons. The direction of the induced change is generally the same as that induced by electrical stimulation. This suggests that neurotransmitter application and electrical activity are affecting outgrowth by a common mechanism.

1.2.3 Changes in Membrane Polarization May Regulate Neurite Outgrowth

Another method to infer how electrical activity may affect neuronal outgrowth, is to grow cells in depolarizing media. Elevated extracellular potassium concentrations depolarize cells relative to the surrounding media. We expect cells grown in a depolarizing medium to become more electrically active although without direct electrophysiological evidence this supposition is tenuous. Nonetheless, because of this anticipated hypersensitivity, one method for mimicking some of the effects of electrical stimulation on neurite outgrowth may be to grow the cells in depolarizing medium.

Growth of NIE-115 neuroblastoma cells in a depolarizing media containing 30 mM potassium increases their rate of neurite elongation (Anglister et al., 1982) suggesting that

these cells would increase their rate of elongation with electrical stimulation. In contrast, growth in depolarizing media impedes the rate of neurite outgrowth from mouse DRG neurons. Since the addition of veratrine, bradykinin, or potassium to the media all cause the cells to stop elongating this effect appears to be independent of the source of the depolarization (Robson and Burgoyne, 1989). This independence suggests, as Fields and collaborators (1990) have shown, that neurite outgrowth from DRG neurons is inhibited by electrical stimulation.

Depolarizing media also inhibit neurite outgrowth from other sensory, spinal cord, and sympathetic neurons. Sussdorf and Campenot (1986) have found that these neurons are all capable of growing in both media containing 5 mM and media containing 20 mM potassium but sensory and spinal neurons would not grow from 5 mM into 20 mM potassium. The threshold for this inhibition is cell-type dependent. Sympathetic neurons from the superior cervical ganglion (SCG) required a greater potassium concentration (50 mM versus 20 mM) to inhibit outgrowth than the other two neuronal cell types. Interestingly, elevated potassium ion concentrations appears to inhibit axonal outgrowth from regenerating sympathetic neurons more than from other cell types.

Electrical activity is also likely to partially inhibit neurite outgrowth from *Xenopus* spinal cord neurons. When Bixby and Spitzer (1984) grew *Xenopus* neurons in medium that prevents electrical activity (Ca^{++} free medium with or without TTX), neurites extend more rapidly than those grown in control cultures.

As with the addition of neurotransmitters, watching the outgrowth of neurons in medium that either inhibits or causes depolarization can suggest how the neurons will react to electrical stimulation. Because the affect of depolarizing medium is different for SCG neurons than for sensory or spinal cord neurons, we suspected they might also show a different response to electrical stimulation. I shall describe the response of SCG neurons to stimulation in Chapters 3 and 4.

1.3 Summary

The literature to date clearly demonstrates that electrical activity is capable of regulating synapse elimination and process segregation and pruning. Yet the evidence that electrical activity, independent of neurotransmitter application, regulates neurite elongation from vertebrate cells is less compelling. There are no examples of activity regulating neurite outgrowth *in vivo*. In fact there is evidence to the contrary: neurite elongation is unaffected by activity in the retino-tectal system (Sretavan et al., 1988) or during reinnervation of the mouse sternomastoid muscle (Rich and Lichtman, 1989).

In contrast, there is evidence from *in vitro* studies that electrical stimulation inhibits outgrowth. Work with the invertebrate *Helisoma* clearly shows that electrical stimulation inhibits neurite outgrowth (Cohan and Kater, 1986). Unfortunately, in studies with vertebrate neurons such as DRG neurons, large imposed electric field rather than depolarization of a portion of the membrane stimulated the cells (Fields et al., 1990). This difference makes these results suspect since the imposed electric field, rather than the stimulation (stimulation was confirmed with intracellular recordings from model cells), may be responsible for the observed inhibition of outgrowth.

Other studies have used neurotransmitters or depolarizing media to both increase and decrease neurite outgrowth *in vitro*. Because these agents stimulate the cells electrically, a cell's response to these agents may foreshadow its response to electrical stimulation. Neither the stimulating chemical agents nor *in vitro* electrical stimulation reproduces the conditions that the neuron would encounter *in vivo*. For instance, growth in depolarizing media affects the energy balance in the cell and increases the flux of ions through the membrane as well as increasing the activity of the cell. In addition, the induced activity may not resemble physiological activity levels.

Although it has been suggested repeatedly in the literature that electrical activity probably inhibits neurite elongation from many cell types, only one cell type clearly stops growing in response to electrical activity. In Chapters 3 and 4, I shall show evidence that at least for neonatal rat SCG neurons in our cultures outgrowth is independent of electrical stimulation.

References

- Anglister, L., Farber, I.C., Shaher, A. and Grinvald, A. (1982). Localization of voltage-sensitive calcium channels along developing neurites: their possible role in regulating neurite elongation. *Dev. Biol.* 94:351-365.
- Bailey, C.H. and Chen, M. (1983) Morphological basis of long-term habituation and sensitization in *Aplysia*. *Science* 220:91-93.
- Bailey, C.H. and Chen, M. (1988) Long-term memory in *Aplysia* modulates the total number of varicosities of single identified sensory neurons. *PNAS, USA.* 85: 2373-2377.
- Bailey, C.H. and Chen, M. (1989) Time course of structural changes at identified sensory neuron synapses during long-term sensitization in *Aplysia*. *J. Neurosci.* 9:1774-1780.
- Bixby, J.L. and Spitzer, N.C. (1984) Early differentiation of vertebrate spinal neurons in the absence of voltage-dependent Ca^{2+} and Na^{+} Influx. *Dev. Biol.* 106:89-96.
- Burd, G.D. and Nottebohm, F. (1985) Ultrastructural characterization of synaptic terminals formed by newly generated neurons in a song control nucleus of the adult canary forebrain. *J. Comp. Neurol.* 240:143-152.
- Callaway, E.M., Soha, J.M. and Van Essen, D.C. (1987) Competition favouring inactive over active motor neurons during synapse elimination. *Nature* 328:422-426.
- Callaway, E.M., Soha, J.M. and Van Essen, D.C. (1989) Differential loss of neuromuscular connections according to activity level and spinal position of neonatal rabbit soleus motor neurons. *J. Neurosci.* 9:1806-1824.
- Callaway, E.M. and Van Essen, D.C. (1989). Slowing of synapse elimination by a-bungarotoxin superfusion of the neonatal rabbit soleus muscle. *Dev. Biol.* 131:356-365.

- Chang F-L.F. and Greenough, W.T. (1984) Transient and enduring morphological correlates of synaptic activity and efficacy change in the rat hippocampal slice. *Brain Research* 309:35-46.
- Cohan, C.S. and Kater, S.B. (1986). Suppression of neurite elongation and growth cone motility by electrical activity. *Science* 232:1638-1640.
- Dahm, L.M., Landmesser, L.T. (1988) The regulation of intramuscular nerve branching during normal development and following activity blockade. *Dev. Biol.* 130:621-644.
- Dahm, L.M., Landmesser, L.T. (1991) The regulation of synaptogenesis during normal development and following activity blockade. *J. Neurosci.* 11:238-255.
- Fawcett, J.W., O'Leary, D.D.M. and Cowan, W.M. (1984) Activity and the control of ganglion cell death in the rat retina. *PNAS* 81:5589-5593.
- Fields, R.D., Neale, E.A. and Nelson, P.G. (1990). Effects of patterned electrical activity on neurite outgrowth from mouse neurons. *J. Neurosci.* 10:2950-2964.
- Glanzman, D.L., Kandel, E.R. and Schacher, S. (1990) Target-dependent structural changes accompanying long-term synaptic facilitation in *Aplysia* neurons. *Science* 249:799-802.
- Goldberg, J.I., Kater, S.B. (1989) Expression and function of the neurotransmitter serotonin during development of the *Helisoma* nervous system. *Dev. Biol.* 131:483-495.
- Goldberg, J.I., Mills, L.R., and Kater, S.B. (1991) Novel effects of serotonin on neurite outgrowth in neurons cultured from embryos of *Helisoma trivolvis*. *J. Neurobiol.* 22:182-194.
- Greenough, W.T. (1984) Structural correlates of information storage in the mammalian brain: a review and hypothesis. *TINS* 7:229-233.
- Haydon, P.G., McCobb, D.P. and Kater, S.B. (1984) Serotonin selectively inhibits growth cone motility and synaptogenesis of specific identified neurons. *Science* 226:561-564.
- Haydon, P.G., McCobb, D.P. and Kater, S.B. (1987). The regulation of neurite outgrowth, growth cone motility, and electrical synaptogenesis by serotonin. *J. Neurobiol.* 18:197-215.
- Jansen, J.K.S. and Fladby, T. (1990). The perinatal reorganization of the innervation of skeletal muscle in mammals. *Prog. in Neurobiol.* 34:39-90.

- Jones, P.G., Rosser, S.J. and Bulloch, A.G.M. (1986) Glutamate enhancement of neurite outgrowth in *Helisoma* neurons. Soc. for Neurosci. Abst. 139.3.
- Lankford, K., De Mello, F.G. and Klein, W.L. (1987) A transient embryonic dopamine receptor inhibits growth cone motility and neurite outgrowth in a subset of avian retina neurons. Neurosci. Letts. 75:169-174.
- Lipton, S.A., Frosch, M.P., Phillips, M.D., Tauck, D.L. and Aizenman, E. (1988). Nicotinic antagonists enhance process outgrowth and rat retinal ganglion cells in culture. Science 239:1293-1296.
- Mattson, M.P., Dou, P. and Kater, S.B. (1988a). Outgrowth-Regulating Actions of Glutamate in Isolated Hippocampal Pyramidal Neurons. J. Neurosci. 8:2087-2100.
- Mattson, M.P., Lee, R.E., Adams, M.E., Guthrie, P.B., and Kater, S.B. (1988b) Interactions between entorhinal axons and target hippocampal-neurons: A role for glutamate in the development of hippocampal circuitry. Neuron 1:865-876.
- McCobb, D.P. and Kater, S.B. (1988) Membrane voltage and neurotransmitter regulation of neuronal growth cone motility. Dev. Biol. 130:599-609.
- Murrain, M., Murphy, A.D., Mills, L.R. and Kater, S.B. (1990). Neuron-specific modulation by serotonin of regenerative outgrowth and intracellular calcium within the CNS of *Helisoma trivolvis*. J. Neurobio. 21:611-618.
- Nelson, P.G., Yu, C., Fields, R.D. and Neale, E.A. (1989) Synaptic connections in vitro: Modulation of number and efficacy by electrical activity. Science 244:585-587.
- Nelson, P.G., Fields, R.D., Yu, C. and Neale, E.A. (1990) Mechanisms involved in activity-dependent synapse formation in mammalian central nervous system cell cultures. J. Neurobiol. 21:138-156.
- Pearce, I.A., Cambray-Deakin, M.A. and Burgoyne, R.D. (1987) Glutamate acting on NMDA receptors stimulates neurite outgrowth from cerebellar granule cells. FEBS Letters 223:143-147.
- Reh, T.A. and Constantine-Paton, M. (1985). Eye-specific segregation requires neural activity in three-eyed *Rana pipiens*. J. Neurosci. 5:1132-1143.
- Ribchester, R.R. (1988) Activity-dependent and -independent synaptic interactions during reinnervation of partially denervated rat muscle. J. Physiol. (Lond.) 401:53-75.
- Ribchester, R.R. and Taxt, T. (1983) Motor unit size and synaptic competition in rat lumbrical muscles reinnervated by active and inactive motor axons. J. Physiol. (Lond.) 344:89-111.

- Ribchester, R.R. and Tuxt, T. (1984) Repression of inactive motor nerve terminals in partially denervated rat muscle after regeneration of active motor axons. *J. Physiol. (Lond.)* 347:497-511.
- Rich, M.M. and Lichtman, J.W. (1989) In vivo visualization of pre- and postsynaptic changes during synapse elimination in reinnervated mouse muscle. *J. Neurosci.* 9:1781-1805.
- Robson, S.J. and Burgoyne, R.D. (1989). L-type calcium channels in the regulation of neurite outgrowth from rat dorsal root ganglion neurons in culture. *Neurosci. Lett.* 104:110-114.
- Schmidt, J.T. and Edwards, D.L. (1983) Activity Sharpens the Map during the regeneration of the retinotectal projection in goldfish. *Brain Research* 269:29-39
- Schmidt, J.T. and Eisele, L.E. (1985) Stroboscopic illumination and dark rearing block the sharpening of the regenerated retinotectal map in goldfish. *Neurosci. Letts.* 14:535-546.
- Schmidt, J.T. (1989) Long-term potentiation and activity dependent retinotopic sharpening in the regenerating retinotectal projection of goldfish: common sensitive period and sensitivity to NMDA blockers. *J. Neurosci.* 10:233-246.
- Small, S.A., Kandel, E.R. and Hawkins, R.D. (1989) Activity-dependent enhancement of presynaptic inhibition in *Aplysia* sensory neurons. *Science* 243:1603-1606.
- Smith, S.J. and Jahr, C. personal communication.
- Sretavan, D.W., Shatz, C.J. and Stryker, M.P. (1988). Modification of retinal ganglion cell axon morphology by prenatal infusion of tetrodotoxin. *Nature* 336:468-471.
- Stryker, M.P. and Strickland, S.L. (1984) Physiological segregation of ocular dominance columns depends on the pattern of afferent electrical activity. *Invest. Ophthalmol. Vis. Sci.* 25:278.
- Sussdorf, W.S. and Campenot, R.B. (1986). Influence of the extracellular potassium environment on neurite growth in sensory neurons, spinal cord neurons and sympathetic neurons. *Dev. Brain Res.* 25:43-52.
- Swindale, N.V. (1981) Absence of ocular dominance patches in dark-reared cats. *Nature* 290:332-333.)
- Thompson, W.J. (1985) Activity and synapse elimination at the neuromuscular junction. *Cell Mol. Neurobiol.* 5:167-182.

- Thompson, W., Kuffler, D.P. and Jansen, J.K.S. (1979). The effect of prolonged, reversible block of nerve impulses on the elimination of polyneuronal innervation of new-born rat skeletal muscle fibers. *Neuroscience* 4:271-281.
- Van Essen, D.C., Gordon, H., Soha, J.M. and Fraser, S.E. (1990). Synaptic dynamics at the neuromuscular junction: mechanisms and models. *J. Neurobiol.* 21:223-249.

Chapter 2

The Effects of Intracellular Calcium on Outgrowth

If electrical activity affects neurite outgrowth, what is the mechanism of the regulation? Kater and his collaborators (1988; 1991) have proposed one possible mechanism. They suggest that the increase in $[Ca]_i$ that accompanies suprathreshold electrical activity is the causative agent in regulating outgrowth. This hypothesis is plausible because calcium enters the growth cone during stimulation and regulates many growth cone associated functions, such as the exocytosis of neurotransmitters (Smith and Augustine, 1988) and actin-based motility (Forscher, 1989; Smith, 1988).

In this chapter, I shall review the relationship between $[Ca]_i$ and neurite outgrowth, starting with experiments where electrical activity or stimuli that mimic electrical activity increase $[Ca]_i$ (Section 2.1). Studies that decouple the effects of calcium and activity will follow (Section 2.2). In Section 2.3, I shall discuss the correlation between growth cone calcium concentrations, $[Ca]_{gc}$ and neurite outgrowth rates. Finally, in Section 2.4, I shall summarize the evidence that $[Ca]_i$ can regulate outgrowth.

2.1 Stimulation, $[Ca]_i$, and Neuron Outgrowth

Kater and collaborators (1988;1991) have proposed that environmental stimuli that influence neurite outgrowth and synaptogenesis act through a common integrator, calcium. Such stimuli include neurotransmitters, electrical stimulation, electrical depolarization, and ion channel blockers. They suggest, on the basis of studies of mammalian (Connor, 1986) and snail (Cohan et al., 1987) neurons, that $[Ca]_i$ can vary between growth-permissive and non-growth-permissive ranges. For example, quiescent growth cones have calcium levels from 40 to 80 nM, whereas actively growing growth cones have calcium levels from 100

to 300 nM (Kater et al., 1988). The authors postulate that increasing the $[Ca]_{gc}$ above the levels permissive for outgrowth would stop the cells from growing.

In support of the hypothesis described in the preceding paragraph, electrical stimulation increases $[Ca]_i$ and $[Ca]_{gc}$ and inhibits neurite outgrowth from *Helisoma* buccal ganglion neurons (Cohan et al., 1987). $[Ca]_{gc}$ rises transiently in *Helisoma* B5 neurons from 100 nM to 300 to 400 nM, before plateauing at 225 to 325 nM in response to stimulation at 3 Hz (Cohan et al., 1987); stimulation at 4 Hz stops outgrowth from these same cells (Chan and Kater, 1986). Likewise, at serotonin concentrations that presumably stimulate *Helisoma* B19 neurons above threshold, serotonin application stops outgrowth (Haydon et al., 1987) and causes calcium to rise from 125 nM to 330 nM (Cohan et al., 1987).

Evidence from studies of mouse DRG neurons also supports the hypothesis proposed by Kater and collaborators. Calcium concentrations in mouse DRG neurons increase when the neurons are stimulated at frequencies that arrest outgrowth (Fields et al., 1990a; 1990b). As in *Helisoma* neurons, $[Ca]_i$ and $[Ca]_{gc}$ transiently increase well above final plateau levels. The magnitude of the calcium increase that accompanied the inhibition of growth was equal to or slightly less than that found with *Helisoma* neurons. Surprisingly, after 24 hours of stimulation, some DRG neurons resumed growth, apparently adapting to the electrical stimulation (Fields et al., 1990b). The $[Ca]_{gc}$ does not differ significantly in neurons that apparently adapted to electrical stimulation and in neurons that remained immobile (personal communication, Fields, 1990).

Electrical activity has other potentially calcium-dependent effects. Chronic depolarization and electrical activity decrease the response of SCG neurons to a cholinergic factor. This decreased response allows adrenergic differentiation (Walicke et al., 1977). The effect is probably calcium dependent since in chronically depolarized or electrically stimulated cells, the addition of calcium transport inhibitors inhibits adrenergic

differentiation, and the addition of extracellular calcium or barium enhances adrenergic differentiation. Barium can prevent cholinergic differentiation in nondepolarizing conditions, further suggesting that the effect is calcium dependent (Walicke and Patterson, 1981).

Application of an appropriate neurotransmitter should stimulate neurons electrically as well as change $[Ca]_i$. Many researchers have correlated these neurotransmitter-induced changes in $[Ca]_i$ with the arrest of outgrowth from certain neurons. Murrain and collaborators (1990), have shown that serotonin application transiently increases $[Ca]_i$ in only those *Helisoma* neurons whose growth stops in response to serotonin application, and not in those neurons whose growth is insensitive to serotonin. The serotonin-sensitive neurons normally have serotonin as a presynaptic agonist, not surprisingly. Serotonin application to serotonin-sensitive *Helisoma* neurons causes $[Ca]_i$ to increase from 130 nM to 290 nM. The $[Ca]_i$ returns to prestimulus levels within 30 minutes. Serotonin application inhibits outgrowth and increases $[Ca]_i$; surprisingly however, the growth inhibition remains even after the $[Ca]_i$ returns to prestimulus levels. The continued inhibition of growth, in spite of the measured decrease in $[Ca]_i$, is inconsistent with the hypothesis that calcium directly regulates neurite outgrowth.

In other experiments that look at the affect of neurotransmitter application on outgrowth regulation, calcium levels were not measured. Correlations between changes in $[Ca]_i$ and outgrowth from these experiments are therefore suspect. In cultured cerebellar granule cells, for instance, glutamate might be necessary for outgrowth, because it allows extracellular calcium to enter the cell through NMDA receptors (Pearce et al., 1987). NMDA receptors, but not other glutamate receptors, mediate these affects, since only NMDA antagonists block outgrowth. We can only suspect that the increase in $[Ca]_i$ is the regulatory agent, without a direct measurement of a decrease in $[Ca]_i$ upon the removal of endogenous glutamate or addition of NMDA antagonists.

In contrast, glutamate limits dendritic outgrowth from hippocampal pyramidal cells grown in co-culture with entorhinal cortex explants, that spontaneously release glutamate. The application of glutamate antagonists reverses the glutamate-induced growth inhibition, the application of tetrodotoxin (TTX), or a reduction in the extracellular calcium concentration (Mattson et al., 1988). The increase in $[Ca]_i$ probably mediates these responses since, in addition to the previously mentioned responses, calcium-channel blockers prevent the glutamate-induced inhibition of dendritic growth and calcium ionophores or chronic depolarization inhibit neurite outgrowth. All this evidence suggests that the opening of voltage-dependent calcium channels, which results in an increase in calcium influx, leads to the observed alteration in dendritic outgrowth (Mattson et al., 1988).

Robson and Burgoyne (1989), suggest that L-type calcium channels regulate neurite outgrowth in rat DRG cultures. Neurons grown in depolarizing conditions, such as high potassium, veratridine, or bradykinin, show up to a 60 percent decrease in the number of neurons with neurites. The addition of nifedipine, an L-type calcium-channel blocker, selectively reversed the inhibitory effects of the depolarizing conditions. Calcium channels also contribute to neuronal plasticity associated with learning behaviors in *Aplysia* (Edmonds et al., 1990).

Growth from neuroblastoma cells also is apparently calcium dependent. Depolarizing medium containing 30 mM potassium causes an increase in growth-cone area and an increase in neurite elongation from neuroblastoma cells. Cadmium, a calcium-channel blocker, blocks these changes. Similar changes occur during incubation with 2 μ M bromo-A23187, a calcium ionophore (Anglister et al., 1982). These results suggest that calcium entry might trigger neurite elongation.

Activity-induced changes in $[Ca]_i$ correlate positively with neuronal growth from cerebellar granular and neuroblastoma cells; are negatively correlated with growth from

DRG, *Helisoma*, and hippocampal neurons; and regulate neurotransmitter changeover from SCG neurons.

2.2 Calcium Alone May Regulate Neurite Outgrowth

The stimuli used to change $[Ca]_i$ in the experiments just described (electrical stimulation, neurotransmitter application or depolarizing media) also affect the membrane potential and are likely to trigger associated second messenger systems. To test whether $[Ca]_i$ can independently regulate neurite outgrowth, an experimenter must manipulate $[Ca]_i$ without simultaneously altering the membrane potential. These experiments differentiate between the effects of changing $[Ca]_i$ and the effects of changing the membrane depolarization or electrical stimulation of the cell. Such treatments include the use of calcium channel blockers or calcium ionophores without electrical activity or neurotransmitter application.

Many studies that correlate $[Ca]_i$ and growth do not directly measure the $[Ca]_i$ in response to the imposed stimuli. Results are interpreted nonetheless with the assumption that calcium concentrations do change. This assumption may not be warranted. For example, as I shall discuss in chapters 3 and 4, bathing SCG neurons in low concentrations of some ionophores does not allow the $[Ca]_i$ and extracellular calcium concentrations to equilibrate. Because $[Ca]_i$ was not measured and is thus unknown, the actual $[Ca]_i$ may be quite different from those expected, and may not be in a range that is physiologically relevant. Nonphysiological changes in $[Ca]_i$ are of little interest in determining whether calcium normally regulates neurite development in vivo. It is nevertheless, instructive to review evidence that changes in $[Ca]_i$ affect neurite outgrowth rate.

For instance, calcium is presumably necessary for outgrowth from X-organ cells of crab and lobster, since the application of cadmium to these cells blocks both calcium inflow

through channels and neurite outgrowth (Cooke et al., 1988). In addition, Goldberg (1988) found that application of calcium-channel blocker or changes in extracellular calcium concentrations affect veil extension and growth from *Aplysia* neurons. Presumably, either the $[Ca]_i$ changed with the addition of calcium channel blockers or with the change in extracellular calcium concentration. A decrease in the extracellular calcium concentration from 11 mM to 1.3 mM stopped growth. The addition of barium or the calcium ionophore, bromo-A23187, which artificially raised the internal divalent ion concentration allowed the growth to resume.

Mattson and collaborators, (1988b), have shown that increases in $[Ca]_i$ caused by the addition of the calcium ionophore bromo-A23187 or decreases in $[Ca]_i$ caused by the addition of calcium channel blockers, inhibit outgrowth from cultured hippocampal neurons. Lanthium, presumably acting as a calcium-channel blocker and thus decreasing the rise of $[Ca]_i$ normally caused by serotonin, blocks the serotonin-induced inhibition of outgrowth (Mattson and Kater, 1987).

Suarez-Isla and collaborators (1984) have also used calcium-channel blockers in cultures of chick retinal neurons to show that a voltage-dependent calcium influx was necessary for both neurite extension and synapse formation between retinal neurons and muscle cells in culture.

Although the studies described in Sections 2.1 and 2.2 suggest that calcium regulates neurite outgrowth, the site and mechanism of action remain undetermined. Since the growth cone is the site of many active channels, we might suspect that, if calcium influx regulates neurite outgrowth, calcium influx at the growth cone must be essential. Yet, calcium influx at the growth cone does not appear to be essential for growth from SCG neurons. Campenot and Draker (1989) found that for sustained neurite growth SCG neurons require neither extracellular calcium nor calcium influx at the growth cone. They

found that growth cones continue to grow, albeit more slowly, in calcium-free media, as long as calcium remains in the medium at the cell body.

2.3 Correlation of Growth Cone Calcium Concentrations with Growth

Neurite outgrowth rate has been correlated with the $[Ca]_i$ levels or with calcium-channel conductivity in a number of systems. Correlations between outgrowth rate and $[Ca]_i$ level seem to be cell-type dependent. In these studies, some of the variability may be due to inadvertent averaging of large variations in the local $[Ca]_i$ during the measurements (Lipscombe et al.; 1988; Connor et al.; 1990; Silver et al., 1990).

Some researchers, nonetheless, have correlated neurite outgrowth rate with $[Ca]_i$. Connor (1986) show that diencephalon cells from the rat central nervous system have outgrowth rates that correlate with increased $[Ca]_i$. Calcium levels in active growth cones are over 200 nM whereas the levels in the soma are 60 to 80 nM. Cells without active growth cones, in comparison, have uniform calcium concentrations of 30 to 70 nM. In *Helisoma* buccal ganglion neurons, the internal free calcium concentrations are three times higher in motile than in non-motile growth cones (Cohan et al., 1987). Interestingly, the calcium sensitivity of neurite elongation is different from that of growth cone movement (Mattson and Kater, 1987).

In contrast to the correlations developed in *Helisoma* neurons, Silver and collaborators (1989) found that $[Ca]_i$ in motile advancing growth cones was low (60 nM), and was equal to $[Ca]_i$ in quiescent growth cones (55 nM). Motile growth cones that are not advancing actively had slightly higher values of $[Ca]_i$, (90 nM), possibly suggesting that a small elevation of $[Ca]_i$ inhibits neurite extension. A further rise of $[Ca]_i$ (225 nM) appears to inhibit motility and to cause retraction of the growth cone back toward the cell body. These results are incompatible with the model that a rise in $[Ca]_i$ is responsible for

activation of quiescent growth cones; however, the data suggests that, in active growth cones, $[Ca]_i$ can regulate morphology and behavior.

If there is a variation in the calcium concentration in active and quiescent growth cones, it may arise from differences in channel activity. Lipton (1987) showed that in regenerating rat retinal-ganglion cells the calcium channels displayed bursting behavior, whereas, channels in quiescent cells did not. Likewise, *Helisoma* growth cones have 70 pS calcium channels that are active in growing growth cones and inactive in stable growth cones (Cohan et al., 1985). The gating of these channels in *Helisoma* is calcium independent. Freeman and collaborators (1985) have shown that steady calcium currents are present only in actively growing filopodia tips. In the growing tip of lamprey giant axons, likewise, there is an additional spike found only in regenerating axons. The spike is due to an increase in a voltage-dependent calcium conductance in the growing axon (MacVicar and Llinas, 1985). Finally, O'Lague and collaborators have shown that there are calcium channels in the growth cones of NGF-induced, polyethylene glycol-fused, PC-12 cells.

One circumstance that may confuse these correlations between $[Ca]_i$ and neurite outgrowth rate is the possibility that spatial inhomogeneities exist within the growth cones (see review, Kater and Mills, 1991). In small growth cones, these inhomogeneities potentially occur over a region that is too small to measure with fura-2. Researchers have found evidence of such inhomogeneities in sympathetic neurons (Lipscombe et al., 1988). Observations with cell-attached patch recordings show that both L- and N-type calcium channels often are concentrated in local hot spots. One channel type sometimes dominates the hot spots (Lipscombe et al., 1988). Using fura-2 and neurons with large growth cones (*Helisoma* and *Aplysia*), Connor and collaborators (1990) sharply defined the calcium gradients within the growth cones (spatial resolution of a few microns) during action

potentials. These changes probably arise from clustering of voltage-gated calcium channels in the membrane.

Silver and collaborators (1989) correlated small spatial gradients of $[Ca]_i$ within the neuroblastoma growth cone with outgrowth rate. The gradients although small, are statistically significant; $[Ca]_i$ is lower by 5 to 10 nM in motile regions. The next year, (Silver et al., 1990), these authors showed that directly below membrane regions where calcium channels cluster, the local calcium concentration could be elevated into the micromolar range. Such areas may reflect the immobile regions observed in the earlier study.

Polak and collaborators (1991) showed recently that the serotonin-mediated inhibition of outgrowth from *Helisoma* neurons involves calmodulin: a calmodulin antagonist, CGS 9343B, blocks the serotonin-induced inhibition of neurite outgrowth. Because calmodulin has a relatively low binding affinity for calcium (Manalan and Klee, 1984), calcium may increase only enough to activate calmodulin dependent pathways in localized regions of the cell.

2.4 Summary

Many experiments correlate changes in the $[Ca]_i$ with changes in neurite outgrowth rates. Both increases and decreases in $[Ca]_i$ from normal physiological levels (generally about 100 nM) inhibit neurite outgrowth in some circumstances. In the majority of cases increases in $[Ca]_i$ correlate with an inhibition of outgrowth, although some studies correlate an increase in $[Ca]_i$ with an increase in neurite outgrowth rate. These experiments are consistent with the hypothesis that there is an optimal range of calcium concentrations for outgrowth. In some cells this optimal range is evidently relatively narrow since

changes as small as 125 to 330 nM in $[Ca]_i$ have been correlated with the arrest of outgrowth (Haydon et al., 1987; Cohan et al., 1987).

Many of the studies discussed in this chapter correlate electrical activity with an increase in $[Ca]_i$ and a reduced rate of neurite outgrowth, but none show that these increases in $[Ca]_i$ cause the interruption of neurite outgrowth observed with electrical stimulation. Furthermore, some experiments are inconsistent with the latter hypothesis. For instance, after Murrain and collaborators (1990) stimulated *Helisoma* neurons for 30 minutes the $[Ca]_i$ had returned to prestimulus levels but neurite outgrowth remained inhibited. Likewise, some DRG neurons resume outgrowth after 24 hours of continuous stimulation, but their average $[Ca]_i$ is not significantly different from that of the other neurons in the culture that do not resume outgrowth (personnel communication, Fields, 1990). The experiments presented in chapters 3 and 4 of this dissertation will present evidence that electrical stimulation and the concomitant increase in $[Ca]_i$ do not inhibit neurite outgrowth from one cell type - namely SCG neurons.

References

- Anglister, L., Farber, I.C., Shafer, A. and Grinvald, A. (1982). Localization of voltage-sensitive calcium channels along developing neurites: their possible role in regulating neurite elongation. *Dev Bio* 94:351-365.
- Campenot, R.B. and Draker, D.D. (1989). Growth of sympathetic nerve fibers in culture does not require extracellular calcium. *Neuron* 3:733-743.
- Cohan, C.S., Haydon, P.G. and Kater, S.B. (1985) Single channel activity differs in growing and nongrowing growth cones of isolated identified neurons of *Helisoma*. *J. Neurosci. Res.* 13:285-300.
- Cohan, C.S., Connor, J.A. and Kater, S.B. (1987). Electrically and chemically mediated increases in intracellular calcium in neuronal growth cones. *J. Neurosci.*, 7:3588-3599.
- Cohan, C. and Kater, S.B. (1986). Suppression of neurite elongation and growth cone motility by electrical activity. *Science* 232:1638-1640.

- Connor, J.A. (1986). Digital imaging of free calcium changes and of spatial gradients in growing processes in single, mammalian central nervous system cells. *P.N.A.S.* 83:6179-6183.
- Connor, J.A., Kater, S.B., Cohan, C. and Fink, L. (1990) Ca^{2+} dynamics in neuronal growth cones: regulation and changing patterns of Ca^{2+} entry. *Cell Calcium* 11:233-239.
- Cooke, I., Graf, R., Grau, S. and Meyers, D. (1988). Crustacean peptidergic secretory neurons in culture: outgrowth, secretory competence, and Ca^{++} currents. *J. of Gen. Physiology* 92:3a-4a.
- Edmonds, B., Klein, M., Dale, N. and Kandel, E.R. (1990) Contributions of two types of calcium channels to synaptic transmission and plasticity. *Science* 250:1142-1147.
- Fields, R.D., Guthrie, P.B. Nelson, P.G. and Kater, S.B. (1990b). Calcium homeostatic capacity is regulated by patterned electrical activity in growth cones of mouse DRG neurons. 16th Soc. of Neurosci. Abst. 197.2: 457.
- Fields, R.D., Neale, E.A. and Nelson, P.G. (1990a). Effects of patterned electrical activity on neurite outgrowth from mouse neurons. *J. Neurosci.* 10:2950-2964.
- Forscher, P. (1989) Calcium and polyphosphoinositide control of cytoskeletal dynamics. *TINS* 12:468-474.
- Freeman, J.A., Manis, P.B., Snipes, G.J., Mayes, B.N., Samson, P.C., Wikswo, Jr., J.P., and Freeman, D.B. (1985) Steady growth cone currents revealed by a novel circularly vibrating probe: A possible mechanism underlying neurite growth. *J. Neurosci. Res.* 13:257-283.
- Goldberg, D.J. (1988). Local role of Ca^{2+} in formation of veils in growth cones. *J. Neurosci.* 8:2596-2605.
- Haydon, P.G., McCobb, D.P. and Kater, S.B. (1987). The regulation of neurite outgrowth, growth cone motility, and electrical synaptogenesis by serotonin. *J. Neurobio.* 18:197-215.
- Kater, S.B., Mattson, M.P., Cohan, C. and Connor, J. (1988). Calcium regulation of the neuronal growth cone. *Trends. in Neurosci.* 11:315-321.
- Kater, S.B. and Mills, L.R. (1991) Regulation of Growth Cone Behavior by Calcium *J. Neurosci.* 11:891-899.
- Lipscombe, D., Madison, D.V., Poenie, M., Reuter, H., Tsien, R.Y. and Tsien, R.W. (1988). Spatial distribution of calcium channels and cytosolic calcium transient in growth cones and cell bodies of sympathetic neurons. *PNAS* 85:2398-2402.

- Lipton, S.A. (1987) Bursting of calcium-activated cation-selective channels is associated with neurite regeneration in a mammalian central neuron. *Neurosci Letts* 82:21-28.
- MacVicar, B.A. and Llinas, R.R. (1985) Barium Action Potentials in Regenerating Axons of the Lamprey Spinal Cord. *J. Neurosci. Res.* 13:323-335.
- Manalan, A.S. and Klee, C.B. (1984) Calmodulin in: *Advances in cyclic nucleotide and protein phosphorylation research*, Vol 18 (Greengard P, Robinson GA, eds), pp 227-278. New York: Raven.
- Mattson, M.P., Dou, P. and Kater, S.B. (1988). Outgrowth-regulating actions of glutamate in isolated hippocampal pyramidal neurons. *J. Neurosci.* 8:2087-2100.
- Mattson, M.P. and Kater, S.B. (1987) Calcium regulation of neurite elongation and growth cone motility. *J Neurosci* 7:4034-4043.
- Mattson, M.P., Lee, R.E., Adams, M.E., Guthrie, P.B. and Kater, S.B. (1988) Interactions between entorhino axons and target hippocampal-neurons: a role for glutamate in the development of hippocampal circuitry. *Neuron* 1:865-876.
- Murrain, M., Murphy, A.D., Mills, L.R. and Kater, S.B. (1990). Neuron-specific modulation by serotonin of regenerative outgrowth and intracellular calcium within the CNS of *Helisoma trivolvis*. *J. Neurobio.* 21:611-618.
- O'Lague, P.H., Huttner, S.L., Vandenberg, C.A., Morrison-Graham, K. and Horn, R. (1985) Morphological properties and membrane channels of the growth cones induced in PC12 cells by nerve growth factor. *J. Neurosci. Res.* 13:301-321.
- Pearce, I.A., Cambray-Deakin, M.A. and Burgoyne, R.D. (1987) Glutamate acting on NMDA receptors stimulates neurite outgrowth from cerebellar granule cells. *FEBS Letters* 223:143-147.
- Polak, K.A., Edelman, A.M., Wasley, J.W.F. and Cohan, C.S. (1991) A novel calmodulin antagonist, CGS 9343B, modulates calcium-dependant changes in neurite outgrowth and growth cone movements. *J. Neurosci.* 11:534-542.
- Robson, S.J. and Burgoyne, R.D. (1989). L-type calcium channels in the regulation of neurite outgrowth from rat dorsal root ganglion neurons in culture. *Neurosci. Lett.* 104:110-114.
- Silver, R.A., Lamb, A.G. and Bolsover, S.R. (1989). Elevated cytosolic calcium in the growth cone inhibits neurite elongation in neuroblastoma cells: correlation of behavioral states with cytosolic calcium concentration. *J. Neurosci.* 9:4007-4020.

- Silver, R. A., Lamb, A. G. and Bolsover, S. R. (1990) Calcium hotspots caused by L-channel clustering promote morphological changes in neuronal growth cones. *Nature* 343:751-754.
- Smith, S.J. (1988) Neuronal cytom mechanics: the actin-based motility of growth cones. *Science* 242:708-715.
- Smith, S.J. and Augustine, G.J. (1988) Calcium ions, active zones and synaptic transmitter release. *TINS* 11:458-464.
- Suarez-Isla, B.A., Pelto, D.J., Thompson, J.M. and Rapoport, S.I. (1984). Blockers of calcium permeability inhibit neurite extension and formation of neuromuscular synapses in cell culture. *Dev. Brain Res.* 14:263-270.
- Walicke, P.A., Campenot, R. and Patterson, P.H.(1977) Determination of transmitter function by neuronal activity. *PNAS, USA* 74:5767-5771.
- Walicke, P.A. and Patterson, P.H. (1981) On the role of Ca²⁺ in the transmitter choice made by cultured sympathetic neurons. *J. Neurosci.* 1:343-350.

Chapter 3

Electrical Stimulation and Changes in $[Ca]_i$ Do Not Affect Neurite Elongation from Sympathetic Neurons

Both electrical activity and the accompanying changes in $[Ca]_i$ have been proposed as common regulatory mechanisms for neuronal outgrowth. In particular, experiments suggest that electrical activity inhibits neurite outgrowth from *Helisoma* (Cohan and Kater, 1986) and mouse DRG (Fields et al., 1990) neurons in culture. To investigate the generality of this control mechanism, I stimulated neurons from the neonatal rat SCG while measuring the neurite outgrowth rate.

$[Ca]_i$ increases during stimulation of both *Helisoma* (Cohan et al., 1987) and DRG (Fields et al., 1990a) neurons. This increase may be the mechanism whereby stimulation inhibits outgrowth. Since electrical stimulation does not appear to inhibit outgrowth from SCG neurons, we postulated that the $[Ca]_{gc}$ may not be increasing to the same extent in SCG neurons as in the other cell types that respond to electrical stimulation. To test this hypothesis, I collaborated with Dr. Wade Regehr in Dr. David Tank's laboratory at Bell Laboratories, Murray Hill, NJ, to measure changes in the $[Ca]_i$ in both the soma and the growth cones of SCG neurons during electrical stimulation. To further test if $[Ca]_i$ regulates outgrowth in general, we attempted (unsuccessfully) to elevate $[Ca]_{gc}$ pharmacologically to greater than 500 nM for prolonged periods. A level of 500 nM is significantly above the concentration postulated to inhibit neurite outgrowth by Kater and collaborators (1988). I shall discuss the results of these experiments in Chapter 4.

In this chapter, I shall discuss why I chose to study the effect of electrical activity on rat SCG neurons (Section 3.1), and the methods that I employed in both the electrical

stimulation and calcium experiments (Section 3.2). In Section 3.3, I shall discuss the reliability of these measurements.

3.1 The Choice of Neonatal Rat SCG Neurons

I chose to use neonatal rat SCG neurons for these studies for four reasons. First, there have been extensive studies of neurite outgrowth from cultured SCG neurons. SCG neurite outgrowth rates in culture are both rapid and steady (Bray, 1973), although the absolute growth rate depends on the age of the ganglion at dissection (Argiro et al., 1984). The average outgrowth rates were 8 to 22 $\mu\text{m}/\text{hour}$ for embryonic SCG neurons, 14 to 29 $\mu\text{m}/\text{hour}$ for perinatal SCG neurons, and 4 to 13 $\mu\text{m}/\text{hour}$ for adult SCG neurons (Argiro et al. 1984) for collagen grown neurons. In our culture system, the cells extend many processes simultaneously.¹ We thought that the continuous nature and speed of neurite growth from SCG neurons would simplify the outgrowth measurements.

Second, SCG neurons have, at the time of dissection, the minimum requirement for electrical activity regulated outgrowth: The neurons already receive presynaptic inputs (Rubin, 1985a), and these presynaptic inputs are electrically competent although they are not necessarily active (Rubin, 1985b). The axons are growing actively toward their targets at this time (Rubin, 1985b). SCG neurons continue to grow into adulthood (Voyvodic, 1987; Purves et al., 1986), and that growth is apparently largely independent of preganglionic innervation (Voyvodic, 1987), unlike growth from the primary sensory systems (see Berry et al., 1978 for a review).

A third reason to study SCG neurons is that results from studies on the effects of depolarizing media suggest that SCG neurons might differ from other neurons in their

¹Although the processes are likely to be axons, I can not verify their identity without assaying them directly with antibodies. I shall refer to the processes as processes or neurites. (See Leins and Higgins, 1989 and Bruchenstein and Higgins, 1988, for descriptions of SCG axons and dendrites in culture.)

response to electrical stimulation. High potassium medium, a depolarizing medium that mimics some of the effects of electrical stimulation, does not appear to impede outgrowth from SCG neurons (Campenot, 1984; 1986; and Sussdorf and Campenot, 1986). SCG neurons, in contrast to sensory and spinal-cord neurons, continue to grow from medium with 5 mM potassium into medium with 20 mM potassium, and are impeded only when they try to grow into medium with 50 mM potassium. SCG neurons are able to grow in 50 mM potassium (Sussdorf and Campenot, 1986), whereas DRG neurons cannot do so (Robson and Burgoyne, 1989). Neurite regeneration from SCG neurons, on the other hand, is relatively more sensitive to elevated potassium concentrations than is similar growth from either spinal or sensory neurons (Sussdorf and Campenot, 1986).

A fourth reason to study SCG neurons is that outgrowth continues even if there is no extracellular calcium at the growth cones (Campenot and Draker, 1989)². This continued growth suggests that outgrowth is not dependent on local calcium influx. The fact that growth continues when there is no external calcium at the growth cone suggests that calcium does not regulate outgrowth. Furthermore, this calcium independence suggests that if electrical activity regulates outgrowth it does so in a calcium independent fashion.

²When SCG neurons are grown in the absence of extracellular calcium at the growth-cone, there is some decrease in the average neurite outgrowth rate.

3.2 Methods

In this section, I shall describe how I did the experiments described in Chapter 4. Specifically, I shall discuss how I prepared and stimulated the cells and how I measured the calcium concentrations.

3.2.1 Cell Culture

I anesthetized rat pups (0 to 3 days old) with Halothane and decapitated them, before removing the superior cervical ganglia. After transferring the ganglia into 2 ml of Hank's balanced salts solution (HBSS) with penicillin/streptomycin and no divalent cations, I cleaned and incubated them at 37 °C in HBSS with 0.125 percent trypsin for 30 minutes in a 5 percent CO₂ environment. I inactivated the trypsin after the incubation by soaking the ganglia in modified Leibovitz's L-15 media (L15) with 32.5 percent horse serum for 10 minutes. Finally, I transferred the ganglia to L15, shredded, triturated and plated them on previously prepared polylysine-laminin coated 35 mm dishes at 3000 neurons/dish. I allowed the cells to settle for 30 minutes to 3 hours before experiments began.

3.2.2 Media

I made the modified L15 by supplementing L15 as described in Mains and Patterson, (1973), except I omitted the bovine serum albumin and methyl cellulose and substituted 10 percent horse serum for rat serum and of 4 ng/ml 2.5 S NGF (Boehringer Mannheim) for 0.5 µg/ml 7 S NGF. The medium used during all outgrowth experiments was L15_{air}. I prepared the L15_{air} by omitting sodium bicarbonate and serum from the L15, adjusting the pH to 7.2 (in air) with NaOH and adjusting the NGF concentration to 2 ng/ml. I adjusted the NGF concentration to 2 ng/ml because of the large volume of buffer

used in these experiments. In preliminary experiments, where I observed outgrowth for up to two weeks, there was no detectable decrease in SCG outgrowth at NGF concentration from 1 to 20 ng/ml. For experiments in high K^+ L15, I decreased the concentration of NaCl from 137 mM to 92 mM and increased the concentration of KCl from 5.6 mM to 50 mM. To make high K^+ /high Ca^{++} L15, I also increased the concentration of $CaCl_2$ from 1.26 mM to 5 mM: I did not compensate for this adjustment by adjusting the concentration of other divalent cations. For experiments with the calcium ionophore, bromo-A23187, I added different amounts of a 20 μ M stock solution (minimum dilution was 1/50) of the ionophore in DMSO to the perfusing medium.

3.2.3 Substrate

I grew the cells on glass coverslips which I had glued under a 6 mm hole in the bottom of 35 mm petri dishes. I had previously soaked the dishes for 30 minutes in fuming nitric acid, rinsed them three times with distilled water, and soaked them overnight in Dulbecco's phosphate buffered saline (DPBS) with 100 μ g/ml polylysine, (Sigma P8905). In the morning, I had rinsed, dried and stored the dishes at 4 °C until use. Just before plating, I soaked them in a 20 μ g/ml solution of laminin (Sigma, L8263) in DPBS for 45 minutes, and rinsed them three times with DPBS.

3.2.4 Stimulation

It is essential to have a reliable stimulation method if we are to study the affects of activity on neurite outgrowth. In preliminary experiments, I found that intracellular and whole-cell electrode techniques stopped neurite outgrowth. Therefore, I used cell-attached patch pipettes to stimulate the neurons non-invasively. I stimulated the cells extracellularly

with cell-attached patch pipettes (KG-33 glass, Garner Glass Co.). Tip diameters were about 1 μm and electrode impedances were 5-15 $\text{M}\Omega$. I used a high-potassium, low-sodium saline in the pipette to depolarize the cell without breaking down the membrane. To make this saline, I modified the recipe from Marty and Neher, (1983); 140 mM KCl, 2 mM MgCl_2 , 11 mM EGTA-KOH (pH 7.3), 1 mM CaCl_2 , and 10 mM HEPES, adjusted to pH 7.2 with KOH and to 320 mOs with sucrose. With this solution in the pipette, I apparently depolarized the portion of the membrane inside the pipette and caused the continuous opening of non inactivating channels, because the pipette potential approached the cell's resting potential, -70 mV relative to the bath, after I obtained a seal. The open channels reduced the impedance of the patch and allowed the passage of enough current to stimulate the cell without damaging the membrane (see Regehr et al., 1989 for a detailed explanation). The reduced patch impedance also increased the signal-to-noise ratio for recording evoked action potentials.

I positioned the electrodes while monitoring the voltage drop produced by a hyperpolarizing current pulse, (50 pA, 2 Hz). After the pipette had touched the cell membrane, indicated by an increase in the measured impedance of the pipette, I applied light suction with a mouth pipette. I stopped the test pulses as soon as a seal had formed. I observed each cell for 30 minutes without stimulation to check for pipette induced damage. I did stimulation experiments only on cells that were undamaged by patching, i.e., continued to grow during this control period. I also rejected cells if I was unable to evoke an action potential without breaking down the membrane. I was usually able to stimulate the neurons reliably at 10 Hz with pulses of 200 to 500 pA lasting 10 to 50 ms. SCG neurons do not spontaneously fire action potentials.

3.2.5 Outgrowth Experiments

I performed outgrowth experiments on a microscope stage with dishes perfused with L15_{air} at 20 ml/hour. I warmed the medium to 35 ± 1 °C as it entered the dish through a channel in a heated stainless steel ring and I continuously monitored the temperature with a thermistor located at the bottom of the dish. Under these experimental conditions, the osmolarity of the medium remained constant.

I recorded outgrowth during the stimulation experiments with time-lapse 35 mm photography through a 20x phase-contrast objective. In experiments where I measured the $[Ca]_i$, I measured outgrowth from fluorescence images recorded by a CCD camera (model 220 Photometrics) and stored on a computer (Macintosh IIx) (Regehr et al., 1989).

I determined the rate of outgrowth in the stimulation experiments by dividing the change in growth cone position by the time elapsed between photographs. For stimulation experiments, I projected each image a fixed distance and traced it on top of the trace of the preceding image. I used the cell bodies and gold marks on the coverslips to align the successive traces. I determined outgrowth from computer generated fura-2 images by comparing the distance from the neurite-cell body attachment point or a branch point to the growth cone tip in successive images. The fura-2 images, and thus the measurements of the growth rate, were too coarse to allow me to see the fine structure of the growth cones. I defined the growth cone position as the outermost point of the semicircle circumscribing the anterograde edge of the lamellapodia. I measured neurite lengths to ± 2 μ m.

I determined the average growth rate of a cell by measuring the growth rates of all photographed, observable³ neurites during a time period and dividing by the number of neurites. After a neurite branched, I counted both daughter branches individually. Occasionally, a neuron was left with one or more stubby processes after trituration. I observed these "stubs" immediately after plating and they never grew or developed into a

³Some neurites appeared to grow along other neurites, making their growth essentially impossible to assess. These neurites were excluded from our measurements.

growth cone during an experiment. The stubs are probably remnants of processes incompletely sheared off during plating. Since they did not grow, they did not contribute to the total outgrowth and I excluded them from the calculation of average growth rate. I used unpatched cells in which I photographed at least half the processes continually for 2 hours or more as controls.

3.2.6 Calcium Measurements

I used the acetomethoxy (AM) form of the calcium-sensitive fluorophore, fura-2, to measure the $[Ca]_i$. I could not use the acid form because SCG neurons stop growing after intracellular penetration. To stain the neurons, I incubated them in 1 ml of a 2 μ M solution of fura-2 AM in L15_{air} at 37 °C for 30 minutes. To make the final 2 μ M solution, I diluted 2 μ l of a 1 mM fura-2 AM (Calbiochem) stock solution to 1 ml of L15_{air}, vortexed the solution to ensure uniform mixing, and removed any remaining undissolved fura-2 AM by centrifuging the solution in a microfuge for 1 minute at 1000 rpm. I made the fura-2 AM stock solution in 25% Pluronic Acid/ 75% dry DMSO and stored it at -20 °C for up to 2 weeks before use. After 30 minutes of staining, I washed the cells three times with L15_{air} and left them to deesterify for 45 minutes before use. I assumed that deesterification was essentially complete after 45 minutes; at this time the R_{min}/R_{max} ratio was greater than 11 in calcium permeabilized cells (10 μ M ionomycin in media with 1.26 mM calcium). Staining of subcellular compartments became noticeable after about 3 hours, and became pronounced after about 5 hours. Therefore, I performed the experiments within 3 hours of staining.

I measured $[Ca]_i$ in collaboration with Dr. Wade Regehr in Dr. Tank's laboratory. The ultraviolet illumination came from a mercury arc lamp. Filters removed most of the 360 nm peak and the light longer than 450 nm before a dichroic filter split the remainder

into two portions. Each portion then passed through a band pass filter and shutter before being recombined. The first band pass filter has a bandwidth of 20 nm, centered at 340 nm, and the second band pass filter has a bandwidth of 10 nm, centered at 380 nm. Neutral density filters adjusted the illumination intensity (and thus absolute fluorescence) to the desired level. We recorded the fluorescent image into a Macintosh IIfx using a software package written by Dr. Tank.

To minimize potentially cytotoxic effects of prolonged exposure to UV light we limited the illumination intensity with neutral density filters. During experiments in which we measured both $[Ca]_i$ and outgrowth rates, we limit the exposure duration and frequency also. While testing for cytotoxicity, we observed continued growth when image pairs were taken every 2 minutes. We, therefore, limited our exposures to no more than one 2-second image pair every 5 minutes for experiments that measured growth and calcium concentration. We averaged calcium measurements in either the growth cone or soma over a $3.3 \mu\text{m}^2$ (4 pixels) area. We measured calcium concentrations in the soma at regions away from the nucleus, the site of pipette attachment, and the cell border (Figure 3.1).

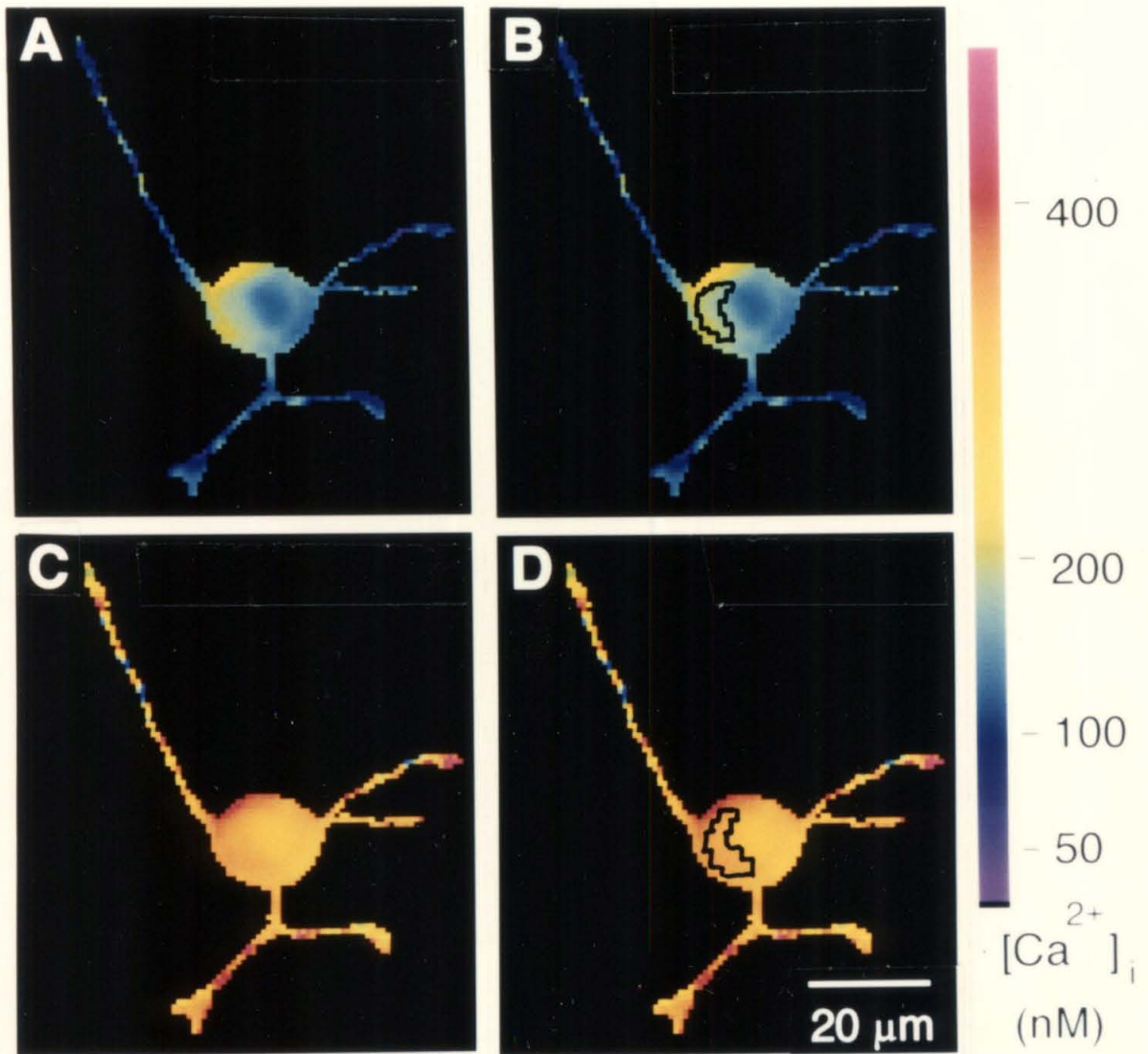


Figure 3.1 These pictures show the variation in calcium concentration across a SCG's soma and the region in which calcium is measured. Pictures A and B are of an SCG before stimulation while pictures C and D are of the same SCG after stimulation. Somatic calcium concentration measurements would be taken from the region outlined in black in pictures B and D. The region in the right-hand portion of the soma with a decreased calcium concentration is the nucleus.

We calculated calcium levels from the fluorescence measurements using the ratio method (Grynkiewicz et al., 1985). Because we always used the ratio of the fluorescence of the dye at different wavelengths in calculating the calcium concentration, we could cancel variations due to the instrumental sensitivity, optical path length, and effective total concentration of the dye. Since the unbound anion has a peak absorption maximum at 362 nm and the bound anion has a peak absorption maximum at 335 nm (Grynkiewicz et al., 1985), we excited the anionic dye with light of 340 and 380 nm.

I derive the equation for calculating the calcium concentration from fluorescence measurements at two different excitation frequencies in this paragraph. This derivation assumes that the dye forms a 1:1 complex with calcium, that the dye behaves in the cell as it does in the calibration medium, and that the dye is dilute such that the fluorescence intensity is linearly proportional to the concentration of the fluorescent species. The fluorescence of the fura-2 with excitation at 340 nm, F_{340} , is

$$F_{340} = S_{f340} c_f + S_{b340} c_b \quad (1)$$

S_{f340} is the proportionality constant of the free fura-2 excited with light at 340 nm (S_{b340} is for the bound fura-2). c_f and c_b are the concentrations of free and bound fura-2. The fluorescence of fura-2 with excitation at 380 nm is

$$F_{380} = S_{f380} c_f + S_{b380} c_b \quad (2)$$

The equation

$$c_b = c_f \frac{[Ca^{2+}]}{K_D} \quad (3)$$

relates the concentration of free and bound dye to the calcium concentration, $[Ca^{2+}]$ and to the dissociation constant, K_D . If we define R to be ratio of the fluorescence in the sample at 340 to 380 nm excitation, we can express R as

$$R = \frac{F_{340}}{F_{380}} = \frac{(S_{f340} c_f + S_{b340} c_b)}{(S_{f380} c_f + S_{b380} c_b)} \quad (4)$$

Substituting equation 3 into equation 4, we obtain

$$R = \frac{\left(S_{f340} + S_{b340} \frac{[Ca^{2+}]}{K_D} \right)}{\left(S_{f380} + S_{b380} \frac{[Ca^{2+}]}{K_D} \right)} \quad (5)$$

We can solve equation 5 for the calcium ion concentration, $[Ca^{2+}]$:

$$[Ca^{2+}] = K_D \left(\frac{R - \left(\frac{S_{f340}}{S_{f380}} \right)}{\left(\frac{S_{b340}}{S_{b380}} \right) - R} \right) \left(\frac{S_{f380}}{S_{b380}} \right) \quad (6)$$

S_{f340}/S_{f380} is the limiting fluorescence ratio when there is no calcium in the solution or R_{min} . S_{b340}/S_{b380} is the limiting fluorescence ratio when there are saturating concentrations of calcium in the solution or R_{max} .

$$[Ca^{2+}] = K_D \left(\frac{R - (R_{min})}{(R_{max}) - R} \right) \left(\frac{S_{f380}}{S_{b380}} \right) \quad (7)$$

In calculating the calcium concentration using equation 7, we used a dissociation constant K_D of 225 nM (Regehr et al., 1989), and Dr. Regehr had previously determined R_{min} and R_{max} in saline (Regehr et al., 1989). We measured S_{f380}/S_{b380} experimentally after determining the optimal intensity of incident light. For consistency with other papers in the field, we did not use a viscosity correction factor (Cohan et al., 1987; Connor, 1986).

3.3 Reliability of Measurements

Our confidence in the results limits the interpretation of any experiment. In the experiment presented in this dissertation we measured outgrowth and calcium concentration. In this section, I shall discuss the reliability of these measurements.

3.3.1 Reliability of Outgrowth Measurements

Outgrowth of neurites from SCG neurons appears to be strikingly regular. This regularity is obvious when we view the drawings of the outgrowth (see Figure 3.2). Although the viewer integrates variations in the outgrowth rates, the random variability of the movement is readily apparent when quantitatively measured. This large variability in measured outgrowth rate is due partially to variation in the growth rate of the neurites, partially to the crudeness of the measurements, and partially to the fluctuation in the shape of the growth cone. The measurements are precise to only ± 2 microns, or about 15% of the average cell growth, during a 30 minute measurement interval. Fluctuations in the shape of the growth cone also increase the variability in the measurements, because they make it difficult to assess the position of the growth cone properly. In Figure 3.3, I show a set of three successive images that display typical variation in the shape and position of a growth cone over 20 minute intervals. The magnitude of the fluctuations in the shape of the growth cone is often comparable to that of the total neurite outgrowth during 20 minutes. These fluctuations are especially pronounced soon after plating, when the growth cones tend to be broad and flat. The fluctuations tend to decrease over the course of our experiments, as the growth cones become more compact. Because it is more difficult to define the growth cone position when the growth cone is broad and flat, this systematic change in the shape of the growth cone during an experiment may partially account for the observed decrease in growth rate in both experimental and control cells.

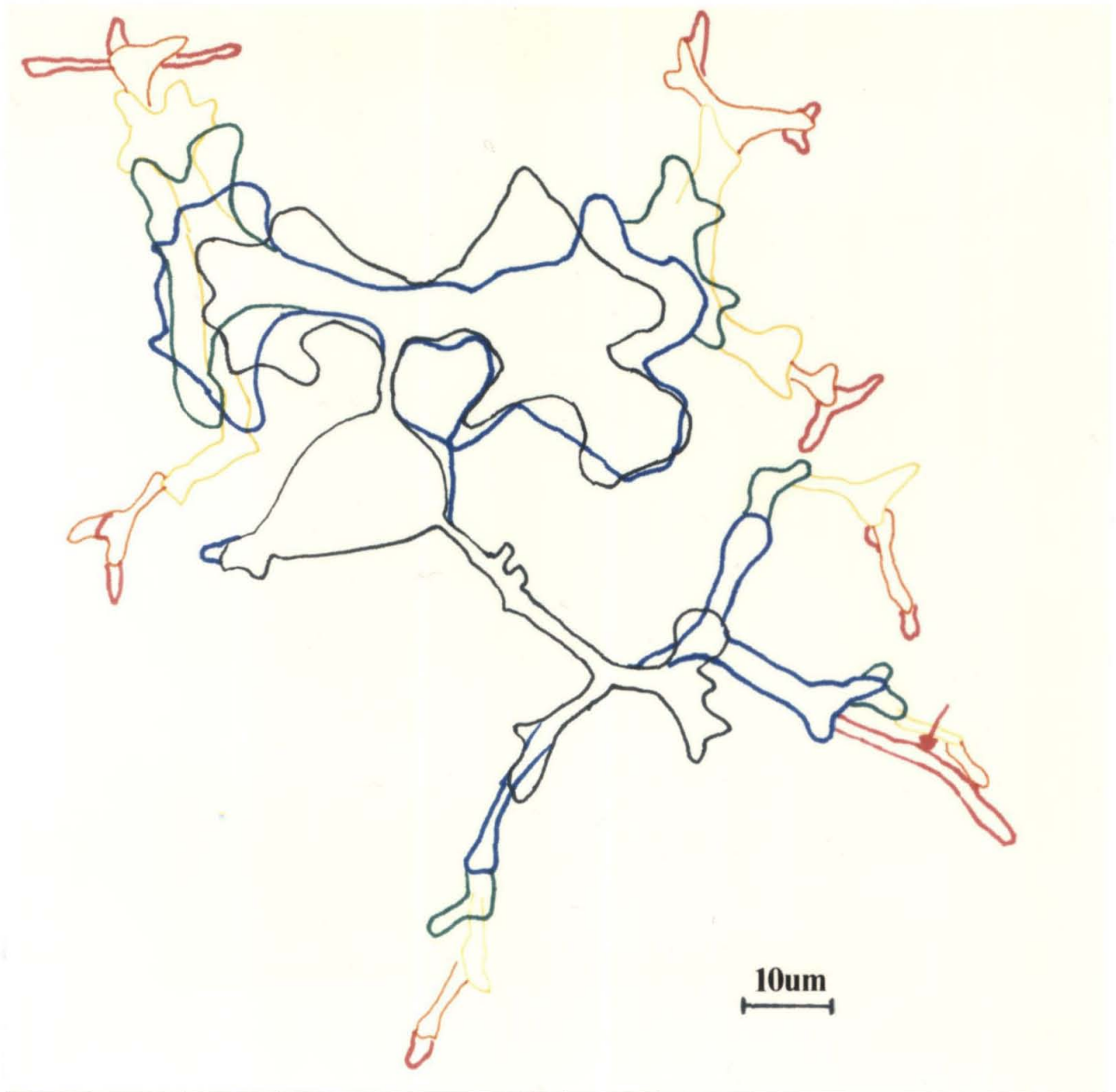


Figure 3.2 An outline drawing of neurite outgrowth from an SCG neuron. The growth was measured from these drawings. This drawing was made from images taken every 20 minutes. I drew the outline from the earliest photograph in black, the next in blue, then green, yellow, orange, and red (last). Figure 3.3 shows the original pictures from which these drawings are made.

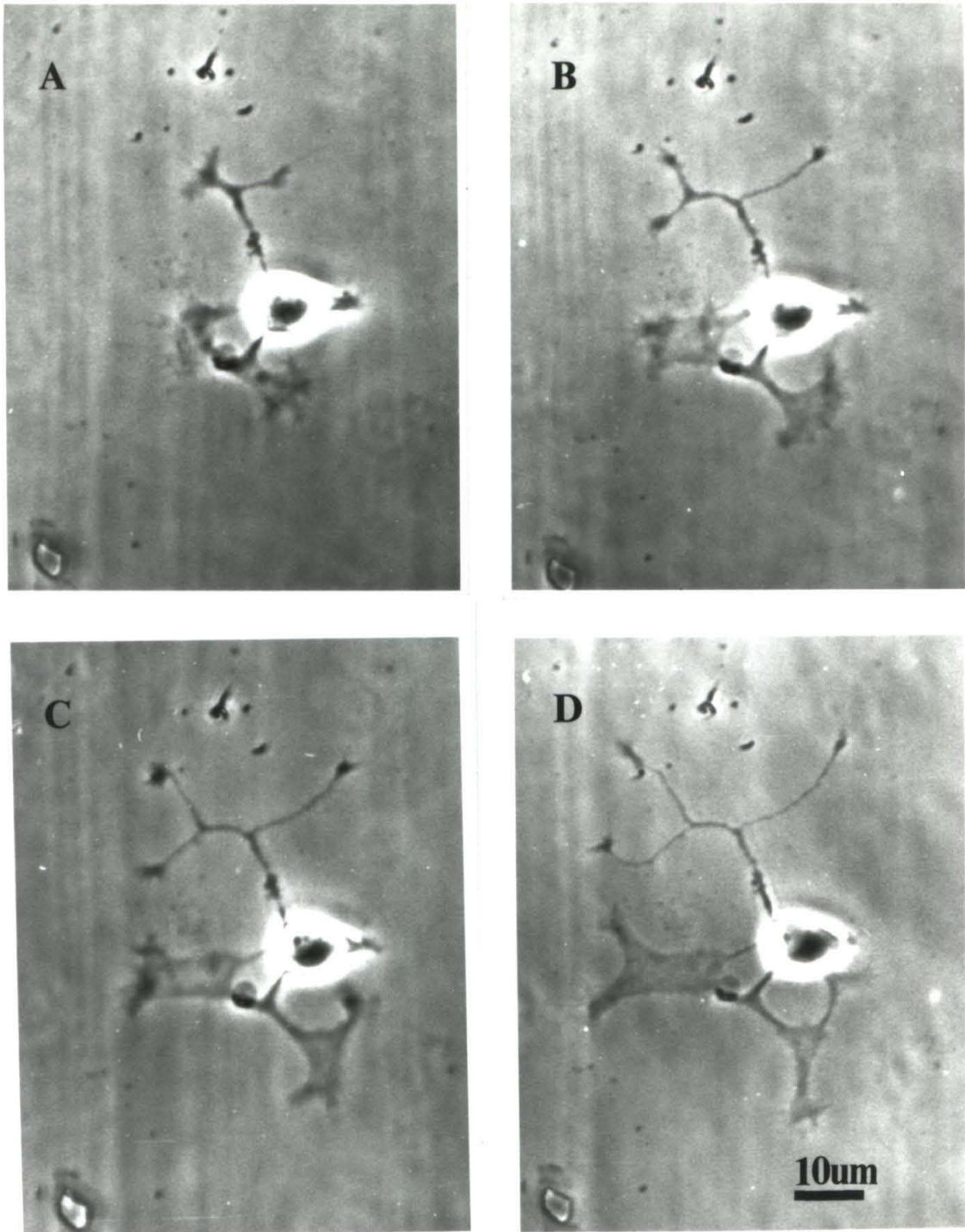


Figure 3.3 *Successive pictures of the SCG neuron outlined in Figure 3.2. The images were taken every 20 minutes. Notice that the growth cones and processes become more compact with time.*

3.3.2 Reliability of Calcium Measurements

One of the best ways of measuring $[Ca]_i$ is to use fura-2, but because of variations in both methodology and experiments, reported calcium concentrations cannot always be compared directly. Since I will compare the calcium measurements presented here with those made by other researchers (notably Fields et al., 1990a; Cohan et al, 1987), it is instructive to look at the magnitude and sign of some of the suspected discrepancies.

One of the largest potential sources of error is incorrectly estimating the values of R_{min} and R_{max} . The choice of R_{min} and R_{max} can easily affect the calculated calcium concentration by a factor of 2 or more. Regehr and collaborators (1989) had previously determined R_{min} and R_{max} in saline. These R_{min} and R_{max} values differed from the ratios we determined using SCG neurons made permeable with ionophores, bromo-A23187, and ionomycin. When we used 5 μ M bromo-A23187 to permeabilize the cells, R_{min} equalled 0.306 ± 0.029 and R_{max} equalled 2.00 ± 0.36 . When we used 200 nM ionomycin to permeabilize the cells, $R_{min} = 0.278 \pm 0.026$ and $R_{max} = 3.34 \pm 0.24$ (we used solutions containing 1 nM and 5 mM Ca^{2+} to determine R_{min} and R_{max} , respectively). As an example of the magnitude of the potential error in the calculated calcium concentration, if the measured fluorescence ratio was 1, the calculated calcium concentration would be about 120 percent greater if we used the R_{min} and R_{max} values obtained with bromo-A23187, rather than those obtained with ionomycin. The larger R_{min}/R_{max} ratio obtained with ionomycin rather than with bromo-A23187 permeabilized cells indicates that ionomycin was more effective at equilibrating the calcium concentration between the interior and exterior of the cell. We do not know whether differences between *in situ* and *in vitro* R_{max} values represent an inability of the ionophore to equilibrate Ca^{2+} across the membrane, or whether the differences represent a real difference in the response of fura-2 in the cell versus in saline. The effect of using the *in vitro* values is a possible underestimation of the true calcium concentration in the cell, in either case.

A related source of error is that, for consistency with other papers in the field (Cohan et al., 1987; Connor, 1986), we did not correct R_{\min} and R_{\max} for the cellular viscosity. In a viscous environment, such as inside a cell, R_{\min} and R_{\max} appear different from in a nonviscous environment, such as the saline used for calibration (Poenie et al., 1986). To correct for the intracellular viscosity, we multiplied the measured fluorescence ratios, R_{\min} and R_{\max} , by a correction factor. The viscosity correction factor is probably dependent on the cell type. For example, Poenie and collaborators, (1986), estimated the correction factor to be 0.7, while Regehr and collaborators, (1989), estimated the correction factor to be 0.85 in PtK₁ and hippocampal cells, respectively. By omitting the viscosity correction factor we tend to underestimate our true calcium concentration.

If fura-2 is transported selectively into intracellular compartments, the measured calcium concentrations would represent that of the intracellular compartments rather than that of the bulk cytoplasm. Intracellular compartments may have much higher calcium concentrations than that of the surrounding cytoplasm. If fura-2 is responding to the local vesicular environment, we would overestimate the average calcium concentration. We were sometimes able to see evidence of vesicular staining (punctate staining within the cell) after about 3 hours. This staining was clearly visible in most cells by 5 hours. To minimize measurement errors due to compartmentalization of the dye, we limited our measurements to the times less than 3 hours after staining, and we did not use cells in which any punctate staining was apparent.

We estimate that 25% of our staining was membrane associated or compartmentalized. We base this estimate on comparisons of fluorescence before and after we obtained whole-cell recordings with a saline-filled pipette. All the fura-2 should rapidly diffuse into the essentially infinite volume of the patch pipette, leaving the cell non-fluorescent if none of the dye was membrane associated or compartmentalized; complete diffusion did not occur. In the three cases in which we entered the cell, roughly

25 percent of the fluorescence remained intracellular after a 15 minute. It is difficult to extrapolate the calcium concentration in the intracellular compartments strictly from the calcium concentration measured by this residual dye, since the ratio of bound to compartmentalized dye is unknown and saline replaced the cytoplasm. If calcium-rich compartments sequester half of this 25 percent and the calcium concentration in those compartments is eight times that in the cytoplasm, our measurements would overestimate the true R value by a factor of 2.

Spatial resolution limits further complicate the fura-2 measurements. We averaged $3.3 \mu\text{m}^2$ for each measurement. This resolution means that the fura-2 measurements are insensitive to more local variations in calcium concentration, but these more local potential variations may contribute to the regulatory mechanisms discussed in the next chapter. As discussed in Chapter 2, some researchers have found evidence for spatial calcium ion gradients using fura-2 (Connor et al., 1990), but these gradients are in invertebrate neurons with growth cones much larger than those of the SCG neurons. Such gradients probably exist in most growth cones, nonetheless, particularly directly below the calcium channels in the membrane. As I shall discuss in Chapter 4, local areas of extremely elevated calcium may be the effective agent in regulating outgrowth. This source of error will average the calcium concentration across the growth cone.

Because of the large potential variations in the calculation of $[\text{Ca}]_i$, from the measured fluorescence of fura-2 stained cells at 340 and 380 nm as described, we must view any direct comparison of absolute calcium concentrations between different cell types or laboratories with some suspicion. Nonetheless, we can compare calcium measurements within an experiment and the percent increase in calcium between experiments.

References

- Argiro, V., Bunge, M.B. and Johnson, M.I. (1984) Correlation between growth form and movement and their dependence on neuronal age. *J. Neurosci.* 4:3051-3062.
- Berry, M., Bradley, P. and Borges, S. (1978) Environmental and genetic determinants of connectivity in the central nervous system-An approach through dendritic field analysis. *Prog. Brain Res.* 48: 133-148.
- Bray, D. (1973). Branching patterns of individual sympathetic neurons in culture, *J. Cell Bio.* 56:702-712.
- Bruckenstein, D.A. and Higgins, D. (1988) Morphological differentiation of embryonic rat sympathetic neurons in tissue culture II. Serum promotes dendritic growth. *Dev. Biol.* 128:337-348.
- Campenot, R.B. (1984) Inhibition of nerve fiber regeneration in cultured sympathetic neurons by local, high potassium. *Brain Research* 293:159-163.
- Campenot, R.B. (1986) Retraction and degeneration of sympathetic neurites in response to locally elevated potassium. *Brain Research* 399:357-363.
- Campenot, R.B. and Draker, D.D. (1989). Growth of sympathetic nerve fibers in culture does not require extracellular calcium. *neuron* 3:733-743.
- Cohan, C.S., Connor, J.A. and Kater, S.B. (1987). Electrically and chemically mediated increases in intracellular calcium in neuronal growth cones. *J. Neurosci.*, 7:3588-3599.
- Cohan, C.S. and Kater, S.B. (1986). Suppression of neurite elongation and growth cone motility by electrical activity. *Science* 232:1638-1640.
- Connor, J.A. (1986). Digital imaging of free calcium changes and of spatial gradients in growing processes in single, mammalian central nervous system cells. *P.N.A.S.* 83:6179-6183.
- Connor, J.A., Kater, S.B., Cohan, C. and Fink, L. (1990) Ca^{2+} dynamics in neuronal growth cones: regulation and changing patterns of Ca^{2+} entry. *Cell Calcium* 11:233-239.
- Fields, R.D., Guthrie, P.B., Nelson, P.G. and Kater, S.B. (1990a). Calcium homeostatic capacity is regulated by patterned electrical activity in growth cones of mouse DRG neurons. 16th Soc. of Neurosci. Abst. 197.2: 457.

- Fields, R.D., Neale, E.A. and Nelson, P.G. (1990b). Effects of patterned electrical activity on neurite outgrowth from mouse neurons. *J. Neurosci.* 10:2950-2964.
- Grynkiewicz, G., Poenie, M. and Tsien, R.Y. (1985). A new generation of Ca^{++} indicators with greatly improved fluorescence properties. *J Biol. Chem.* 260: 3440-3450.
- Kater, S.B., Mattson, M.P., Cohan, C. and Connor, J. (1988). Calcium regulation of the neuronal growth cone. *Trends. in Neurosci.* 11:315-321.
- Lein, P.J. and Higgins, D. (1989) Laminin and a basement membrane extract have different effects on axonal and dendritic outgrowth from embryonic rat sympathetic neurons *in vitro*. *Dev. Biol.* 136:330-345.
- Mains, R.E. and Patterson, P.H. (1973). Primary cultures of dissociated sympathetic neurons. I. Establishment of long-term growth in culture and studies of differential properties. *J. Cell Bio.* 59:329-345.
- Poenie, M., Alderton, J., Steinhardt, R. and Tsien, R. (1986) Calcium rises abruptly and briefly throughout the cell at the onset of anaphase. *Science* 233:886-889.
- Purves, D., Hadley, R.D. and Voyvodic, J.T. (1986) Dynamic changes in the dendritic geometry of individual neurons visualized over periods of up to three months in the superior cervical ganglion of living mice. *J. Neurosci.* 6:1051-1060.
- Regehr, W.G., Connor, J.A. and Tank, D.W. (1989). Optical imaging of calcium accumulation in hippocampal pyramidal cells during synaptic activation. *Nature* 341:533-536.
- Robson, S.J. and Burgoyne, R.D. (1989). L-type calcium channels in the regulation of neurite outgrowth from rat dorsal root ganglion neurons in culture. *Neurosci. Lett.* 104:110-114.
- Rubin, E. (1985a) Development of the rat superior cervical ganglion: Ingrowth of preganglionic axons. *J. Neurosci.* 5:685-696.
- Rubin, E. (1985b) Development of the rat superior cervical ganglion: Initial stages of synapse formation. *J. Neurosci.* 5:697-704.
- Sussdorf, W.S. and Campenot, R.B. (1986). Influence of the extracellular potassium environment on neurite growth in sensory neurons, spinal cord neurons and sympathetic neurons. *Dev. Brain Res* 25:43-52.
- Voyvodic, J.T. (1987) Development and regulation of dendrites in the rat superior cervical ganglion. *J. Neurosci.* 7:904-912.

Chapter 4

Effects of Electrical Stimulation and Changes in $[Ca]_i$ on Neurite Outgrowth from SCG Neurons II

In this chapter, I shall present and discuss results from experiments that measure the effect of electrical activity and the concomitant increase in $[Ca]_i$ on neurite outgrowth from neonatal rat SCG neurons in culture. In the experiments described, neurite outgrowth, from rat SCG neurons, continues during chronic stimulation at 10 Hz and during the accompanying increase in $[Ca]_i$. These results suggest that neither electrical activity nor $[Ca]_i$ generally regulates neurite outgrowth. In Section 4.1, I present the results of these experiments. I discuss these results in Section 4.2.

4.1 Results

Neurites of cultured neonatal rat SCG neurons are formed by the steady advance of growth cones which divide, apparently at random, to form branches (Bray, 1973). On polylysine-laminin substrates, processes were usually evident 30 to 90 minutes after plating. Initially, many processes have large flat growth cones which become more punctate with time.

Neurons showed a diversity of morphologies; some had thinner neurites and smaller growth cones even at the beginning of the experiments. Figure 4.2 shows the outgrowth from a second cell, over 2.5 hours. The change in this cell's growth cone structure is considerably less pronounced than the change in the growth cone structure of the cell in Figure 4.1. The pictures were taken every 30 minutes.

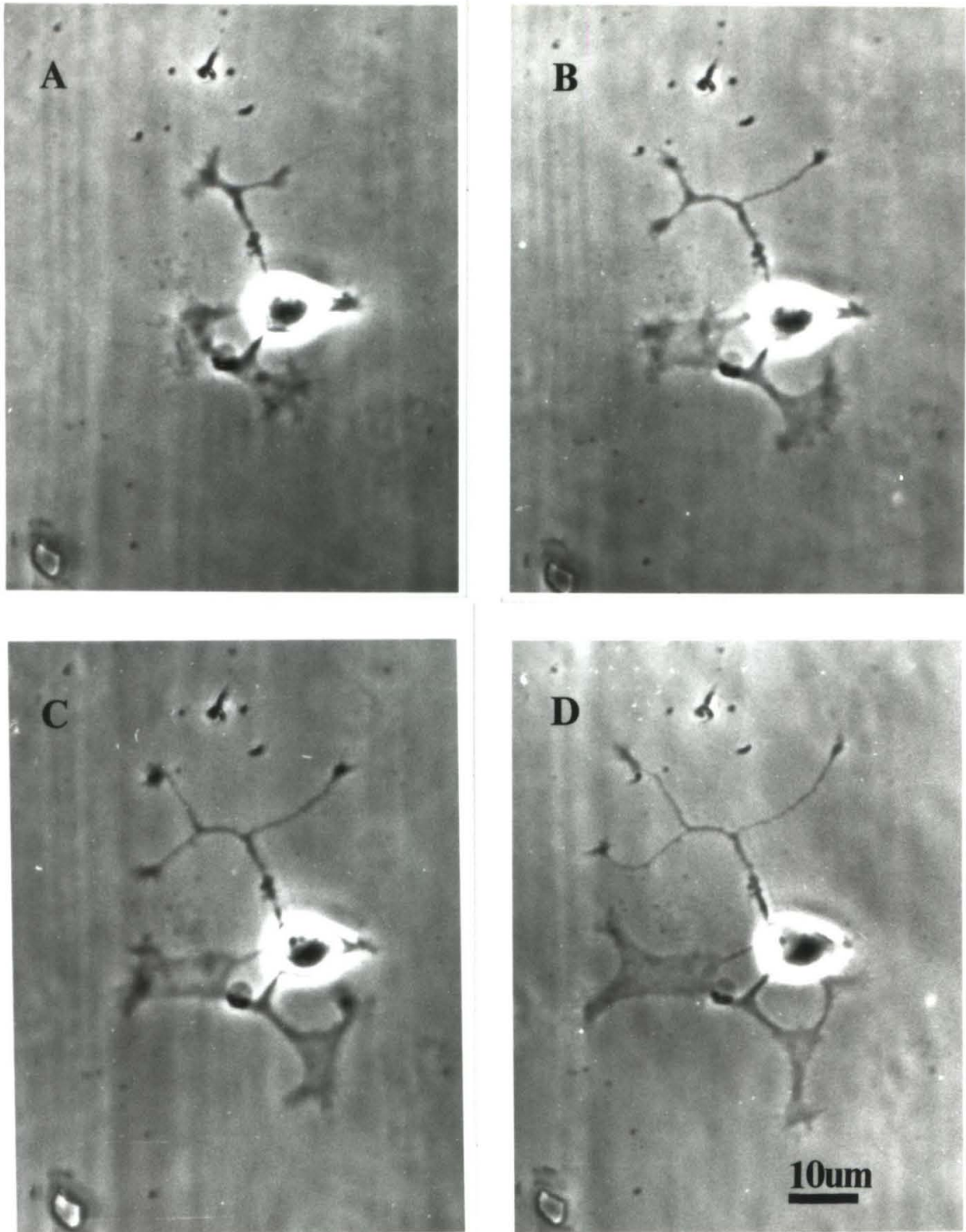


Figure 4.1 Growth from a typical SCG neuron on polylysine-laminin coated substrate. The pictures are taken every 20 minutes starting about 4 hours after plating. Notice the decrease in growth cone size and neurite width that occurs with time, particularly from the bottom portion of this cell.

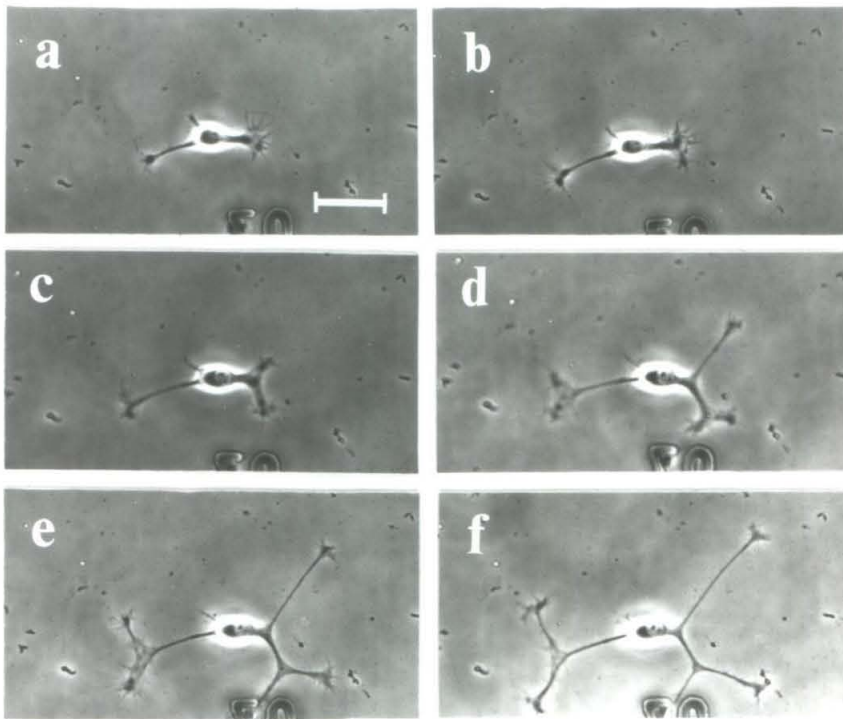


Figure 4.2 *Neurite outgrowth from a second cell.* Thirty minutes elapsed between photographs.

I measured neurite outgrowth (as described in Chapter 3) from drawings of the projections of negative photographic images. Figure 4.3 is an example of one of these drawings: it is of the cell in Figure 4.1. The succession of colors is black, blue, green, yellow, orange, and red; each drawing represents 20 minutes of growth.

The consistency of the outgrowth from a single neuron is striking. Average outgrowth rates were generally in the tens of $\mu\text{m}/\text{hour}$ and the neurites continued to advance throughout the experiments. I watched 251 neurites of which only 16 (6.4 percent) stopped permanently or retreated, and only one resumed growth after initially retreating.

To assess growth, I can plot either the total outgrowth or the average growth rate. Total outgrowth is the sum of the measured outgrowth from all neurites on a given cell. Total outgrowth is not normalized to the number of neurites observed. In Figure 4.4, I plot the total outgrowth versus time from the cell shown in Figure 4.2. The slope of total outgrowth versus time increases slightly with time because the neurites branch during the experiments. I add the growth of each branch separately whether the branch continues to grow, stops growing, or retracts. The negative growth tends to decrease the slope of total growth versus time.

¹A control cell is a neuron which did not have a patch pipette attached to it and was not stimulated electrically. All neurons in which at least half of their neurites were photographed every 30 minutes for 2 hours or more were "control" cells. We had nine control cells with about 40 observable growth cones by this definition. The number of observable growth cones varied over time since some neurites branched and others grew out of the field of view or onto other processes.

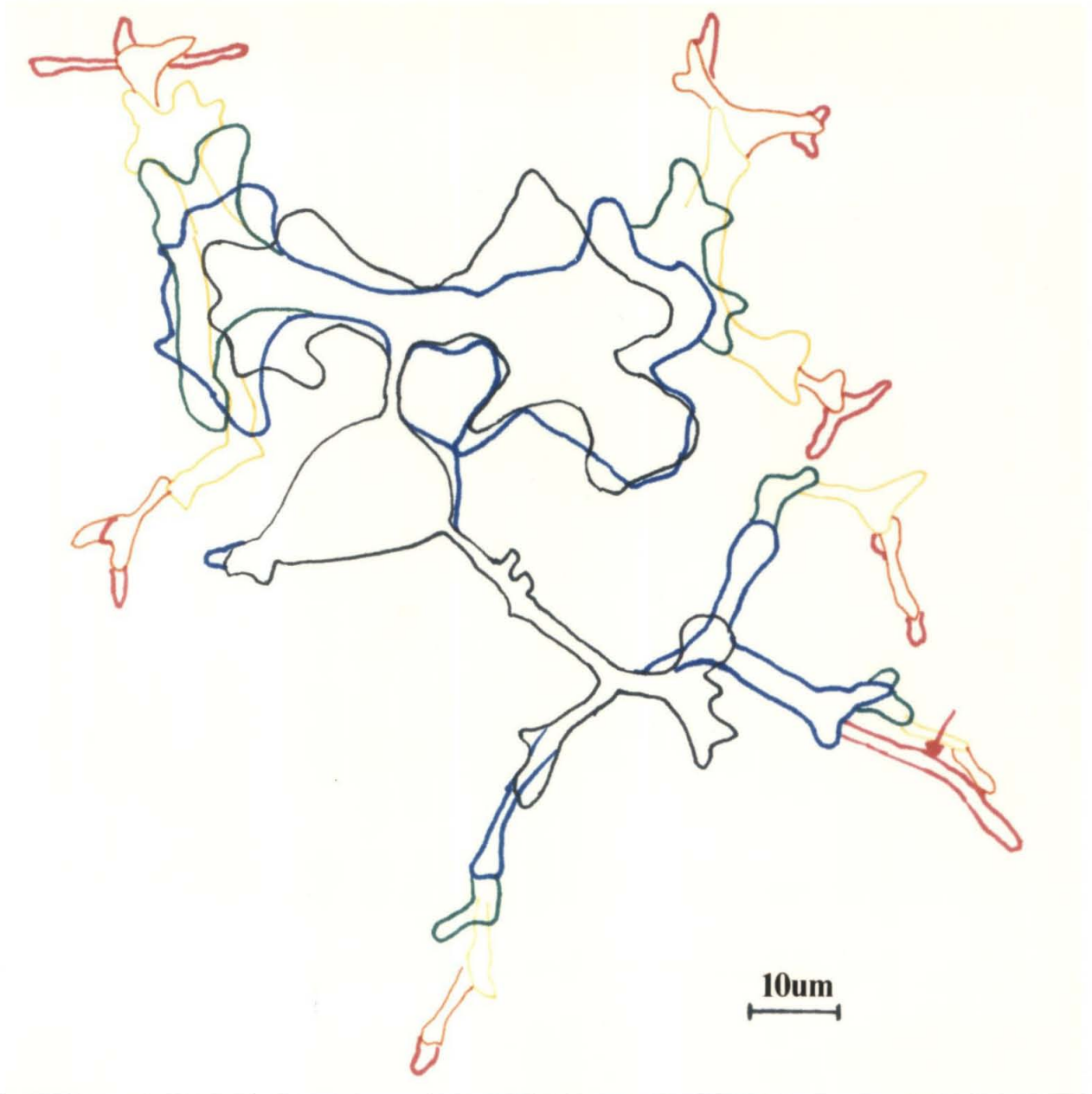


Figure 4.3 Drawing of outgrowth from the typical cell shown in Figure 4.1. The succession of colors is black, blue, green, yellow, orange, and red; each drawing represents 20 minutes of growth.

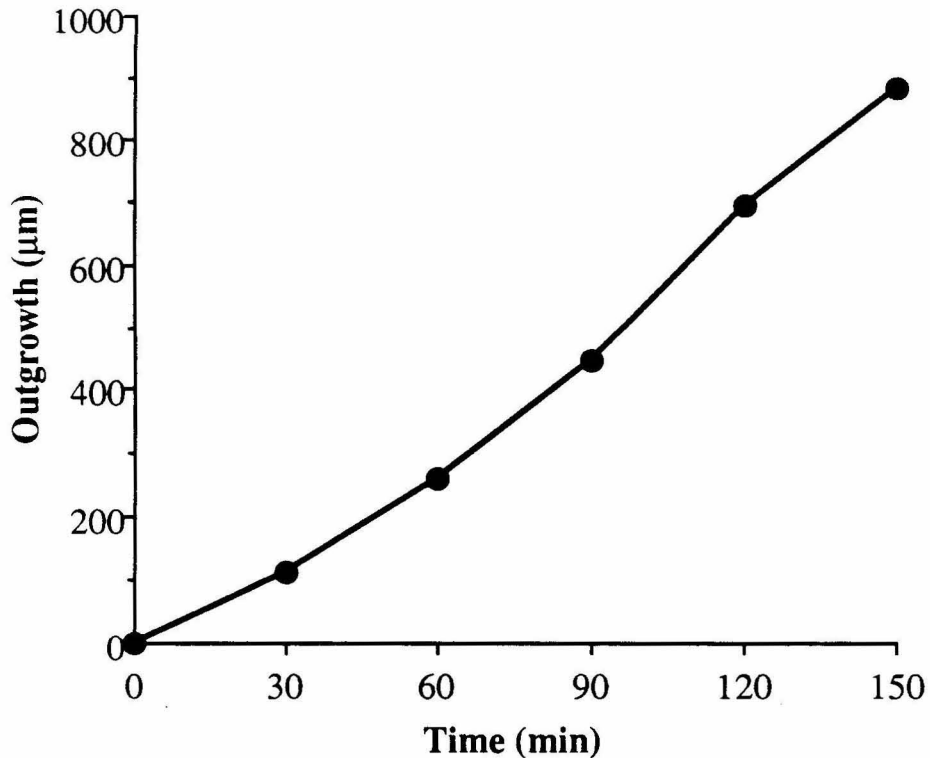


Figure 4.4 Plot of the total outgrowth of all processes from the control cell versus time shown in Figure 4.2.

The average growth rate is the average of the outgrowth rate of each neurite. The outgrowth rate of each neurite is that neurite's measured growth over a time interval divided by the length of the time interval. Therefore, the average growth rate, unlike the total outgrowth, is normalized to the number of neurites observed. As in calculations of the total outgrowth, calculations of the average growth rate include all processes, whether the latter grew steadily or retracted (of all the neurites observed, only 16 of 251 retracted, and only one did so reversibly). Average growth rates from control cells during successive 30 minute time periods, starting 2 to 6 hours after plating, were 24 ± 3 (42 growth cones, (gc), on 9 neurons, (n), \pm standard error of the mean, (SEM)), 21 ± 2 (40 gc on 9 n), 18 ± 3 (36 gc on 9 n) and 16 ± 2 $\mu\text{m}/\text{hour}$ (32 gc on 9 n). There was a decrease in the number of growth cones observed with time, because some growth cones either grew into

other neurites or grew out of the field of view. Figure 4.5 is a plot of the average growth rate versus time. The average growth rates for most control and experimental cells declined with time. I shall discuss this decline in Section 4.1.1.

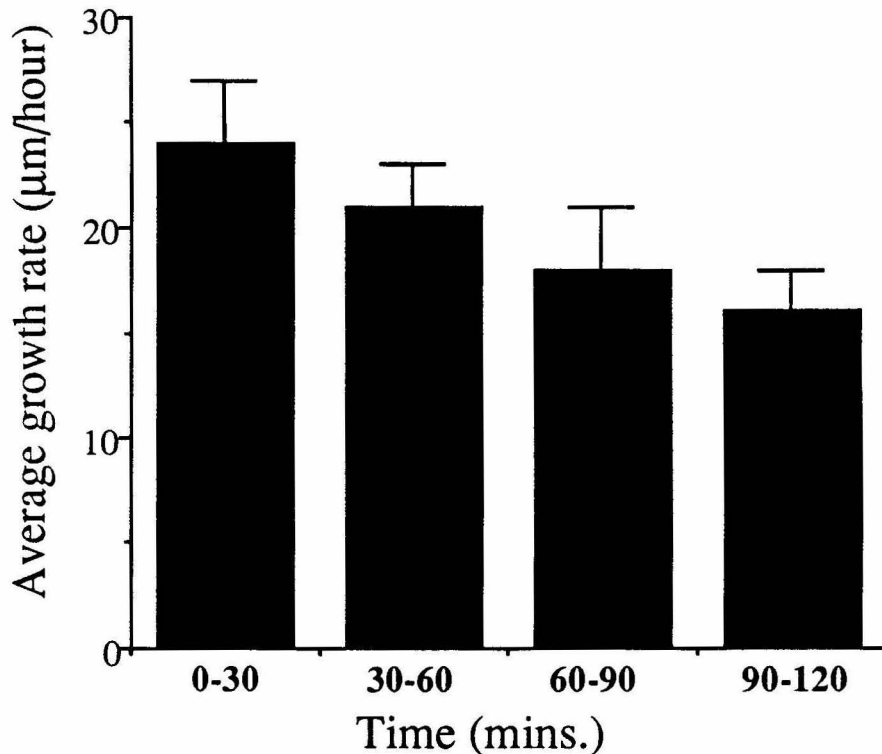


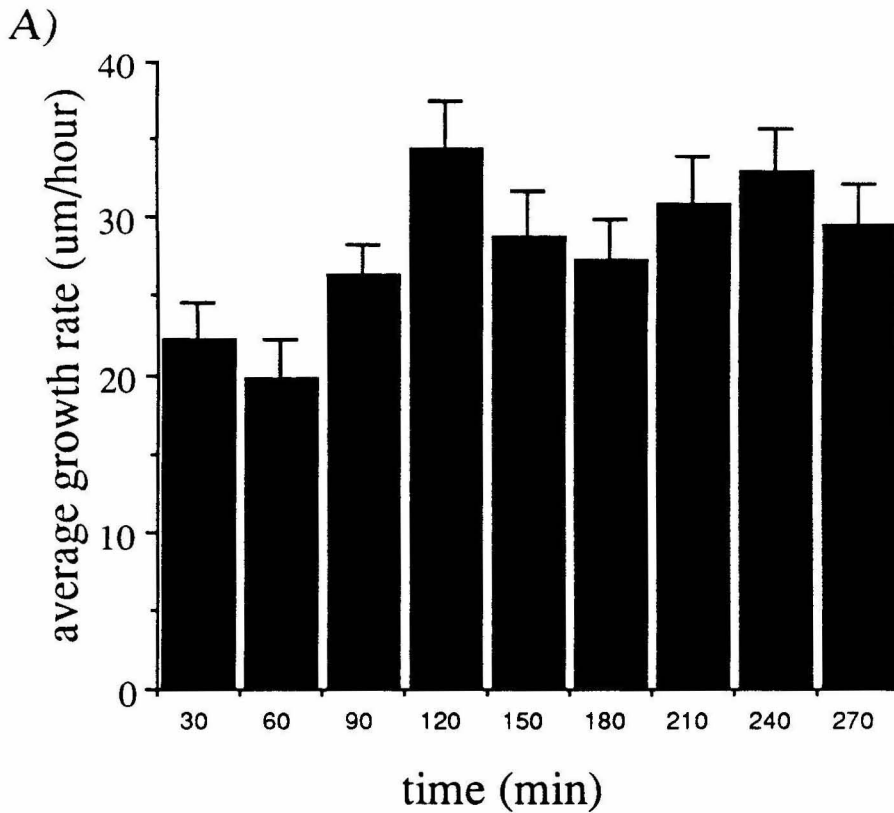
Figure 4.5 Average growth rate versus time for the nine control cells studied.

Processes often branched during an experiment. Each branch grew at approximately the same rate as did the parent. Of the 47 neurites that branched into 102 neurites, the average growth rates of the parent neurites during the 30 minutes before branching and 30 minutes during which a split in the growth cone became apparent, and of the daughter neurites during the 30 minutes following the branching event were 32.9 ± 2.4 , 37.1 ± 1.8 and 33.7 ± 2.1 µm/hour (\pm SEM), respectively.

4.1.1 Possible Reasons Why Neurite Outgrowth Slows

The average growth rates for most control and experimental cells declined with time. On average our control cells slowed 33 ± 10 percent, and our experimental cells slowed 41 ± 48 percent (\pm SEM), over the 2 hours of experiments. Although I do not know the reason for this decrease, there are a number of potential explanations for it. One possibility is that the rate of neurite outgrowth from all SCG neurons decreases with time in culture on a polylysine-laminin substrate. The control experiments, however, did not support this hypothesis. In our experiments, the rate of neurite outgrowth remained constant (Figure 4.6) in L15 medium at 37° C in a five percent CO_2 incubator,.

Another possible reason for this observed slowing of growth is that processes often branched during an experiment. If the daughter branches grow at substantially different rates than do the parent branches, this differential growth rate could account for the measured decrease in the average growth rate. Again, however, the data do not support this hypothesis. The average outgrowth rates of neurites just before and after branching were 32.9 ± 2.4 $\mu\text{m}/\text{hour}$ and 33.0 ± 2.1 $\mu\text{m}/\text{hour}$ (\pm SEM), respectively.



B)

	time (min)								
	0-30	30-60	60-90	90-120	120-150	150-180	180-210	210-240	240-270
AGR	22.2	19.7	26.3	34.3	28.7	27.3	30.8	33.0	29.5
SEM	2.3	2.4	2.0	3.2	3.0	2.6	3.1	2.7	2.7
# n	7	7	7	7	7	7	7	7	7
# gc	26	28	30	32	34	40	43	44	44

Figure 4.6 Average SCG neurite outgrowth rates (AGR) for control cells grown in CO_2 buffered medium in a 5 percent CO_2 incubator. A) is a plot of the average growth rate of all the processes from all of the control cells. B) is a table of the same data. The number of neurons and number of growth cone observed during each time interval is included on the table. SEM = standard error of the mean. AGR = average growth rate. n = neurons. gc = growth cones.

I originally plated the neurons in a CO₂ buffered medium at 4 ng/ml NGF but during experiments I grew the cells in room air with only 2 ng/ml NGF in the medium. These changes could account for the observed decrease in growth rate. Control experiments do not support this explanation, however, since seven cells grown for 1 hour in a 5 percent CO₂ incubator (4 ng/ml NGF) and then switched into an incubator with air (2 ng/ml NGF) continue to grow at a constant rate (Figure 4.7).

condition	CO ₂	CO ₂	air	air
AGR ± SEM	31.7±2.8	27.2±3.1	33.0±2.3	39.0±3.3
# of neurons	7	7	7	7
# growth cones	24	24	34	28
time (min)	30	60	90	120

Figure 4.7 Average growth rates (AGR) for SCG neurons grown in a 5 percent CO₂ environment and then switched into an incubator with air. Growth was assessed every 30 minutes. SEM = standard error of the mean.

I cannot rule out other possible explanations for the decreased growth rate at this time. The cells grown in CO₂ already had compact growth cones and thin neurites during these experiments, for instance. The change in growth cone morphology, which we often observed in our experimental and control cells, but did not observe in this batch of CO₂ grown cells, could account for the decrease in growth rate. The decrease in growth rate could be due to either a systematic bias in the measurement or an actual slowing of the processes, if this were the case. Another possibility is that growth on the microscope stage slows neurite outgrowth. The exposure to light or small variations in the temperature might slow down the cells, for instance. The cells are temperature sensitive. They stop growing

at 25° C or just 2 degrees above the experimental temperature. The small decrease in growth rate with time should not affect the main conclusion of this study.

4.1.2 Stimulation

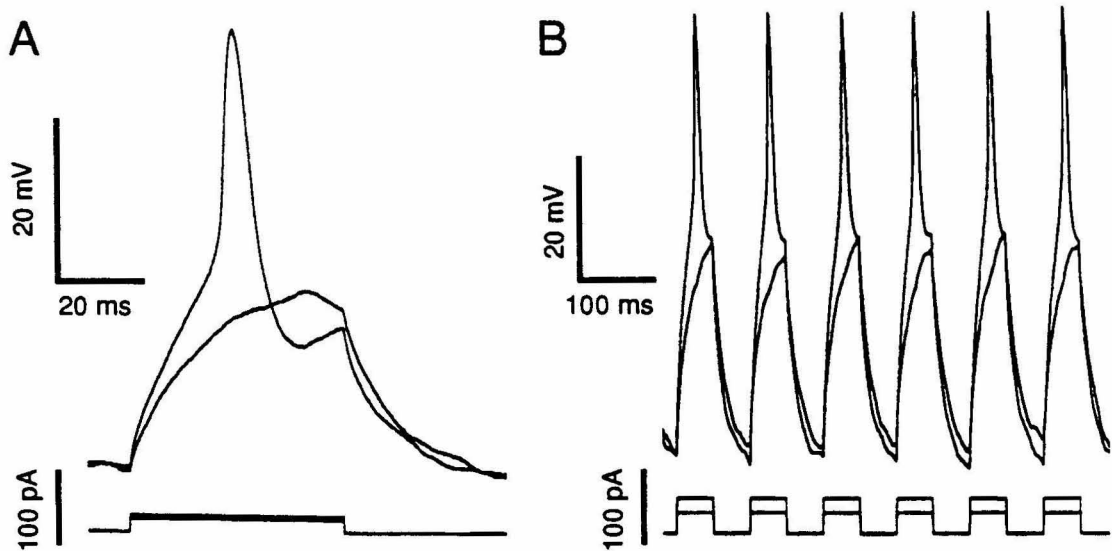


Figure 4.8 *Stimulation of a SCG neuron with a cell-attached pipette at 1 and 10 Hz. In the bottom trace, stimulation is just below threshold; in the top trace, stimulation is increased to just above threshold.*

It was essential to have a reliable stimulation method to study the effects of activity on neurite outgrowth. In preliminary experiments, we found that intracellular and whole-cell electrode techniques stopped neurite outgrowth, so we used extracellular cell-attached patch pipettes to stimulate neurons non invasively as described in Chapter 3. Action potential amplitudes recorded with extracellular pipettes were typically between 4 and 40 mV in magnitude. In Figure 4.8, I show recordings from a cell stimulated at 1 and 10 Hz: the stimulus current is just below threshold in the bottom trace, and the stimulus current is just above threshold in the top trace. The magnitude and shape of the recorded action

potentials varied over the course of an experiment, presumably as the impedance of the seal and patch fluctuated. All experiments used 10 Hz chronic stimulation, because preliminary experiments had shown that stimulation at 1 and 2 Hz did not affect neurite outgrowth rates and 10 Hz was the fastest rate at which we could stimulate the neurons consistently.

4.1.3 Outgrowth During Stimulation

To determine whether electrical activity is likely to regulate the rate of process outgrowth from SCG neurons, I monitored outgrowth before, during, and after stimulation. To control for any effect of the application of the patch pipette on growth rate, I monitored the growth before the application of the patch pipette to the cell. In these experiments, I took pictures every 30 minutes. In Figure 4.9, I show the photographs from one typical experiment. In Figures 4.9a and 4.9b, I show the cell at the beginning of the experiment and 30 minutes later, respectively. At the time represented in Figure 4.9b, I attached a pipette to the cell, but did not stimulate it. In Figure 4.9c, I show the cell 30 minutes later, when 10 Hz stimulation has begun. In Figures 4.9d and e, I show the cell after 30 and 60 minutes of chronic stimulation. I stopped the stimulation at the time corresponding to Figure 4.9e. In Figure 4.9f, I show the cell 30 minutes after stopping electrical stimulation.

Throughout these stimulation experiments, the neurons continued to grow and branch. I observed two branching events during stimulation. The number of branching events expected to originate during stimulation was four. I calculated this expected value by dividing the total number of observed branching events by the fraction of time the neurite were stimulated. Two observed branching events are not statistically significantly different from the four expected events. Stimulation also did not affect the frequency

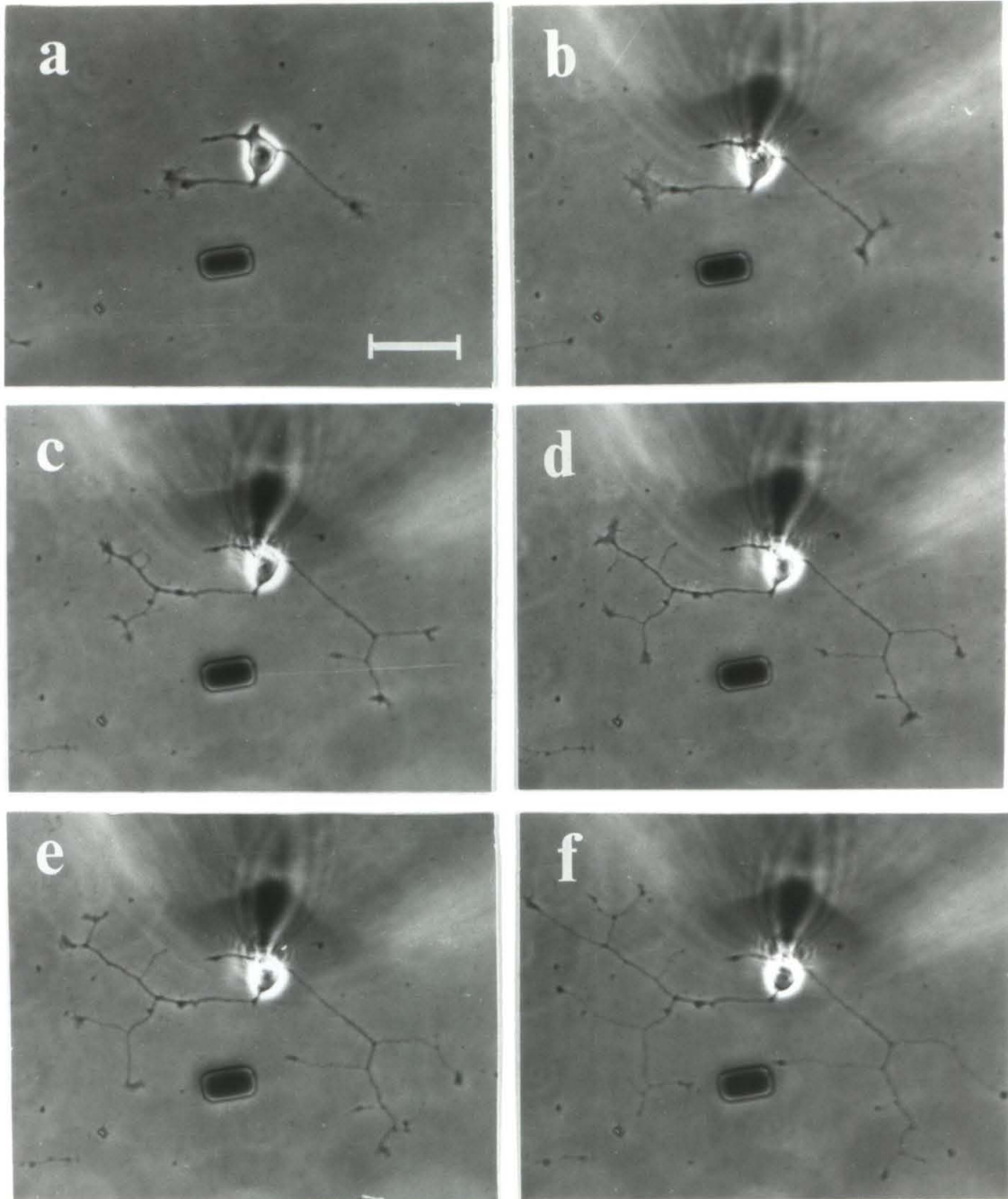


Figure 4.9 *Neurite outgrowth before, during, and after electrical stimulation at 10 Hz.* The photographs were taken at 30 minute intervals. (a) The cell at the beginning of the experiment. (b) After 30 minutes, when a patch pipette was added. (c) After 30 minutes, when electrical stimulation at 10 Hz began. (d) After 30 minutes of electrical stimulation. (e) After 60 minutes of electrical stimulation, when stimulation was stopped. (f) Thirty minutes after the cessation of electrical stimulation.

at which neurites stopped growing or retracted. Neurites rarely retracted during these experiments, and only one neurite retracted during 10 Hz stimulation (the expectation value for retraction events, as calculated for branching events, is 1.6).

In Figure 4.10, I plot total outgrowth from all neurites from the cell in Figure 4.9 versus time. I also plot the total outgrowth from the control cell shown in Figure 4.2, for comparison. Cumulative growth was similar between the two cells, and showed a slight increase in slope with time due to neurite branching.

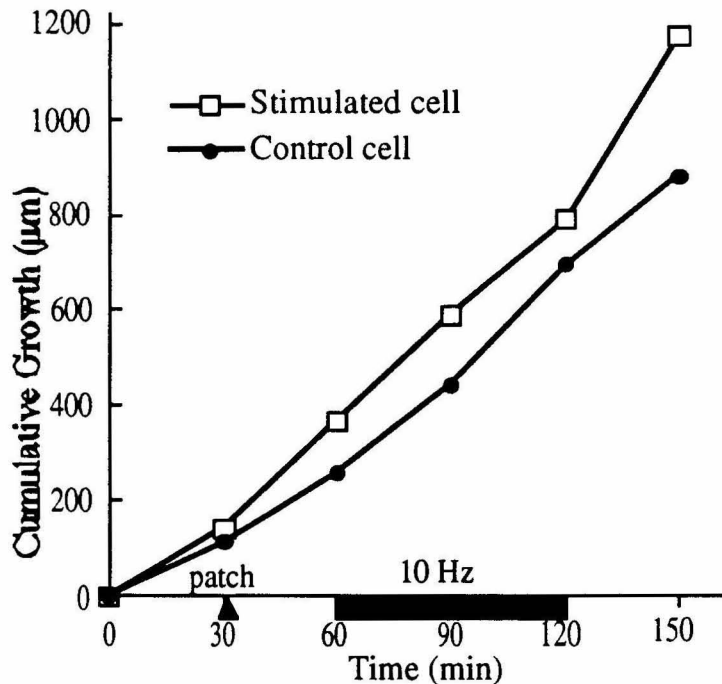
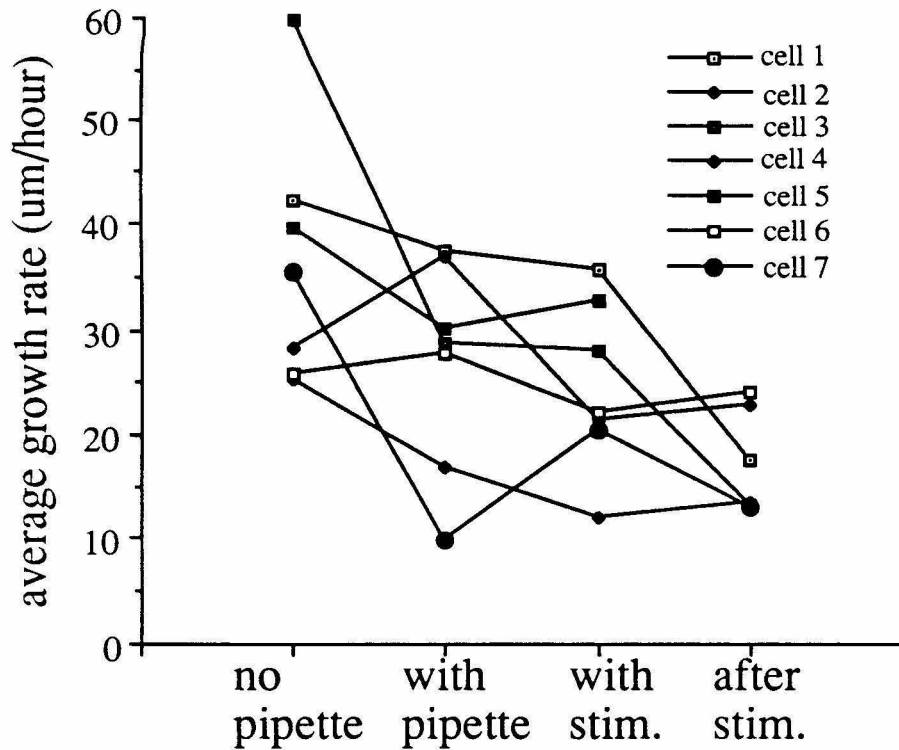


Figure 4.10 Plot of the total outgrowth of all processes from the stimulated cell shown in Figure 4.9 and the control cell shown in Figure 4.2, versus time.

Average growth rates during successive 30 minute periods are the same for stimulated or experimental cells and for control cells. The average growth rates for the 30 minutes before patching or stimulation was $34 \pm 2 \mu\text{m}/\text{hour}$ (62 gc on 7 n, \pm SEM). I



	no pipette	with pipette	stim. 10 Hz	no stim.
cell 1	42.1 \pm 2.3	37.4 \pm 9.9	35.6 \pm 4.2	17.7 \pm 10.2
cell 2	28.3 \pm 4.4	36.9 \pm 5.1	21.4 \pm 2.7	22.9 \pm 3.0
cell 3	59.8 \pm 16.3	28.6 \pm 4.1	27.9 \pm 4.2	13.2 \pm 7.0
cell 4	25.4 \pm 3.7	16.8 \pm 2.7	12.1 \pm 2.1	13.6 \pm 2.6
cell 5	39.4 \pm 3.9	30.1 \pm 1.7	32.8 \pm 6.5	
cell 6	25.8 \pm 3.7	27.7 \pm 3.3	22.2 \pm 1.5	24.2 \pm 3.3
cell 7	35.4 \pm 3.2	9.9 \pm 9.5	20.5 \pm 4.4	13.1 \pm 3.2

Figure 4.11 Average neurite growth rates for seven experimental cells in $\mu\text{m}/\text{hour} \pm$ SEM. Cells were studied on different days. Notice that there is a two fold variation between cells.

attached a cell-attached patch pipette to the cell at the end of this period. The cells grew at $28 \pm 2 \mu\text{m}/\text{hour}$ (71 gc on 7 n) during the 30 minute period with this pipette on the cell. At the end of this second period, 10 Hz stimulation began. The cell grew at $25 \pm 2 \mu\text{m}/\text{hour}$ during 30 minutes of stimulation. At the end of this third period, stimulation stopped. The fourth rate is for growth during the 30 minutes directly after the cessation of stimulation $20 \pm 2 \mu\text{m}/\text{hour}$ (46 gc on 6 n). To calculate the average growth rates, we used neurites on all the cells whose stimulation followed this time course. In Figure 4.11, I give the average growth rates of neurites from each of these cells separately.

The average growth rates of experimental cells and control cells were similar. I show a plot of the average growth rates for all experimental cells, normalized to the growth rate during the initial time period, versus time in Figure 4.12. I did the normalization to facilitate the comparison between the control and experimental average growth rates, because each cell had a different average growth rate. The average growth of the seven experimental cells was 20 percent faster than was the average growth rate of the nine control cells. The average growth rates of experimental cells and control cells were similar. I show a plot of the average growth rates for all experimental cells, normalized to the growth rate during the initial time period, versus time in Figure 4.12. I did the normalization to facilitate the comparison between the control and experimental average growth rates, because each cell had a different average growth rate. The average growth of the seven experimental cells was 20 percent faster than was the average growth rate of the nine control cells.

4.1.4 Growth-Cone Calcium and Neurite Outgrowth

We determined the calcium levels in control cells before determining how electrical stimulation affected $[Ca]_i$. The calcium concentration in the cell body ($[Ca]_{soma}$) was 96 ± 4 nM and that of $[Ca]_{gc}$ was 127 ± 33 nM (21 growth cones from five cells, \pm SEM). These levels were similar to those reported for frog SCGs (Lipscombe et al., 1988), rat diencephalon (Connor, 1986) and *Helisoma* neurons (Cohan et al., 1987).

To determine the effect of electrical stimulation on $[Ca]_{gc}$, we measured the response of $[Ca]_{gc}$ to 10 Hz stimulation (Figures 4.13 and 4.14). In the absence of electrical stimulation, patch-electrode placement did not affect $[Ca]_{gc}$. Occasionally, we

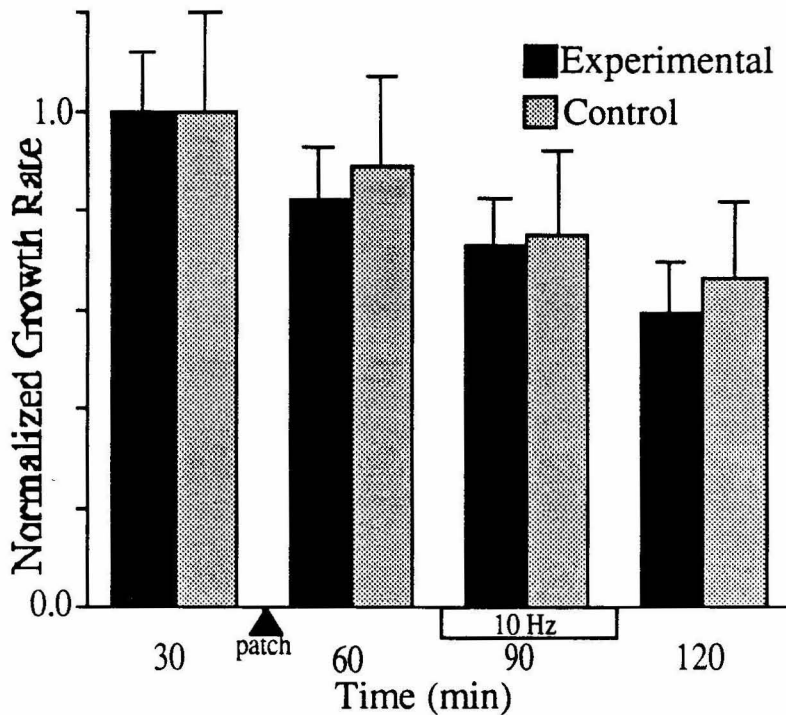


Figure 4.12 The normalized average growth rates of experimental and control cells versus time. I added a pipette to the experimental cells after 30 minutes. I began stimulation after 60 minutes and I stopped stimulation after 90 minutes. The rate of growth of the six experimental cells, whose growth was measured after stimulation, was $23 \mu\text{m/hr}$ during stimulation. This is statistically equivalent (90% confidence) to their expected growth rate $22 \mu\text{m/hr}$ calculated by fitting a line through their growth rates at 60 and 120 minutes.

observed a small increase of less than 40 nM in $[Ca]_{soma}$ localized to the area adjacent to the pipette. Chronic electrical stimulation at 10 Hz increased $[Ca]_{gc}$ first, with $[Ca]_{soma}$ following slowly as shown in the cell in Figures 4.13 a through 4.13 e. Growth cone calcium increased from 128 ± 23 to peak levels of 575 ± 165 nM in 10 to 15 sec (\pm SD across growth cones, $gc = 16$, $n = 4$). Within 2 to 3 minutes, $[Ca]_{gc}$ decreased to steady-state levels of 336 ± 61 nM. $[Ca]_{soma}$ increased more slowly from prestimulus levels of 65 ± 14 nM to peak values of 364 ± 77 nM, with a plateau level of 332 ± 93 nM. Calcium returned to pre-stimulus levels within minutes when stimulation ended (Figure 4.13 f).

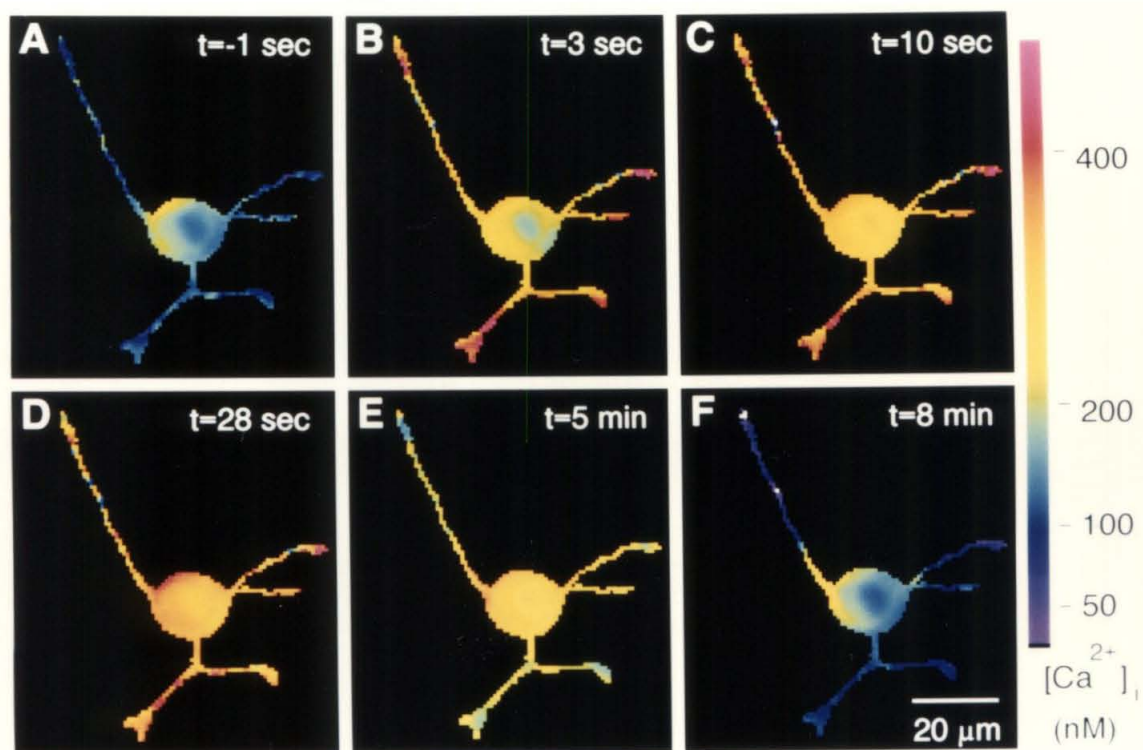


Figure 4.13 *The effect of electrical stimulation on intracellular calcium concentrations as measured with fura-2.* (a) This picture was before 10 Hz electrical stimulation. (b-e) These pictures were taken during electrical stimulation at the times shown. Stimulation ceased at 5 minutes. (f) This picture shows that the intracellular-calcium concentration returned to essentially prestimulus levels after 3 minutes.

In Figure 4.14, I show a plot of the calcium concentration in a second cell as a function of time and of 10 Hz stimulation. The initial calcium concentration is about 120 nM in both the soma and growth cone. Following the onset of stimulation, the $[Ca]_{gc}$ shoots up to over 800 nM transiently, before decreasing to a new steady-state level of about 300 nM. The change in $[Ca]_{soma}$ changes less drastically; $[Ca]_{soma}$ increases to 440 nM and slowly plateaus at about 400 nM. After 17 minutes of stimulation, I turned off the stimulus. Three minutes later, both $[Ca]_{soma}$ and $[Ca]_{gc}$ had returned to prestimulus levels. In a set of such experiments, SCG neurons increased their $[Ca]_{gc}$ transiently, from 128 ± 23 nM to 575 ± 165 nM (at the highest point measured) before plateauing at 336 ± 61 nM ($n = 3$, $gc = 5$, \pm SEM).

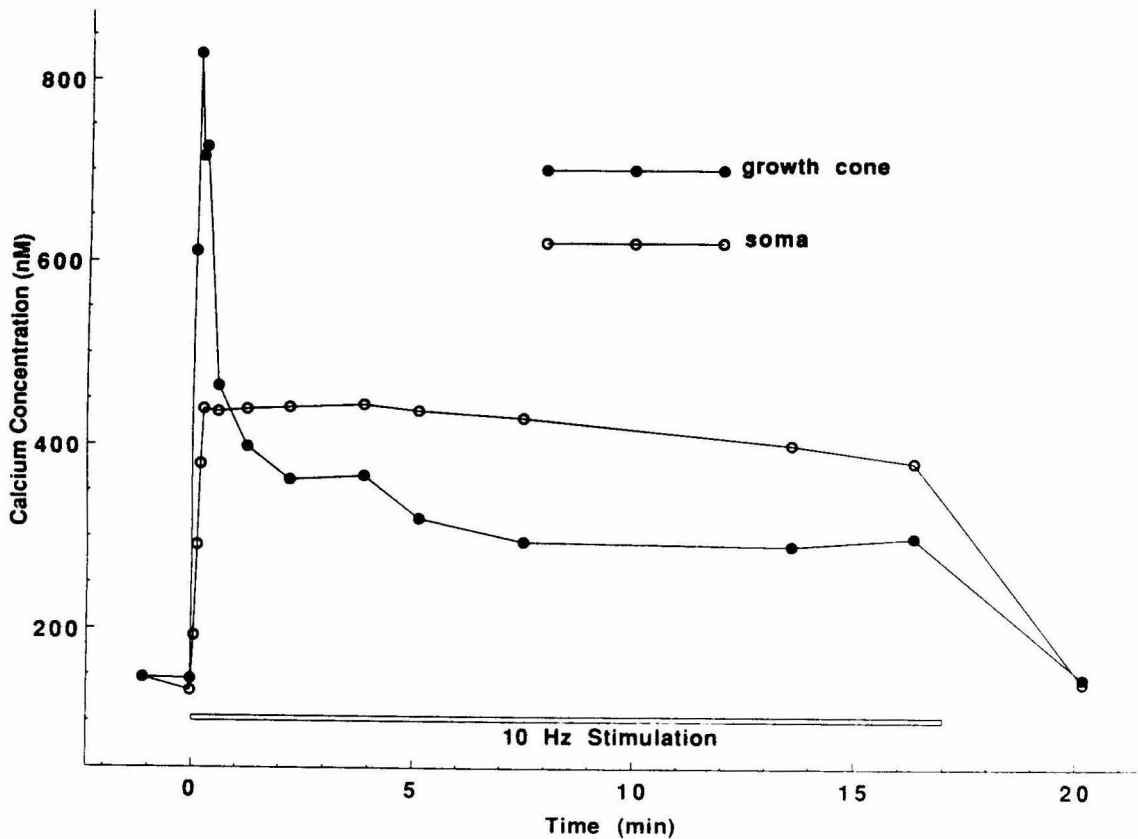


Figure 4.14 Calcium concentrations in the growth cones and soma of the cell shown in Figure 4.13.

We also determined the calcium levels reached during extended periods of stimulation (see Figure 4.10 for an example with one cell). Since we could not reduce the illumination intensity further and retain the necessary signal-to-noise ratio, we conducted a series of experiments during which images were taken every 10 minutes to prevent a reduction in growth rate. $[Ca]_{gc}$ increased from 109 ± 44 nM to steady-state values of 294 ± 101 nM and $[Ca]_{soma}$ increased from 75 ± 51 nM to 283 ± 160 nM (\pm SD, $gc = 24$, $n = 8$). We determined steady-state values from 10 to 40 minutes after the beginning of stimulation. The SCG neurons continued growing during these experiments; I show pictures of one such cell in Figure 4.15.

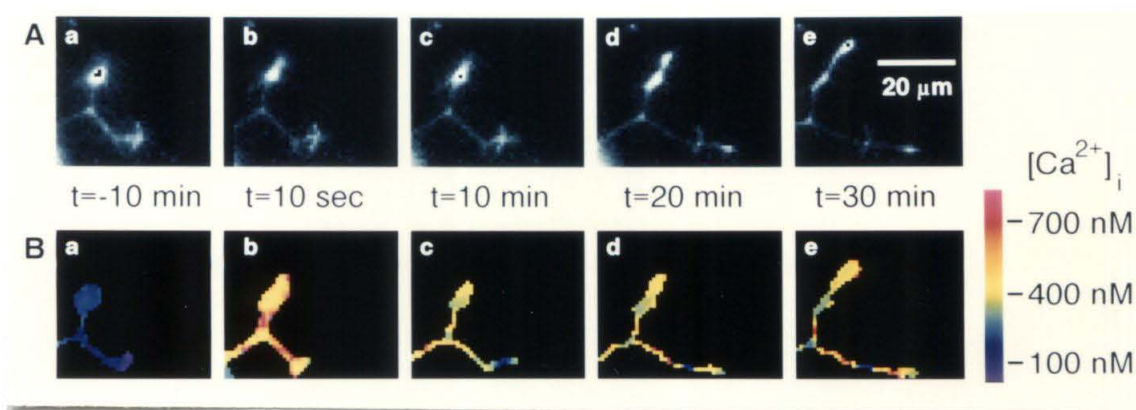


Figure 4.15 Phase and fluorescence images of an SCG neuron growing during electrical stimulation. We measured the calcium concentration with fura-2 in the fluorescence images. The times are relative to the start of electrical stimulation at 10 Hz.

To strengthen my evidence that neurite outgrowth from SCG neurons is independent of the $[Ca]_i$, I wanted to increase the $[Ca]_i$ to levels significantly greater than those that had been shown to stop outgrowth from *Helisoma* (Cohan et al., 1987) and DRG (Fields et al., 1990a) neurons. Therefore, my target level for $[Ca]_i$ was above that of the stimulated *Helisoma* neurons, 300 to 400 nM, but low enough to be physiological,

below 1 μM . I attempted to change $[\text{Ca}]_i$ by growing the SCG neurons in depolarizing media or with calcium ionophores. When I abruptly switched the solution from standard medium to high K^+ saline or high K^+ / high Ca^{++} saline, the $[\text{Ca}]_{\text{gc}}$ briefly rose to greater than 300 nM; within minutes, however, it returned to steady-state levels of less than 200 nM. Because I was unable to increase the $[\text{Ca}]_{\text{gc}}$ to levels above 300 nM with depolarizing medium, I attempted to raise the $[\text{Ca}]_{\text{gc}}$ further by growing the cells with the calcium ionophore, bromo-A23187. In the presence of 20 to 100 nM bromo-A23187 (1.26 mM Ca^{++} in the medium) the $[\text{Ca}]_{\text{gc}}$ increased to less than 200 nM. Increasing the concentration of bromo-A23187 to 400 nM produced large calcium accumulations that oscillated between about 200 and 500 nM. Therefore, I was unable to measure the effect of steady-state calcium concentrations above that I attained with tonic 10 Hz stimulation by growing SCG neurons in these conditions.

4.2 Discussion

My results indicate that neither electrical activity nor $[\text{Ca}]_{\text{gc}}$ affect neurite outgrowth rates from SCG neurons. Electrical stimulation at the fastest feasible rate, 10 Hz, produced no observable changes in outgrowth from SCG neurons. Electrical stimulation at 10 Hz did cause a large increase in $[\text{Ca}]_{\text{gc}}$. Even when steady-state calcium levels increased by a factor of 3 from resting levels of 128 ± 23 nM to steady-state levels of 336 ± 61 nM, outgrowth was unaffected.

4.2.1 *Electrical Activity and Neurite Outgrowth?*

The response of rat SCG neurons to electrical stimulation is strikingly different from that of the other cell types whose responses have been studied, mouse DRG neurons and *Helisoma* buccal-ganglion neurons. DRG neurons immediately retract their filopodia and lamellipodia when electrically stimulated with an electric field at 2.5 to 10 Hz (Fields et al., 1990b). For instance, in response to 10 Hz stimulation, DRG neurons retract their filopodia, lamellipodia, and 75 percent of their neurites. B19 cells from the buccal ganglion of *Helisoma* also stop neurite outgrowth (but do not retract) when stimulated with a cell-attached patch pipette at 4 Hz (Cohan and Kater, 1986).

I have presented evidence that outgrowth from cultured SCG neurons is insensitive to electrical stimulation at frequencies up to 10 Hz. There has also been evidence from the following *in vivo* studies that electrical activity does not regulate neurite outgrowth. Voyvodic (1987) has shown that outgrowth from SCG neurons *in vivo* continues in the absence of presynaptic innervation, although the targeting of ganglionic projections is abnormal. Rich and Lichtman (1989) have also shown that electrical stimulation does not affect neurite elongation during the reinnervation of the mouse sternomastoid muscle (Rich and Lichtman, 1989). Many studies of the outgrowth of retinal-ganglion neurons have shown that outgrowth to the tectum is unaffected by retinal activity or lack thereof, in contrast, the proper segregation at the target is activity dependent (Harris, 1980; Reh and Constantine-Paton, 1985; Schmidt and Edwards, 1983; Sreter et al., 1988). Both SCG neurons (Purves et al., 1986) and mitral cells (Pomeroy et al., 1990), in addition, continue to modify their dendritic arbor into adulthood; this modification is at a time when the cells are presumably electrically active. *In vivo*, therefore, outgrowth either is not regulated by electrical activity or accommodates to chronic electrical stimulation. If the neurons have accommodated to chronic stimulation, large changes in the stimulation amplitude or frequency might inhibit outgrowth. Fields and associates, (1990a), have found evidence

that cultured DRG neurons can accommodate to chronic electrical stimulation and resume growth.

Purves and collaborators have shown that in vivo SCG neurons continue to grow at least into early adulthood (Purves et al., 1986). Since the cells receive presynaptic input during this time (Iggo and Vogt, 1960), and are likely to be at least somewhat electrically active, it would be surprising if physiological stimuli inhibited outgrowth completely. This activity, of course, may slow or otherwise regulate outgrowth.

4.2.2 $[Ca]_i$ and Outgrowth

Since Cohan and collaborators (1987) have correlated activity-induced growth inhibition with changes in $[Ca]_{gc}$, and Kater and associates (1988; 1991), have suggested that increases in $[Ca]_{gc}$ cause the observed inhibition of outgrowth, we determined whether activity increases the $[Ca]_{gc}$ in SCG neurons. In response to 10 Hz chronic stimulation, SCG neurons increase their $[Ca]_{gc}$ transiently from 128 ± 23 nM to 575 ± 165 nM, before plateauing at 336 ± 61 nM. These changes are similar to those that correlated with an inhibition of outgrowth from *Helisoma* neurons. $[Ca]_{gc}$ rises transiently in *Helisoma* B5 neurons from about 100 nM to 300 to 400 nM before plateauing at 225 to 325 nM with 3 Hz stimulation (Cohan et al., 1987). Although stimulation at 3 Hz has not been shown to stop outgrowth it probably does since 4 Hz stimulation stops outgrowth from these cells (Cohan and Kater, 1986). More direct correlations can be made from experiments in which Haydon and associates (1987), applied serotonin to *Helisoma* B19 neurons at concentrations known to stop outgrowth (Haydon et al., 1987). At these concentrations, serotonin application causes calcium to rise from 125 nM to 330 nM (Cohan et al., 1987). Transient increases in $[Ca]_{gc}$ of 4- to 7-fold and steady-state changes of 3- to 5-fold occur

in *Helisoma* buccal ganglion (Cohan et al., 1987), DRG (Fields et al., 1990a) and SCG neurons, but are correlated with an inhibition of outgrowth in only the first two cell types.

Several other studies have shown a correlation between the inhibition of neurite outgrowth and the increase of intracellular calcium. The application of calcium-channel blockers (Robson and Burgoyne, 1989; Cooke et al., 1988; Suarez-Isla et al., 1984), neurotransmitters (Pearce et al., 1987; Mattson et al., 1988; Mattson and Kater, 1987) and calcium ionophores (Anglister et al., 1982; Goldberg, 1988) to cells in culture affects neurite outgrowth from some cell types. The rate of neurite outgrowth and $[Ca]_i$ correlate in some cell types (Connor, 1986; Silver et al., 1989). Adding to the circumstantial evidence that calcium may be important in regulating neurite outgrowth, two groups have shown differential calcium-channel behavior in active versus quiescent growth cones (Lipton, 1987; Cohan et al., 1985).

Evidence that calcium may not regulate neurite outgrowth is also being accumulated from cells in culture. For instance, in some of the studies cited above, although calcium increased in response to growth-inhibiting stimuli, it did not remain elevated or neurite outgrowth resumed despite a continued elevation in $[Ca]_i$. Fields and collaborators (1990a) have shown that, in DRG neurons that accommodate to continued electrical stimulation after 24 hours by resuming outgrowth, the calcium concentration is the same as that in DRG neurons that do not resume growth: Calcium concentration remains between 200 and 400 nM. Murrain and collaborators (1990) have shown that in serotonin-sensitive *Helisoma* neurons dissected as an intact nervous system, the calcium concentration rises transiently in response to serotonin, but returns to prestimulus levels while outgrowth remains inhibited. Both of these examples suggest that either calcium levels do not regulate outgrowth or the critical concentration changes with adaptation.

In related investigations, Ivins and collaborators, (1990), have shown that the contact-mediated growth cone collapse is not a calcium-dependent phenomenon, since fura-

2 measured $[Ca]_{gc}$ did not change during collapse. They were able to increase the $[Ca]_{gc}$ 2 to 3 fold with ionomycin without affecting growth cone morphology, growth cone motility or rate of growth cone advance. Campenot and Draker (1989) have shown that the growth cone does not require calcium for neurite elongation. This finding suggests that calcium may not be used to regulate neurite outgrowth.

Kater and collaborators (1988; 1991) suggested that $[Ca]_i$ regulates neurite outgrowth and that there is a permissive range of $[Ca]_i$. Experiments by Cohan and collaborators (1987) and by Fields and coworkers (1990a) have supported this hypothesis although its generality is under attack. In our experiments, neurite outgrowth is not regulated by calcium at the levels suggests by Kater and collaborators (1988 and 1991).

4.2.3 Different Responses from SCG Neurons

Electrical stimulation does not stop outgrowth from SCG neurons as it does from DRG and *Helisoma* neurons. Since electrical stimulation causes similar increases in $[Ca]_{gc}$ in SCG, DRG, and *Helisoma* neurons, it is unlikely that the $[Ca]_{gc}$ alone is responsible for these differences. One possible explanation is that a SCG neuron's calcium sensitivity is very different from the calcium sensitivity of a DRG or *Helisoma* neuron, and 10 Hz electrical stimulation did not increase $[Ca]_{gc}$ enough to stop outgrowth from SCG neurons. It is also possible that SCG and other neurons may employ cues other than $[Ca]_i$ to control outgrowth. For example, there is evidence that bag-cell neurons from *Aplysia* use cyclic adenosine monophosphate (cAMP) to regulate growth cone structure (Forscher et al., 1987), and dopamine inhibits outgrowth from chick retinal neurons in a cAMP-dependent manner (Lankford et al., 1988). Gunderson and Barrett (1980), in addition, found that chick DRG neurons turned toward sources of mono and dibutylryl cAMP and cyclic guanosine monophosphate (cGMP).

Perhaps high local, ($[Ca]_i$), rather than bulk calcium levels regulate outgrowth in DRG and *Helisoma* neurons. High calcium concentrations activate many cellular processes that have a low calcium affinity. Release of neurotransmitter is an example of such a process: It is only near the mouth of open voltage-dependent calcium channels that calcium reaches levels sufficient to support significant release of neurotransmitter; the average calcium concentration in a presynaptic terminal is sufficient to support only extremely low levels of release (Simon and Llinas, 1985; Fogelson and Zucker, 1985). Variations in $[Ca]_i$, such as elevations in $[Ca]_i$ near calcium channels or clusters of channels (Lipscombe et al., 1988; Silver et al., 1990), probably exist even in a relatively thin structure, such as a growth cone. Fura-2 imaging is relatively insensitive to $[Ca]_i$ due in part to spatial and temporal averaging. No experiments have yet been performed that would clearly distinguish between high bulk calcium levels and high $[Ca]_i$ being responsible for stopping outgrowth. A possible interpretation of recent experiments demonstrating the involvement of calmodulin (Polak et al., 1991) in the activity-dependent stoppage of outgrowth is that $[Ca]_i$ may be involved. Calmodulin is a protein with multiple calcium binding sites and relatively low calcium affinity (Manalan and Klee, 1984). Calcium probably activates calmodulin in a nonlinear manner, so that high calcium concentrations greater than those measured in the bulk of the growth cone may be needed to activate this protein. If proteins such as calmodulin do regulate outgrowth, differences either in the localization of calcium ions or in the affinity of the calcium-activated proteins could explain the observed differences in the regulation of outgrowth between cell types.

4.2.4 *in Vitro* Results Relate to Growth *in Vivo*

Elevated rates of electrical activity probably do not regulate neurite elongation from SCG neurons *in vivo*, since SCG activity rates are likely to be substantially lower than the

10 Hz that failed to inhibit outgrowth *in vitro*. The estimate of *in vivo* activity rate is based on observed spontaneous activity rates (average about 1 Hz) of sympathetic preganglionic neurons in both frog and cat (Blackman et al., 1963; Polasa, 1968; Janig and Schmidt, 1970; Iggo and Vogt, 1960: I was unable to find the corresponding data from unanesthetized rat SCG neurons). The supposition that electrical activity does not regulate neurite outgrowth from SCG neurons *in vivo* is consistent with the observation that the neurons continue to modify their dendritic arbors throughout young adulthood when they are electrically active (Purves et al., 1986). On the basis of *in vitro* experiments, it is possible that activity regulates outgrowth *in vivo* from *Helisoma* and DRG neurons. No one has established whether these neurons actually employ this mechanism in development, however.

4.2.5 Conclusions

My findings suggest that electrical activity and the accompanying rise in calcium may not regulate neurite elongation even if they do regulate some of neuronal development. The observation that SCG neurites continue to elongate during stimulation in these experiments suggests that increased rates of electrical activity and increases in $[Ca]_{gc}$ are not universal signals to stop neurite elongation. The regulation of outgrowth *in vivo* is a complex task. We can reasonably assume that nature uses a variety of mechanisms to regulate it; electrical activity accompanied by an increase in $[Ca]_i$ is probably only one of these mechanisms.

References

- Anglister, L., Farber, I.C., Shaher, A. and Grinvald, A. (1982). Localization of voltage-sensitive calcium channels along developing neurites: their possible role in regulating neurite elongation. *Dev. Biol.* 94:351-365.

- Bixby, J.L. and Spitzer, N.C. (1984) Early differentiation of vertebrate spinal neurons in the absence of voltage-dependent Ca^{2+} and Na^{+} influx. *Dev. Biol.* 106:89-96.
- Blackman, J.G., Ginsberg, B.L. and Ray, C. (1963) Spontaneous synaptic activity in sympathetic ganglion cells of the frog. *J. Physiol. (Lond.)* 167:389-401.
- Bray, D. (1973). Branching patterns of individual sympathetic neurons in culture, *J. Cell Biol.* 56:702-712.
- Campenot, R.B. and Draker, D.D. (1989). Growth of sympathetic nerve fibers in culture does not require extracellular calcium. *Neuron* 3:733-743.
- Cohan, C.S., Connor, J.A. and Kater, S.B. (1987). Electrically and chemically mediated increases in intracellular calcium in neuronal growth cones. *J. Neurosci.*, 7:3588-3599.
- Cohan, C.S., Haydon, P.G. and Kater, S.B. (1985) Single channel activity differs in growing and nongrowing growth cones of isolated identified neurons of *Helisoma*. *J. Neurosci. Res.* 13:285-300.
- Cohan, C. and Kater, S.B. (1986). Suppression of neurite elongation and growth cone motility by electrical activity. *Science* 232:1638-1640.
- Connor, J.A. (1986). Digital imaging of free calcium changes and of spatial gradients in growing processes in single, mammalian central nervous system cells. *P.N.A.S.* 83:6179-6183.
- Cooke, I., Graf, R., Grau, S. and Meyers, D. (1988). Crustacean peptidergic secretory neurons in culture: outgrowth, secretory competence, and Ca^{++} currents. *J. of Gen. Physiology* 92:3a-4a.
- Fields, R.D., Guthrie, P.B., Nelson, P.G. and Kater, S.B. (1990a). Calcium homeostatic capacity is regulated by patterned electrical activity in growth cones of mouse DRG neurons. 16th Soc. of Neurosci. Abst. 197.2: 457.
- Fields, R.D., Neale, E.A. and Nelson, P.G. (1990b). Effects of patterned electrical activity on neurite outgrowth from mouse neurons. *J. Neurosci.* 10:2950-2964.
- Fogelson, A.L. and Zucker, R.S. (1985) Presynaptic calcium diffusion from various arrays of single channels: Implications for transmitter release and synaptic facilitation. *Biophys. J.* 48:1003-1017.
- Forscher, P., Kaczmarek, L.K., Buchanan, J. and Smith, S.J. (1987) Cyclic AMP induces changes in distribution and transport of organelles within growth cones of *Aplysia* bag cell neurons. *J Neurosci* 7:3600-3611.

- Goldberg, D.J. (1988). Local role of Ca^{2+} in formation of veils in growth cones. *J. Neurosci.* 8:2596-2605.
- Gundersen, R.W. and Barrett, J.N. (1980) Characterization of the turning response of dorsal root ganglion neurites toward nerve growth factor. *J. Cell Biol.* 87:546-554.
- Haydon, P.G., McCobb, D.P. and Kater, S.B. (1987). The regulation of neurite outgrowth, growth cone motility, and electrical synaptogenesis by serotonin. *J. Neurobiol.* 18:197-215.
- Harris, W.A. (1980) The effects of eliminating impulse activity on the development of the retinotectal projection in salamander. *J. Comp. Neurol.* 194:303-317.
- Iggo, A. and Vogt, M. (1960) Preganglionic sympathetic activity in normal and in reserpine-treated cats. *J. Physiol.* 150: 114-133.
- Ivins, J.K., Raper, J.A. and Pittman, R.N. (1990). Calcium levels do not change during contract mediated growth cone collapse. 16th Soc. Neurosci. Meeting Abst 417.1;1009.
- Janig, W. and Schmidt, R.F. (1970) Single unit responses in the cervical sympathetic trunk upon somatic nerve stimulation. *Pflugers Arch.* 314:199-216.
- Kater, S.B., Mattson, M.P., Cohan, C., and Connor, J. (1988). Calcium regulation of the neuronal growth cone. *Trends. in Neurosci.* 11:315-321.
- Kater, S.B. and Mills, L.R. (1991) Regulation of growth cone behavior by calcium *J. Neurosci.* 11:891-899.
- Lankford, K.L., DeMello, F.G. and Klein, W.L. (1988) D1-type dopamine receptors inhibit growth cone motility in cultured retina neurons: evidence that neurotransmitters act as morphogenic growth regulators in the developing central nervous system. *P.N.A.S.* 85:4567-4571.
- Lankford, K., De Mello, F.G. and Klein, W.L. (1987) A transient embryonic dopamine receptor inhibits growth cone motility and neurite outgrowth in a subset of avian retina neurons. *Neurosci. Letts.* 75:169-174.
- Lipscombe, D., Madison, D.V., Poenie, M., Reuter, H., Tsien, R.Y and Tsien, R.W. (1988). Spatial distribution of calcium channels and cytosolic calcium transient in growth cones and cell bodies of sympathetic neurons. *P.N.A.S.* 85:2398-2402.
- Lipton, S.A. (1987) Bursting of calcium-activated cation-selective channels is associated with neurite regeneration in a mammalian central neuron. *Neurosci. Letts.* 82:21-28.

- Manalan, A.S. and Klee, C.B. (1984) Calmodulin in: Advances in cyclic nucleotide and protein phosphorylation research, Vol 18 (Greengard P, Robinson GA, eds), pp 227-278. New York: Raven.
- Mattson, M.P., Lee, R.E., Adams, M.E., Guthrie, P.B. and Kater, S.B. (1988) Interactions between entorhinal axons and target hippocampal-neurons: A role for glutamate in the development of hippocampal circuitry. *Neuron* 1:865-876.
- Mattson, M.P. and Kater, S.B. (1987) Calcium regulation of neurite elongation and growth cone motility. *J. Neurosci.* 7:4034-4043.
- McCobb, D.P. and Kater, S.B. (1988) Membrane voltage and neurotransmitter regulation of neuronal growth cone motility. *Dev. Biol.* 130:599-609.
- Murrain, M., Murphy, A.D., Mills, L.R. and Kater, S.B. (1990). Neuron-specific modulation by serotonin of regenerative outgrowth and intracellular calcium within the CNS of *Helisoma trivolvis*. *J. Neurobio.* 21:611-618.
- Pearce, I.A., Cambray-Deakin, M.A. and Burgoyne, R.D. (1987) Glutamate acting on NMDA receptors stimulates neurite outgrowth from cerebellar granule cells. *FEBS Letters* 223:143-147.
- Polak, K.A., Edelman, A.M., Wasley, J.W.F. and Cohan, C.S. (1991) A novel calmodulin antagonist, CGS 9343B, modulates calcium-dependant changes in neurite outgrowth and growth cone movements. *J. Neurosci.* 11:534-542.
- Polosa, C. (1968) Spontaneous activity of sympathetic preganglionic neurons. *Can. J. Physiol. Pharmacol.* 46:887-896.
- Pomeroy, S.L. Lamantia, A.S. and Purves, D. (1990) Post natal construction of neural circuitry in the mouse olfactory bulb. *J. Neurosci.* 10:1952-1966.
- Purves, D., Hadley, R.D. and Voyvodic, J.T. (1986) Dynamic changes in the dendritic geometry of individual neurons visualized over periods of up to three months in the superior cervical ganglion of living mice. *J. Neurosci.* 6:1051-1060.
- Reh, T. A. and Constantine-Paton, M. (1985). Eye-specific segregation requires neural activity in three-eyed *Rana pipiens*. *J. Neurosci.* 5:1132-1143.
- Rich, M.M. and Lichtman, J.W. (1989) *In vivo* visualization of pre- and postsynaptic changes during synapse elimination in reinnervated mouse muscle. *J. Neurosci.* 9:1781-1805.
- Robson, S.J. and Burgoyne, R.D. (1989). L-type calcium channels in the regulation of neurite outgrowth from rat dorsal root ganglion neurons in culture. *Neurosci. Lett.* 104:110-114.

- Schmidt, J.T. and Edwards, D.L. (1983) Activity sharpens the map during the regeneration of the retinotectal projection in goldfish. *Brain Research* 269:29-39
- Silver, R.A., Lamb, A.G. and Bolsover, S.R. (1989). Elevated cytosolic calcium in the growth cone inhibits neurite elongation in neuroblastoma cells: Correlation of behavioral states with cytosolic calcium concentration. *J. Neurosci.* 9:4007-4020.
- Silver, R.A., Lamb, A.G. and Bolsover, S.R. (1990) Calcium hotspots caused by L-channel clustering promote morphological changes in neuronal growth cones. *Nature* 343:751-754.
- Simon, S.M. and Llinas, R.R. (1985) Compartmentalization of the submembrane calcium activity during calcium influx and its significance in transmitter release. *Biophys. J.* 48:485-498.
- Sretavan, D.W., Shatz, C.J. and Stryker, M.P. (1988). Modification of retinal ganglion cell axon morphology by prenatal infusion of tetrodotoxin. *Nature* 336:468-471.
- Suarez-Isla, B.A., Pelto, D.J., Thompson, J.M. and Rapoport, S.I. (1984). Blockers of calcium permeability inhibit neurite extension and formation of neuromuscular synapses in cell culture. *Dev. Brain Res.* 14:263-270.
- Voyvodic, J.T. (1987) Development and regulation of dendrites in the rat superior cervical ganglion. *J. Neurosci.* 7:904-912.

Part II

Wells: Devices for Chronic Recording and Stimulation of Cultured Neurons

Neurobiologists want improved methods for chronically recording from and stimulating neurons. Such devices will help elucidate the secrets of neuronal morphological and electrical development by helping us understand how electrical activity affects synaptic strength, how small neuronal networks interconnect, and how neuronal morphology is affected by activity. Chronic recording from or stimulation of identified neurons in the brain could also allow scientists to understand thought and memory. A method that allows chronic recording from and stimulation of neurons, either in vivo and in culture, has tremendous potential for expanding our understanding of neurobiology.

Existing technology has only a limited ability to record from and stimulate neurons repeatedly and for extended periods of time. If an experimenter wants to study the effects of electrical activity on neurite outgrowth over the course of a month, she would be limited by a scarcity of long-term techniques. To study synapse formation from a ten cell culture, he would also have difficulty looking at that many individual cells simultaneously. In Part II of this dissertation, I shall present the development of a technique that promises to make such an experiment doable, the well electrode. In Chapter 5, I shall compare the ability of the well electrodes and existing stimulation and recording methods. I shall also discuss the theoretical basis for the well design and the design specifications. In Chapter 6, I shall discuss how well electrodes are made and prepared for use. I shall discuss how wells are used for stimulating and recording from neurons in Chapter 7. In Chapter 8, I shall briefly discuss where this research is leading; the shortcomings of the current well design, possible solutions to these shortcomings, and discuss future in vivo designs and experiments.

Chapter 5

Chronic Electrode to Neuron Interfaces

5.1 Introduction

Throughout history the development of new experimental methods has led to advances in our understanding of the nervous system. The development of the Nissel stain for example, which allows investigators to stain individual neurons at random, may have provided the single largest leap in the elucidation of neuronal morphology. Similarly, understanding the emergent behavior of the nervous system depends on the development of methods for elucidating the electrical activity of groups as well as individual neurons.

Most experiments aimed at elucidating the electrical properties of the nervous system have been done with glass pipettes. Glass pipettes have many limitations, however. These limitations include severely restricting both the number of cells that can be studied concurrently and the length of an experiment. The nervous system is composed of billions of neurons that grow and interact over the life time of the organism. Extending our understanding of the nervous system to large numbers of cells or to longer term developmental questions will require developing methods for investigating the interactions of groups of cells over days, weeks, and years. In this chapter, I shall compare the utility of currently available methods for simultaneously stimulating and recording from individual neurons with a new technique, the well electrode. How well each technique performs the hypothetical experiment of daily mapping the electrical connections in a ten cell culture for one month will be compared. Such an experiment would act as a control for future experiments in which the effect of imposed electrical activity on the synapses is evaluated. In Section 5.2, I shall focus on the advantages and disadvantages of currently available techniques for studying electrical activity, in general, and performing the experiment just described, in particular. In Section 5.3, I shall present the theoretical bases for stimulating

and recording from individual neurons with the well electrodes. In Section 5.4, I shall summarize the design criterion for the well electrodes.

5.2 Comparison of Recording and Stimulation Techniques

In Table 5.1, I summarize the most common of techniques for stimulating and recording from individual neurons. The table includes classical neurobiological as well as state-of-the-art recording and stimulating techniques. Although there are different requirements for every application, an ideal technique would be easy to use, non-invasive, specific, and able to both stimulate and record from many neurons for weeks at a time. None of the techniques described in Table 5.1 meet these specifications, but electrode wells promises to do so. A brief discussion of each of stimulation and recording technique will follow.

	Glass Pipettes				Electrode arrays	Diving boards	Electrode Wells
	Intra-cellular	Whole Cell Patch	Cell attached Patch	Extra-cellular			
Number of electrodes	1-4	1-4	1-4	1-4	1-100	1-10	1-100
# observed/electrode	1	1	1	1-10	1-10	1	1
Length of Experiment	hrs-days	hours	hours	months	months	months	months
Invasive to the cell	yes	yes	no	no	no	no	no
Ease of stimulation	easy	easy	doable	doable	doable	doable	doable
Ease of recording	easy	easy	do able	difficult	difficult	do able	do able
Ease of manufacture	easy	easy	easy	easy	easy	do able	easy

Figure 5.1 A comparison of seven techniques for recording from and stimulating neurons. Categories include the *number of electrodes* that can be used concurrently, the *number of cells observed per electrode*, the *maximum length of a single experiment* with a single cells, whether the technique is *invasive to the cell* being observed, the *ease of stimulating* a single cell, the *ease of recording* from a single cell, the *ease of manufacturing* and using these electrodes.

5.2.1 Glass-Pipette Electrodes

Researchers make glass-pipette electrodes by drawing a glass tube into a fine capillary at one end and filling the other end with a conducting saline. The drawn tip connects to the neuron and the butt end to electronics. The electronics either record the cellular activity or stimulate the cell electrically. Researchers use glass-pipette electrodes in a number of configurations; intracellular, whole-cell patch, cell-attached patch, and extracellular. All four configurations allow the experimenter to reliably stimulate and record from neurons in culture, but because the electrodes must be individually manipulated and held in place, the simultaneous use of more than two pipettes is unwieldy. Using more than four pipettes simultaneously is virtually impossible. Small vibrations of the pipette relative to the cell limits the duration of experiments and makes it nearly impossible to move the dish and/or pipette during an experiment. Despite these limitations, researchers routinely use glass pipette electrodes to stimulate and record from cultured cells. I shall describe the four commonly used configurations in the remainder of this section.

During intracellular recording, the fine electrode tip literally pierces the neuron. After penetration, the tip is within the cell, the intrapipette saline is contiguous with the cytoplasm, and the intracellular potential is measured directly. Intracellular penetration also facilitates stimulation since the stimulation current is injected directly into the cell rather than across a membrane. Intracellular pipettes can not be used for the hypothetical ten-cell, long-term experiment described earlier, however. The first limitation is that a researcher can not use more than four pipettes simultaneously. Second, with no more than four electrodes in a ten cell culture, a researcher would have to pierce individual neurons repeatedly to map all the connections in a culture. Unfortunately, most neurons could not survive these repeated penetrations. A third limitation is that the pipette saline will dialyze the cytoplasm: this dialysis will damage the neuron.

Whole-cell patching has the same limitation as intracellular recording except that the first penetration is less damaging to very small cells. In whole-cell patching, the researcher brings the cellular membrane and the pipette together and then applies suction to pull the membrane into the tip. Mysteriously, the membrane often binds to the glass forming a very high impedance seal. Suction breaks the membrane within the tip of the electrode after the seal has formed and creates a direct connection between the pipette and the cytoplasm. Whole-cell patch electrodes have all the limitation of intracellular pipettes except that the initial penetration is less damaging to small neurons. Whole-cell patch electrodes can not be used for repeated penetrations, however, because they can not be removed from most cells.

Cell-attached patch pipettes are similar to whole-cell patch pipettes except that the membrane at the tip of the pipette is not broken. The cell-attached pipettes are less invasive than either intracellular or whole-cell patch pipettes because the membrane is left intact. Nonetheless, the researcher can not remove the pipette without damaging the neuron because of the strong membrane seal. The ten-cell, long-term experiment can not be done with cell-attached patches, whole-cell patches or intracellular pipette.

Extracellular stimulation and recording is the fourth common glass pipette technique. To extracellularly stimulate or record from a neuron, a pipette is brought close to but not touching the cellular membrane. Because the pipette does not touch the neuron, extracellular stimulation and recording, unlike any of the preceding techniques, is both non-invasive and repeatable. Unfortunately, extracellular pipettes present other difficulties in performing the hypothetical experiment. Extracellular pipettes, like other glass pipette techniques, require bulky manipulators to position them over the cell of interest. These manipulators limit the number of electrodes that a researcher can use concurrently, so it is virtually impossible to simultaneously record the response of ten neurons. Another serious limitation is that extracellular pipettes can not directly contact a cell, therefore, more than

one cell may be stimulated simultaneously. In cultures of SCG neurons, for instance, extracellular electrodes might stimulate more than one axon simultaneously (Chien, 1990). A third limitation is that because the electrical coupling from cell to electrode is loose, the pipette can only record action potentials, not subthreshold synaptic potentials.

In response to the shortcomings of conventional electrodes, researchers have developed three types of microfabrication-based electrodes for chronic stimulation of and recording from individual neurons in culture. These electrodes are multi-electrode arrays, diving board electrodes, and well electrodes: I shall describe these electrodes below.

5.2.2 Multi-Electrode Culture-Dish Arrays

Multi-electrode culture-dish arrays are metal electrodes imbedded in a culture dish. The metal leads are insulated from the culture medium except at their tips, where stimulation and recording occur. In Figure 5.2, I show a cross-section through a single electrode from a typical array. Many laboratories including; Thomas and collaborators, (1972), Gross and collaborators, (1977; 1982), Pine, (1980), Israel and collaborators, (1984), and Novak and Wheeler, (1986) have developed arrays. The researchers in these laboratories use the arrays to chronically record from and stimulate individual cells.

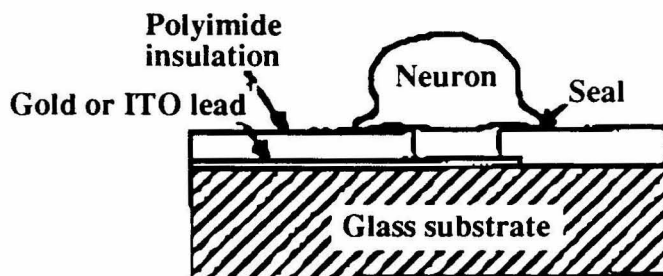


Figure 5.2 *Cross-section of one electrode in a typical multi-electrode array.* From Regehr (1988a).

The arrays have many useful features for long-term stimulation and recording from cultured neurons. Because the cell culture is grown over spatially-fixed electrodes, the array can stimulate and record from cells repeatedly and chronically. A second feature is that the arrays can easily be expanded to monitor more cells, since it is just as easy to fabricate an array with two electrodes as 100 electrodes. Finally, I use simple integrated-circuit technology to make the arrays so I can produce them cheaply.

Unfortunately there are also problems associated with the electrode arrays. The signal to noise ratio of the recordings can be quite low, typically less than 100 μV action potentials with 15 μV_{pp} of Johnson noise, because the recordings are extracellular, the distance between the cell and electrode is variable, and the cell is in a low-resistance, essentially infinite-volume conductor (the bath). The low signal to noise ratio limits experimenters to only measuring action potentials of the cells closest to the electrodes. In addition, any activity whose voltage signature can be mistaken for noise can not be distinguished. In high density cultures, the cellular origin of a given signal is not easily identifiable since the electrode records the potential in the medium at the electrode tip and not at a given cell body. Meister and collaborators (1991b) have somewhat circumvented this problem. They were able to recognize the signature of more than one neuron per electrode by shape and magnitude of the recorded signal. There are also problems associated with stimulation through the electrode arrays. Because the electrode is not associated with only one cell's soma and axons, it is difficult if not impossible to specify what cell is going to be excited by a current pulse from an electrode. Because of this difficulty, researchers independently verify the stimulation with a second recording technique such as voltage-sensitive dyes (Chien, 1990).

In some instances, researcher have used electrode arrays successfully. Success is often achieved when the bath resistance can be limited either by having a solid mass such as that of a retina (Meister et al., 1991a) covering the array or by using the array with neurons

large enough to completely cover an individual electrode (Regehr et al., 1989). Perhaps the most striking success of the multi-electrode arrays to date was when Meister and collaborators (1991) recorded from up almost 100 individual retinal neurons concurrently using the arrays. In this experiment, the arrays provided the spatial resolution necessary to see waves of activity travel across the developing retina in the dish.

5.2.3 Diving Boards

Regehr and collaborators (1988a; 1988b) designed diving board electrodes to investigate how a cup around the tip of a metal electrode, held in close contact to a cell body, might improve its recording and stimulation ability. Diving board electrodes (see Figure 5.3) are metal electrodes embedded in the underside of a microscopic platform shaped to resemble a diving board. The base which can be glued to the culture dish supports the tethered end of the board. The electrode-to-neuron interface is at the free end of the board. To use the diving board electrode, a researcher glues the base to the dish so that the tip of the board touches the cell surface.

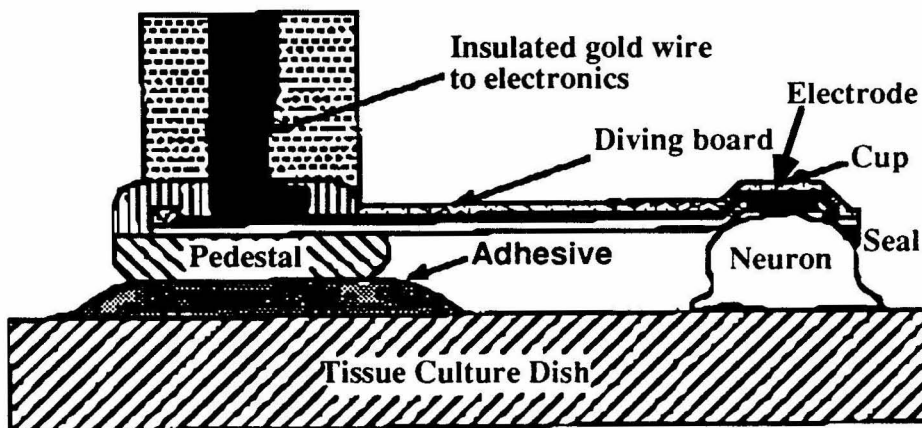


Figure 5.3 A schematic representation of a diving board. From Regehr (1988a).

Diving board electrodes have many of the same advantages as the multi-electrode arrays, for instance, diving board electrodes can stimulate and record from more than one

neuron and more than four can be used concurrently. Multi-electrode arrays are, however, easier to fabricate than diving board electrodes. Because of these fabrication limitations, it is difficult to make the boards small enough for some mammalian cells (personal communication with Wade Regehr, see Regehr, 1988a for more discussion of the uses and limitations of diving boards). It is also awkward to place more than a few diving boards in any single culture. Regehr and collaborators (1988b) have however used the diving board electrodes successfully with large invertebrate neurons in culture. In these cultures, the diving board's electrode cup will "seal" to the neuronal membrane.

5.2.4 Well Electrodes

Well electrodes are yet another technique for chronic stimulation of and recording from individual neurons. Well electrodes and multi-electrode arrays are similar except that for well electrodes the metal electrodes are embedded into the bottom of individual neuron-sized wells rather than in a flat culture dish. I show a typical cross-section through a line of four such wells in Figure 5.4.

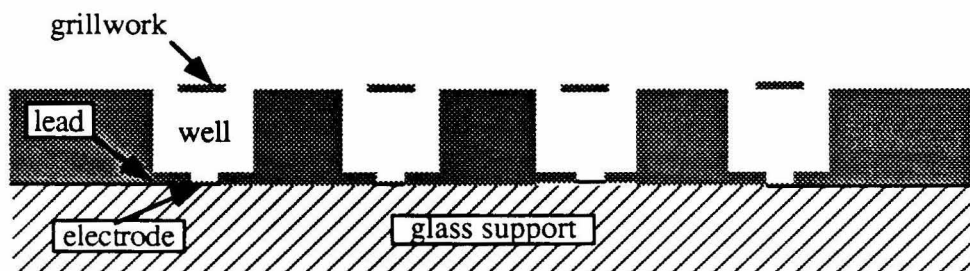


Figure 5.4 A typical cross-section through a line of four wells in a well electrode device.

Well electrodes have all the advantages of planer multi-electrode arrays listed earlier in this chapter, but the well electrodes are potentially preferable because of their theoretical electrical characteristics. I shall discuss the development of the well electrodes in the rest of this thesis. In Section 5.3, I shall discuss why the well electrodes are expected to improve

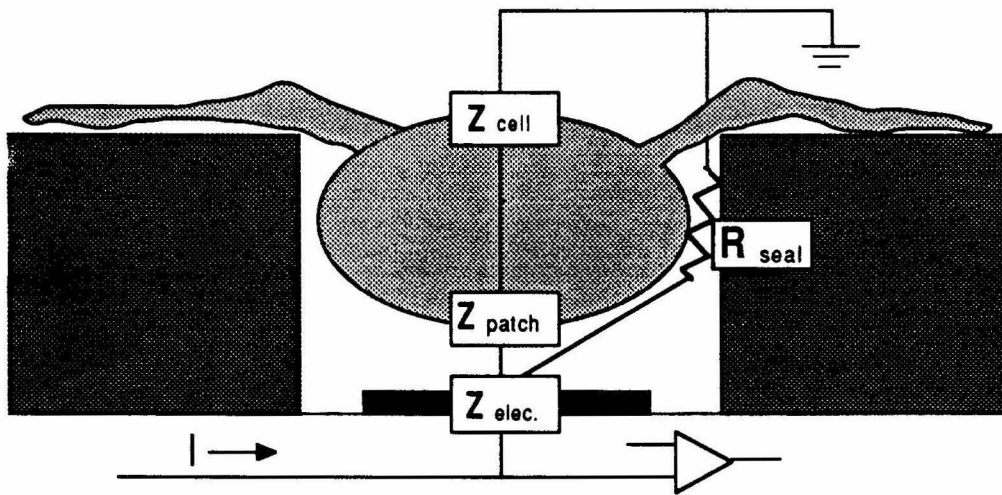
the stimulation and recording characteristics of the electrodes and in section 5.4, I shall summarize the design criterion for the well electrodes.

5.3 Stimulation and Recording with Well Electrodes: The Theory

Stimulation and recording with the well electrodes is similar to extracellular stimulation and recording with glass-pipettes or flat multi-electrode arrays. I shall discuss the basic theory behind extracellular recording and stimulation as well as the advantages afforded by the wells in this section.

5.3.1 Stimulation

There are three advantage of well electrodes as compared to other multi-electrode extracellular stimulation methods: increased specificity, increased reproducibility, and increased ease of stimulation. The well electrodes are more specific because one and only one cell is trapped in a well at the beginning of an experiment. As long as processes from other neurons do not grow under the neuron in the well, only one cell should be stimulated by an electrode (In SCG cultures, processes from many neurons grow adjacent to any cell body, see dissertation by Chien, 1990). Repeated stimulation of a given cell should be routine because neurons are trapped in a well for weeks at a time.



Stimulation

The objective is to maximize the current entering the patch without producing gas at the electrode.

$$I_{\text{patch}} = \frac{IR_{\text{seal}}}{Z_{\text{Patch}} + Z_{\text{cell}}}$$

$$I_{\text{max}} = \frac{V_{\text{gas}}}{Z_{\text{electrode}}}$$

Figure 5.5 Stimulation with a well electrode. R_{seal} is assumed to be much smaller than $Z_{\text{patch}} + Z_{\text{cell}}$.

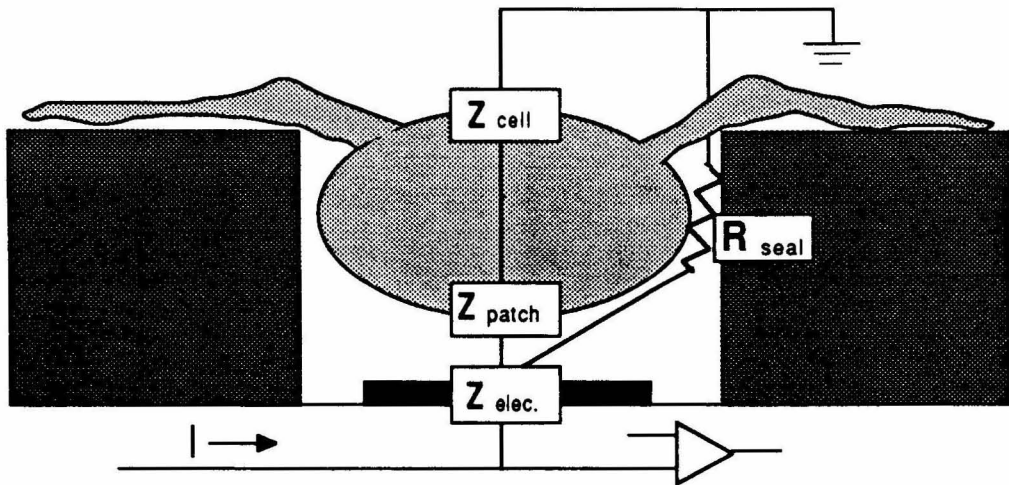
During extracellular stimulation a decrease of about 15 mV relative to the bath potential in a region near the electrode electrically stimulates the neuron. The current produced by the stimulating electrode, I_{stim} , produces the necessary potential across the membrane by producing a potential drop across the height of the well and the bottom of the cell membrane. Because the product of R_{seal} and I_{stim} produces the stimulation pulse, an increase in either R_{seal} or I_{stim} will make it easier to stimulate the cell.

Gas production at the gold electrode limits I_{stim} , because the production of gas will kill an over lying cell. The maximum current that can be introduced across the electrode is the potential at which gas is produced (V_{gas}) divided by the impedance of the electrode (Z_{elec}). A gold electrode will produce gas by hydrolyzing water when the electrode potential increases above about 1 V. Because of the electrodes enormous impedance, without electroplating the electrode, even a small current will produce more than a volt at the electrode. Electroplating the electrode with platinum black decreases the impedance of the electrode allowing the researcher to use more stimulation current

We designed the wells to require less stimulation current than flat arrays by increasing the resistance to ground, R_{seal} . A well traps a small neuron just after plating. As the cell grows it fills the well, the distance between the cell membrane and the walls of the well decreases. This decrease causes the resistance, R_{seal} , between the electrode and the ground in the bath to increase. The resistance of a 22 μ m diameter well, 10 μ m tall, filled with L15 media (resistivity is about to be 100 Ω cm) is about 26 K Ω . If the same well is filled with a 10 μ m diameter cell that impedance will increase to approximately 30 K Ω . If the cell grows to 20 μ m in diameter, nearly filling the well, the impedance increases to about 140 K Ω . As the resistance increases, a given stimulus current will produce a larger potential drop across the cell. Therefore, a stimulating current will depolarize the cell more easily (Figure 5.5).

5.3.2 Recording

Researchers record neuronal electrical activity by measuring the potential at an electrode tip located between the cytoplasm and ground. For extracellular recording, the electrode is just outside the membrane, so the potential recorded at the electrode is simply the potential drop through the bath. Since the impedance of the cell membrane is large compared to the resistance of the bath, the recorded signal can be very small. Changing the ratio of the pre- and post- electrode resistances in the recording circuit changes the magnitude of the recorded potential. Usually the membrane resistance is fixed. Therefore, to increase the magnitude of the recorded signal, a researcher must increase the resistance of the bath. The wells as compared to multi-electrode arrays should increase this resistance (R_{seal} in Figure 5.6).



Recording

The objective is to maximize the potential at the electrode by increasing the seal resistance while minimizing noise.

$$V_{\text{elec}} = R_{\text{seal}} \times I_{\text{patch}}$$

$$\text{noise} \propto \sqrt{Z_{\text{elec}}}$$

Figure 5.6 Recording with the well electrode. The noise equation assumes that R_{elec} is much greater than R_{seal} .

5.3.2a Noise

Recording electrical activity is relatively straightforward. Recording is limited by the signal-to-noise ratio of the recorded signal. If the expected signal is $25 \mu\text{V}$ at the electrode, the noise and electrical interference must be significantly less $25 \mu\text{V}$.

If the non-random noise of the amplifier and other electronic noise is negligible, random noise will be limiting. The major components of the random noise are: Johnson, shot, and 1/f noise. Johnson noise is

$$V_{\text{noise(VMS)}} = (4kTRB)^{0.5} \quad (1)$$

with k = Boltzmann's constant, T = absolute temperature, B = bandwidth in hertz, R = resistance, and $4kT = 1.62 \times 10^{-20} \text{ V}^2/\text{Hz}\Omega$ at room temperature. Decreasing the bandwidth or the recording electrode resistance, therefore, decreases the Johnson. In our system, the Johnson noise should be $15.5 \mu\text{V}_{\text{RMS}}$ when the bandwidth is limited with a 3-pole low-pass filter with 50% attenuation at 4 KHz and an electrode resistance of $1 \text{ M}\Omega$ or $4.9 \mu\text{V}_{\text{RMS}}$ with the same low-pass filtering and an electrode resistance of $100 \text{ K}\Omega$. The Johnson noise is at or below this value in practice.

Shot noise is due to the nature of electrical current being discrete charges rather than a continuum. The shot noise is

$$I_{\text{noise(VMS)}} = (2qI_{\text{DC}}B)^{0.5} \quad (2)$$

where q is the electron charge ($1.6 \times 10^{-19} \text{ C}$), B is the bandwidth, and I_{DC} is the DC current. Our bandwidth is 4 KHz and our I_{DC} is 1 nA. For $100 \mu\text{V}$ signal, the shot noise is $1.2 \text{ pA}_{\text{(RMS)}}$ with an electrode with $100 \text{ K}\Omega$ impedance or $1.2 \mu\text{V}$ with a $100 \text{ K}\Omega$ impedance. Shot noise is negligible.

The 1/f noise or flicker is dependent on the composition of the resistors in the circuit and the voltage applied across them. Typical values are $0.1 \mu\text{V}$ to $3 \mu\text{V}$ per 1 V for a carbon composition resistor vs. $0.02 \mu\text{V}$ to $0.2 \mu\text{V}$ per 1 V (depending on frequency) for a metal film resistor. Because the applied voltages in this circuit are generally small, less than 5 V, this source of noise is expected to be small in comparison to the Johnson noise.

5.3.2b Interference

Interference comes from 60 Hz pick-up and the stimulus artifacts. We can limit 60 Hz pick-up to less than $10 \mu\text{V}_{\text{RMS}}$ with proper shielding. Furthermore, synchronizing the stimulator output to the 60 Hz line frequency further minimizes the effect of pick-up on the recording of small signals.

The stimulus artifact decay at the electrode is much larger than any of the previous mentioned sources of interference. This decay is often in the millivolt range immediately after the stimulus pulse and when the evoked action potential is expected. If I do not subtract this decay, it will totally obscure the signal when I attempt to record activity evoked by stimulation. I shall discuss methods for minimizing the stimulus artifact in Chapter 7.

5.4 Design Criteria for the Well Electrodes

Like the multi-electrode arrays described in Section 5.2.2, I designed the well electrodes to record from and stimulate a small group of neurons for weeks or months. I originally designed the wells to do the experiment described at the beginning of this chapter, i.e., monitor synapse formation and the connections of a defined set of neurons with and without stimulation. First however, I hoped to use the well electrodes to assess the effects of electrical activity on neurite outgrowth from SCG neurons. I chose SCG neurons for this latter experiment, mainly because SCG neurons are easy to grow and they grow steadily and rapidly in culture. To record from and stimulate young SCG neurons (10-20 μm in diameter) soon after plating, as required for this experiment, I sized the wells to be less than or equal to 22 μm in diameter and 10 μm in depth. The size is perhaps the most critical design feature of the wells since the advantages of a snug fit include improvements in the recording and stimulation efficacy as discussed above.

SCG neurons, like many cell types, will move across the surface of a culture dish as they grow. To prevent movement of the cells out of the wells, I covered the top of the wells with a lattice or grillwork (see Figure 5.7). To allow the movement of freshly plated SCG neurons into the wells, the grillwork has a central opening about 15 μm across. The grillwork also has four side openings that allow the cell processes to grow out of the well and along the surface of the culture dish.

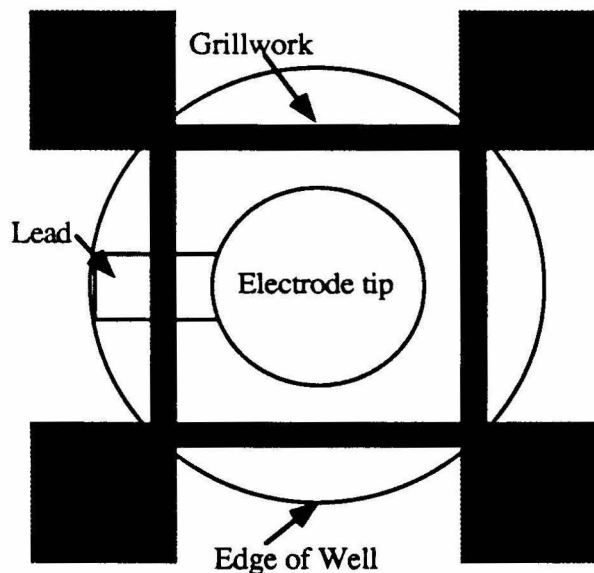


Figure 5.7 *Top view of a well electrode.*

I designed the wells to be transparent. With transparent wells I can use trans- rather than epi- illumination for moving cells into the wells, and for electrophysiological experiments. The inherent advantage of trans-illumination is that the objective may be placed below the specimen well away from the working area above. Trans-illumination is helpful though not essential. To study a network of five to ten neurons concurrently, I

started with sixteen wells per chip. I shall discuss the exact layout of the well electrode array and its fabrication in Chapter 6.

References

- Chien, C.B. (1990) Voltage-sensitive dye recording from networks of cultured neurons. Thesis: California Institute of Technology.
- Gross, G.W., Reiske, E., Kreuzberg, G.W. and Meyer, A. (1977) A new fixed-array multi-electrode system designed for long term monitoring of extracellular single unit neuronal activity *in vitro*. *Neurosci Lett.* 6:101-105.
- Gross, G.W., Williams, A.N. and Lucas, J.H. (1982) Recording of spontaneous activity with photoetched microelectrode surfaces from mouse spinal neurons in culture. *J. Neurosci. Meth.* 5:13-22.
- Israel, D.A., Barry, W.H., Edell, D. and Mark, R.G. (1984) An array of microelectrodes to stimulate and record from cardiac cells in culture. *Am. J. Physiol.* 247:H669-H674.
- Meister, M., Wong, R.O.L., Baylor, D.A. and Shatz, C.J. (1991a) Synchronous bursts of action potentials in ganglion cells of the developing mammalian retina. *Science* 252:939-943.
- Meister, M., Pine, J. and Baylor, D.A. (1991b) Recording visual signals in the retina with a multielectrode array. submitted 1991.
- Novak, J.L. and Wheeler, B.C. (1986) Recording from the *Aplysia* abdominal ganglion with a planar microelectrode array. *IEEE Trans. Biomed. Eng.* BME-33:196-202.
- Pine, J. (1980) Recording action potentials from cultured neurons with extracellular microcircuit electrodes. *J. Neurosci Meth.* 2:19-31.
- Regehr, W.G. (1988a) Neuron-Microdevice Connections. Thesis California Institute of Technology p.20.
- Regehr, W.G., Pine, J. and Rutledge, D.B. (1988b) A long term In Vitro Silicon-Based Microelectrode-neuron connection. *IEEE Trans Biomed. Eng.* BME-35:1023-1032.
- Regehr, W.G., Pine, J., Cohan, C.S., Mischke, M. and Tank, D.W., (1989) Sealing cultured invertebrate neurons to embedded dish electrodes facilitates long term stimulation and recording. *J. Neurosci. Meth.* 30:91-106.
- Thomas, C.A.J., Springer, P.A., Loeb, G.E., Berwald-Netter, Y. and Okun, L.M. (1972) A miniature microelectrode array to monitor the bioelectric activity of cultured cells. *Exp. Cell Res.* 74:61-66.

Chapter 6

Fabrication of the Well Electrodes

In this chapter, I shall discuss the fabrication and use of the well electrodes. I shall summarize the fabrication of well electrodes in Section 6.1, give a general outline of the protocol used to manufacture the wells in Section 6.2, emphasize the unusual aspects of the fabrication, concentrating on those techniques specifically developed for making wells in Section 6.3. I provide a detailed fabrication protocol in Appendix A. In the remainder of the chapter, I explain how wells are prepared for cells. In Section 6.4, I discuss how wells are connected to the external electronics, (described in Chapter 7). In Section 6.5, I discuss the platinization of well electrodes. In Section 6.6, I describe the protein coats used to make the dishes appealing to neurons, and in Section 6.7, the plating of cells onto the dishes is outlined. I discuss how cells are moved into the wells and survival in Sections 6.8 and 6.9.

6.1 Fabrication: Introduction

I use photolithography, a common technique in integrated circuit fabrication, extensively to fabricate the well electrodes. Photolithography enables the low cost manufacturing of many identical structures on almost any substrate; microlithography extends this ability to hundreds or thousands of structures on a single silicon wafer. Microlithography is done by spreading (actually, spinning) a thin layer of light-sensitive plastic photoresist over a surface, exposing the surface to light only where one wants the resist to vanish, and then developing the exposed resist away¹. The exposed surface can be etched or augmented as desired.

¹This technique is for positive resists, for negative resists the resist will remain only where it has been exposed.

To make the well electrodes I take advantage of the repetitive nature of micromachining. Typically, I make 16 wells per array and four arrays per 25 mm² coverslip, for a total of 60 wells per coverslip (i.e., substrate). I show the actual layout of one coverslip in Figure 6.1. The well electrodes are arranged in a four by four array with one of the corner slots reserved for a reference ground electrode. The well electrodes are spaced 100 μm center-to-center and each array is 1.1 cm center-to-center from the others on the coverslip. Four arrays are made on one 2.5 cm² coverslip. Generally, a fabrication run consists of 6, 12, or 18 coverslips. A six coverslip run makes 24 devices in one and a half days, while a 12 coverslip run makes 48 devices in two long days, and an 18 coverslip run makes 72 devices in three comfortable days.

The well structures are built up as a series of layers as shown in Figure 6.2. The well electrodes consist of a coverslip for support (1), chrome-gold leads (2), a primary insulation layer of polyimide (3), a second insulation layer in which the actual wells are carved (4) and an overlying grillwork for trapping cells in the wells (5). I make each of the layers by depositing either metal or plastic, and then patterning it using microlithography. Microlithography, as I have done it in Dr. David Rutledge's laboratory at Caltech, is capable of producing structures with line widths down to one to two microns.

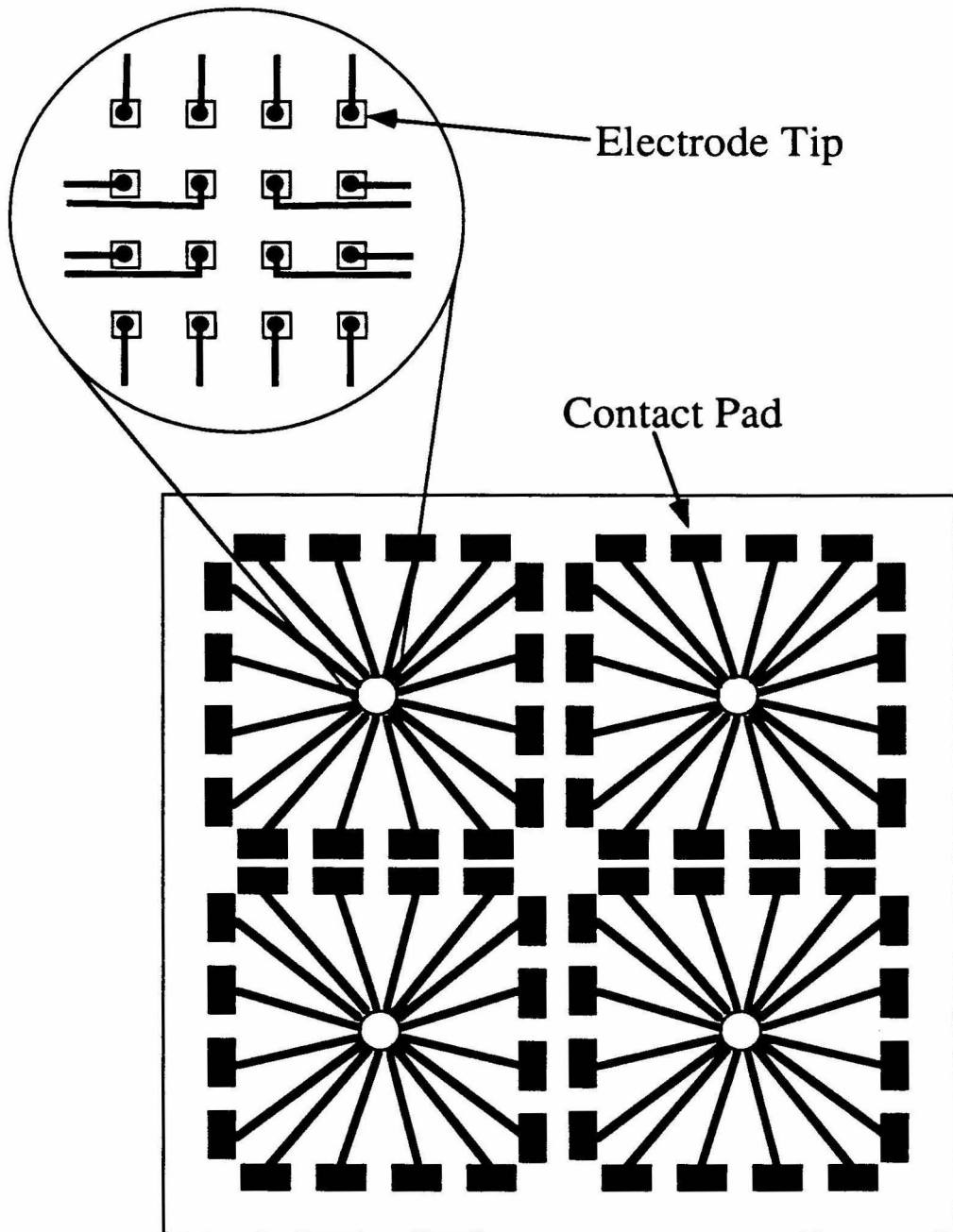


Figure 6.1 *Layout of wells on a 25 mm² coverslip with close-up of the center pattern.*

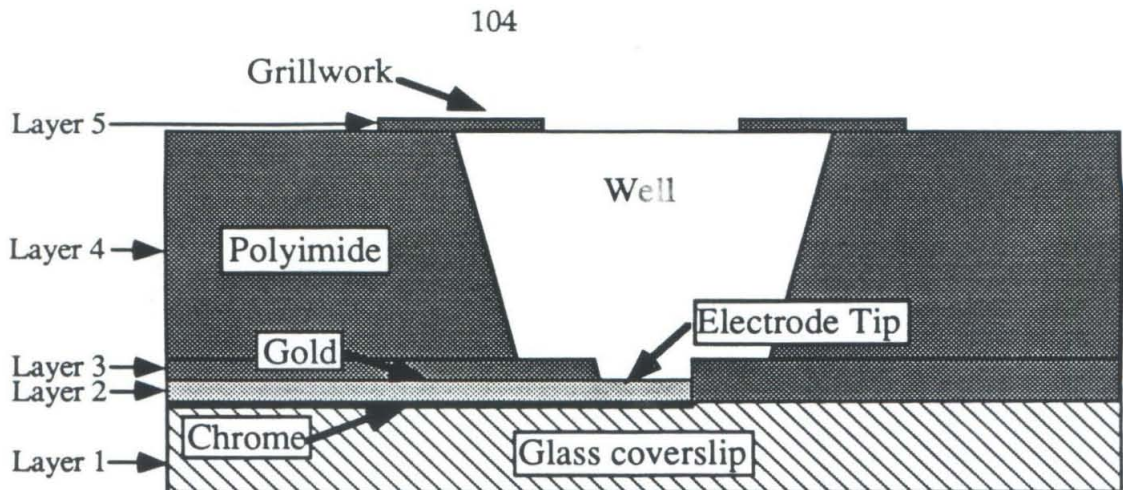


Figure 6.2 Cross section through the middle of a single well.

I size the wells to accommodate a single cell body, in this case that of a SCG neuron from a neonatal rat. When first dissected these cells are 10 to 20 μm in diameter but they may grow to about 25 μm . The opening in the top of the grillwork is 10 to 15 μm in diameter and the wells have a total volume of about 3000 μm^3 . Figure 6.3 is an electron micrograph of a well.

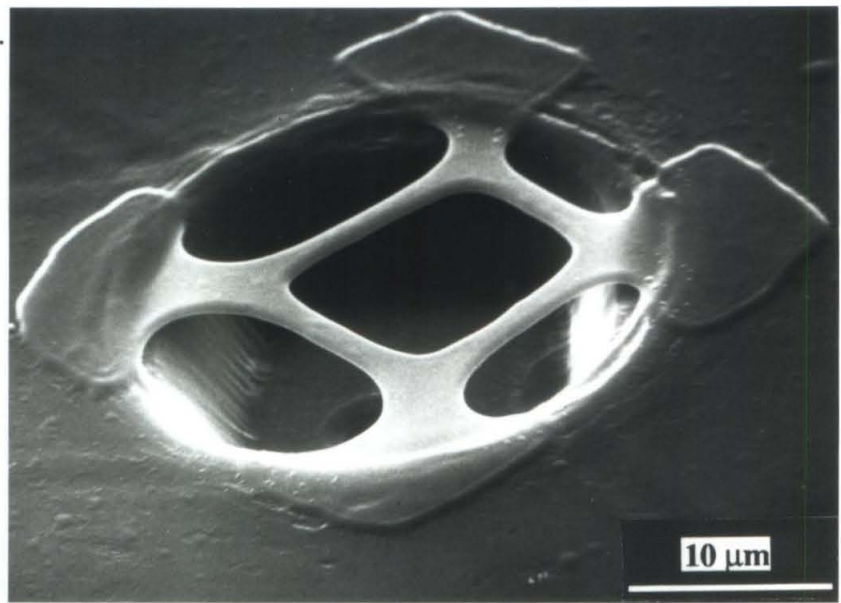


Figure 6.3 Scanning electron micrograph of a well.

6.2 Fabrication:

I describe the fabrication procedure in general terms in this section; the actual protocol is given in Appendix A. To make the wells I first make the gold leads using a technique called a "lift off". To do a lift off, I clean a set of glass coverslips with organic solvents (Figure 6.4a) and spin a thin layer of positive photoresist onto the surface (Figure 6.4b). The photoresist acts as a substrate for lithography. Spinning the resist-coated

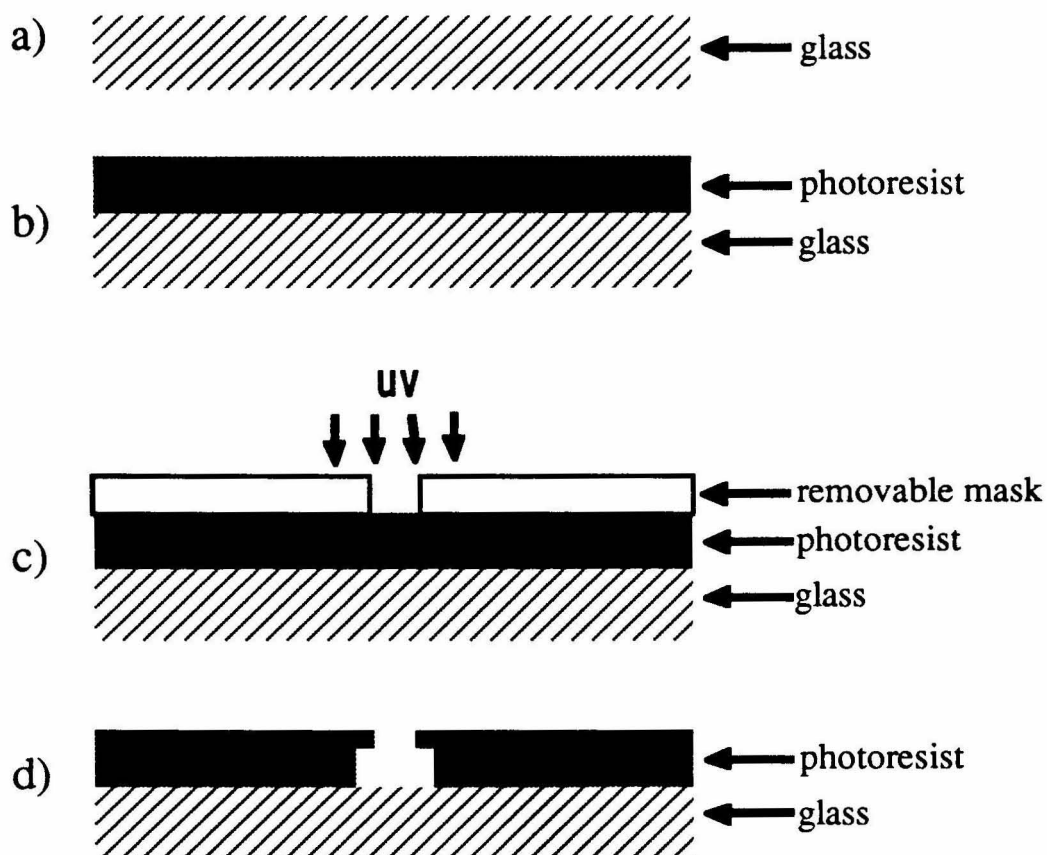


Figure 6.4 The coverslip is prepared for the evaporation of the metal that will form the leads. a) The glass coverslips are cleaned with a series of organic solvents. b) A positive photoresist is spun onto the surface and partially solidified. c) The photoresist is exposed to ultraviolet (UV) light only where it is not blocked by a removable mask. d) The surface of the photoresist is hardened in chlorobenzene before the exposed portion is developed away leaving the hardened overhangs.

coverslip effectively expels all but a thin even layer from the surface. I then gently bake this layer at 85 °C for 25 minutes, till it is firm, before selectively exposing the resist to UV

light only in the areas that will later become the leads. I select the exposure pattern by exposing through a UV opaque removable mask that I put directly onto the resist-coated coverslip (Figure 6.4c). Following exposure, I remove the mask and develop the photoresist so that an overhang in the photoresist remains (Figure 6.4d). I can make the overhang in one of two ways. Either I can softly expose the back of the wafer with UV light to soften the entire bottom of the resist layer or I can harden the top of the resist with chlorobenzene before developing the photoresist. Both techniques allow more of the lower layers of resist to be removed than of the top surface.

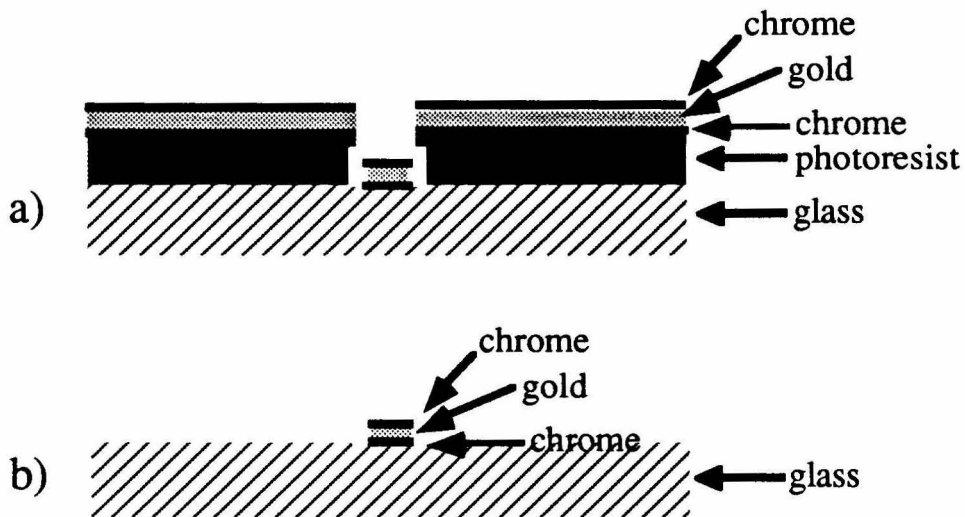


Figure 6.5 *The formation of the electrical leads.* a) Three layers of metal, chrome-gold-chrome are evaporated onto the coverslip to form the leads and electrode tips. b) All of the unwanted metal is removed with the underlying photoresist by desolving the photoresist in acetone. Only the metal that forms the leads remains.

Next I evaporate the metal for the leads onto the surface of the resist (Figure 6.5a). Gold does not adhere well to glass so I evaporate a thin layer of chrome onto the glass before evaporating the gold. I cover the top of the gold with a thin layer of chrome to improve the adhesion between the gold leads and the polyimide that will cover them. To form the leads, I dissolve the remaining photoresist away with acetone, lifting off the

overlaying chrome gold chrome layer. Only the metal that was in contact with the glass surface remains (Figure 6.5b).

After making the leads, I insulate them electrically from what will eventually be the bath with a layer of photosensitive polyimide (Selectilux-50). Selectilux-50 is a negative resist made primarily of polyimide. The polyimide will not adhere well to glass or other polyimide layers without the addition of an adhesion layer. To form the adhesion layer, I can either spin an adhesion promoter on to the coverslip and bake the coverslip, or evaporate a thin layer of aluminum oxide onto the surface of the coverslip. Since most adhesion promoters require curing at temperatures that blacken the polyimide, I used a thin aluminum layer instead (Figure 6.6a). To make the insulation, I spin Selectilux-50 onto the coverslip (Figure 6.6b), and then flood it with UV light from the bottom and the top (Figure 6.6c). Exposing the polyimide through the bottom of the coverslip (i.e, using the lead pattern as a mask) exposes all the polyimide except over the electrodes or contacts or thicker leads. The additional exposure from the top insures that the polyimide over the thicker leads is also exposed and sharpens the edge of the insulation layer to effectively decrease the volume of the well. Following exposure, I develop the unexposed polyimide over the electrodes away (Figure 6.6d).

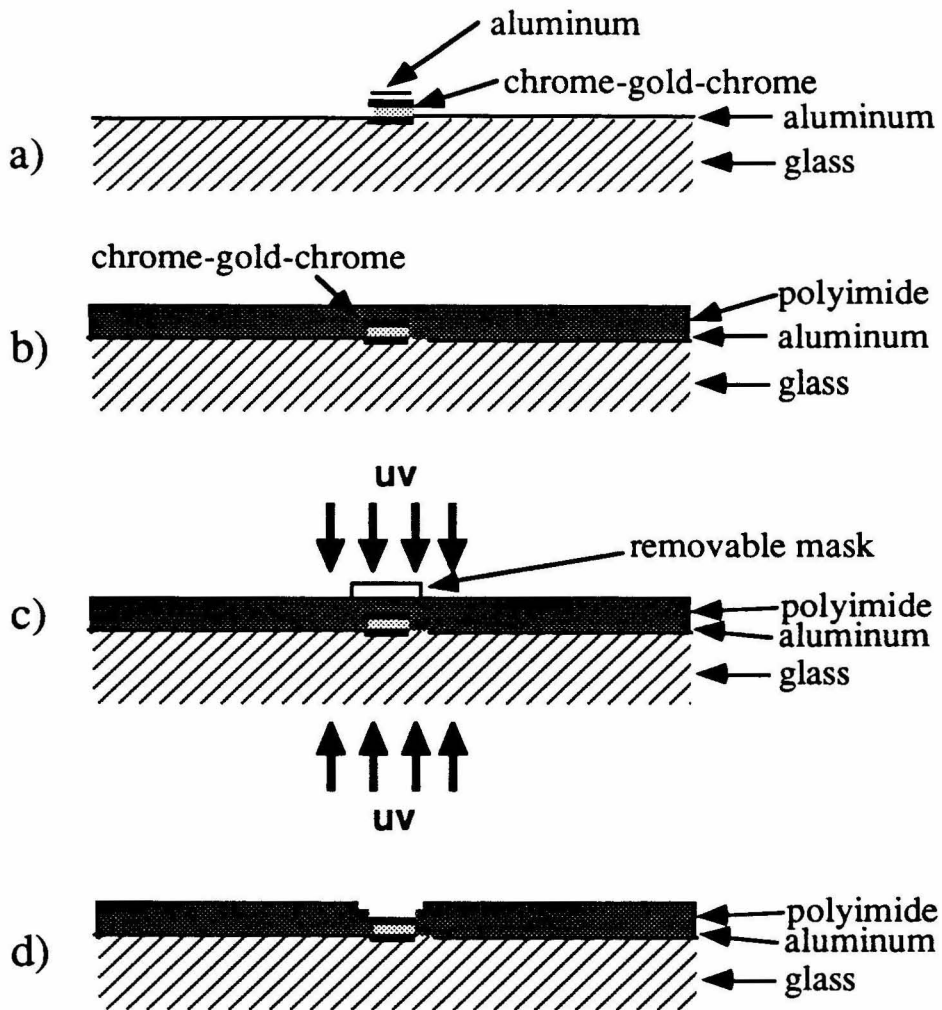


Figure 6.6 *The application of the first insulating polyimide layer.* a) A 30 Å layer of aluminum is evaporated onto the glass and metal surfaces to improve the adhesion of the polyimide to the surface. b) A thin layer of polyimide (Selectlux-50) is spun onto the coverslip and partially solidified by baking. c) The polyimide is exposed to UV light through the coverslip and from the top surface through a removable mask. The polyimide will remain where ever it is exposed. d) The unexposed polyimide is developed out from on top of the metal lead pattern.

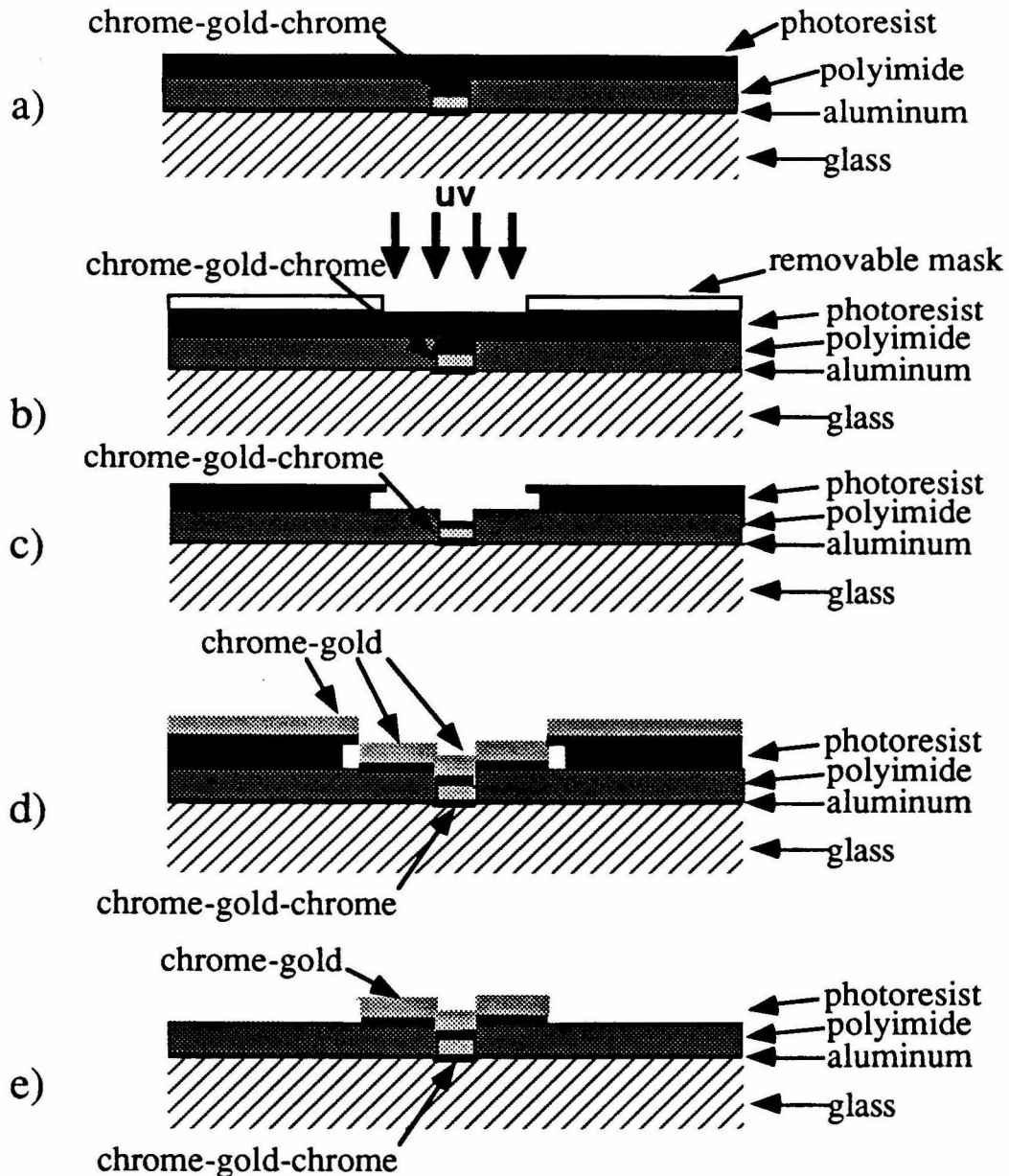


Figure 6.7 A sacrificial mask is made in preparation for the formation of the wells. a) A sacrificial mask, necessary for making the wells, is made out of chrome and gold. First, photoresist is spun onto the surface of the coverslip and partially hardened. b) The photoresist is then exposed to UV light through a removable mask. c) The exposed photoresist is removed after the top surface has been hardened with chlorobenzene to produce an overhang. d) 200 Å of chrome and 1000 Å of gold are evaporated onto the surface. e) The excess metal is removed with the remaining photoresist.

After insulating the leads I build the wells. I also make the wells made out of a Selectilux brand polyimide (Selectilux-200) and pattern them by back-illumination using a gold sacrificial mask. I make the mask for the wells the same way I made the leads (Figure 6.7 a-e) except that I use a thicker layer of chrome as the primary adhesion layer and I do not use chrome on top of the gold. The thick bottom layer of chrome allows me to remove the mask without etching the gold electrode tip directly beneath. I do not add chrome to the surface to discourage adhesion of the polyimide in the bottom of the wells. As with the leads, I make the mask for the wells by patterning a layer of positive resist (Figure 6.7 a-c), evaporating the metal (Figure 6.7 d) and lifting off the unwanted metal by dissolving the resist (Figure 6.7 e).

I make the wells themselves by spinning a thick layer of polyimide (Selectilux-200) on to the coverslip and exposing it to UV light only where it is to remain (Figure 6.8 a). Exposing the polyimide through the bottom of the coverslip solidifies the bottom of the well layer more than the top. The long exposure, needed to fully expose the top of the polyimide from the bottom alone, tends to excessively harden the polyimide in the bottom of the wells. This hardened polyimide can insulate the electrodes even after development. To prevent this problem, I expose the well layer from both the top, using a removable mask, and the bottom (Figure 6.8 b) and I have gold as the top layer of the sacrificial mask. I then clear the well by developing away the unexposed polyimide inside (Figure 6.8 c).

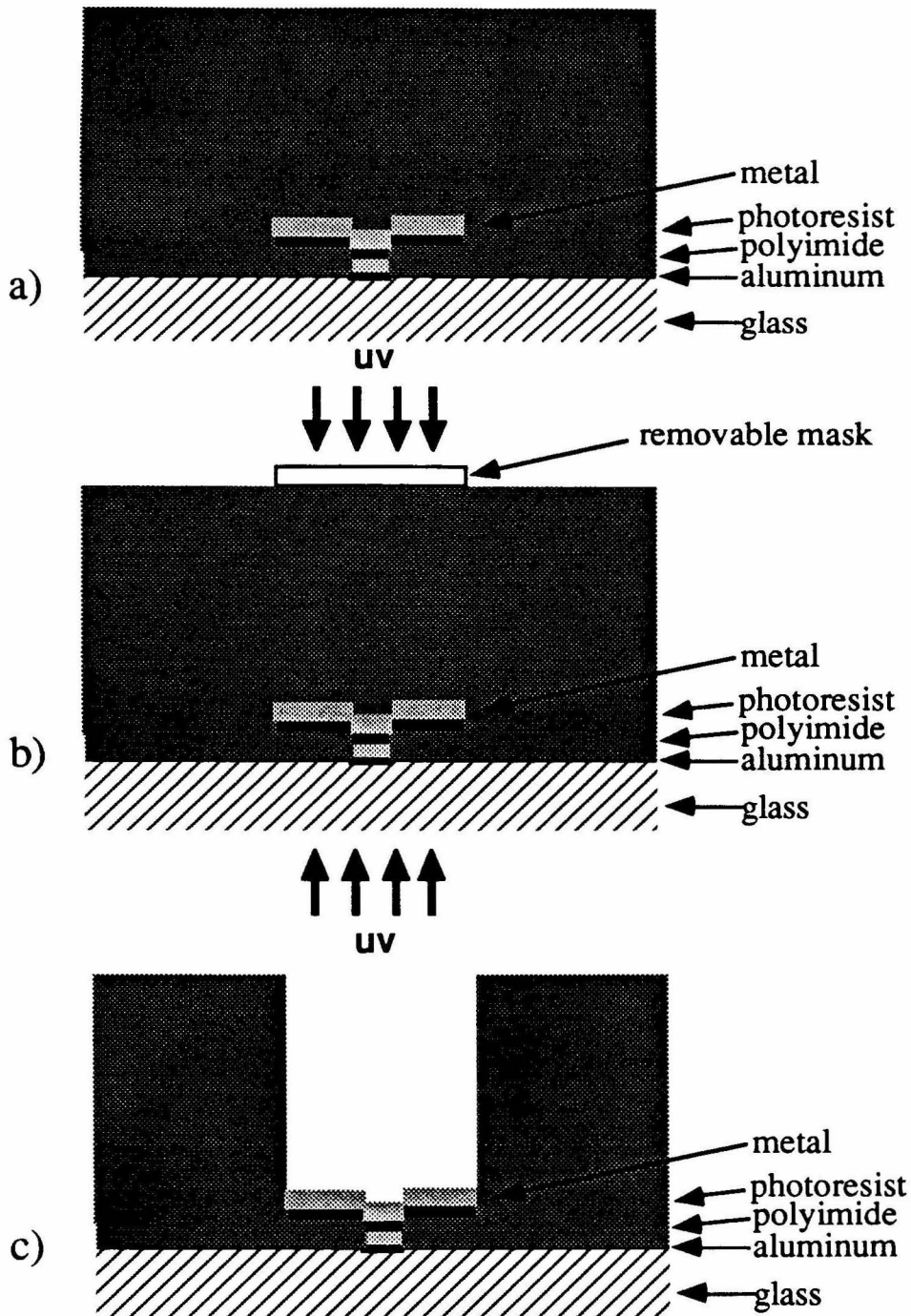


Figure 6.8 The wells are made out of a viscous polyimide, *Selectilux-200*. a) A thick layer of polyimide (*Selectilux-200*) is spun on and hardened. b) The polyimide is exposed with UV light through the coverslip and a removable mask. c) The unexposed polyimide is removed from what is now a well.

The next step in the fabrication is to remove the sacrificial chrome-gold mask. The gold mask is etched away in two steps, first with gold etchant and then with chrome etchant (Figure 6.9).

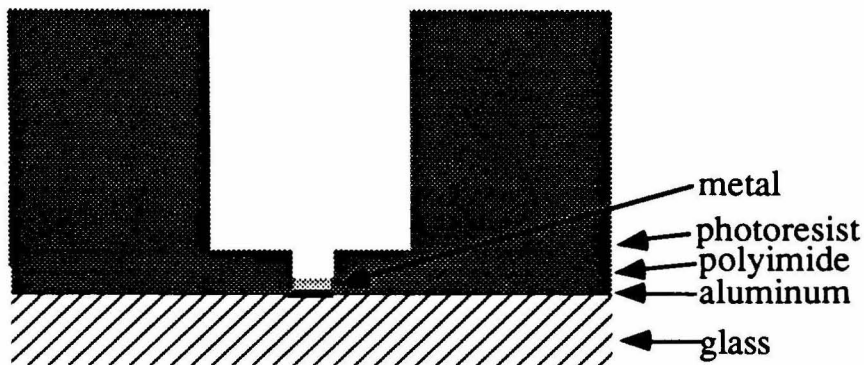


Figure 6.9 *The sacrificial metal layer at the bottom of the well is removed.*

The last layer I add to the wells is the grillwork. The grillwork is also made of polyimide. To make the grillwork, I spin a thin layer of polyimide (Selectilux-50) onto the coverslip filling in the well (Figure 6.10 a). I then lightly expose this last layer from the top with UV light only where the grillwork is to be. Because the duration of the exposure is sufficient to solidify only a very thin layer of the polyimide (Figure 6.10 b), subsequent development of the structure cleans out the well and leaves the grillwork as a thin covering over the hole (Figure 6.10 c). The attachment of the grillwork to the well is strong enough to support the grillwork and to allow the placement of cells into the wells without detachment.

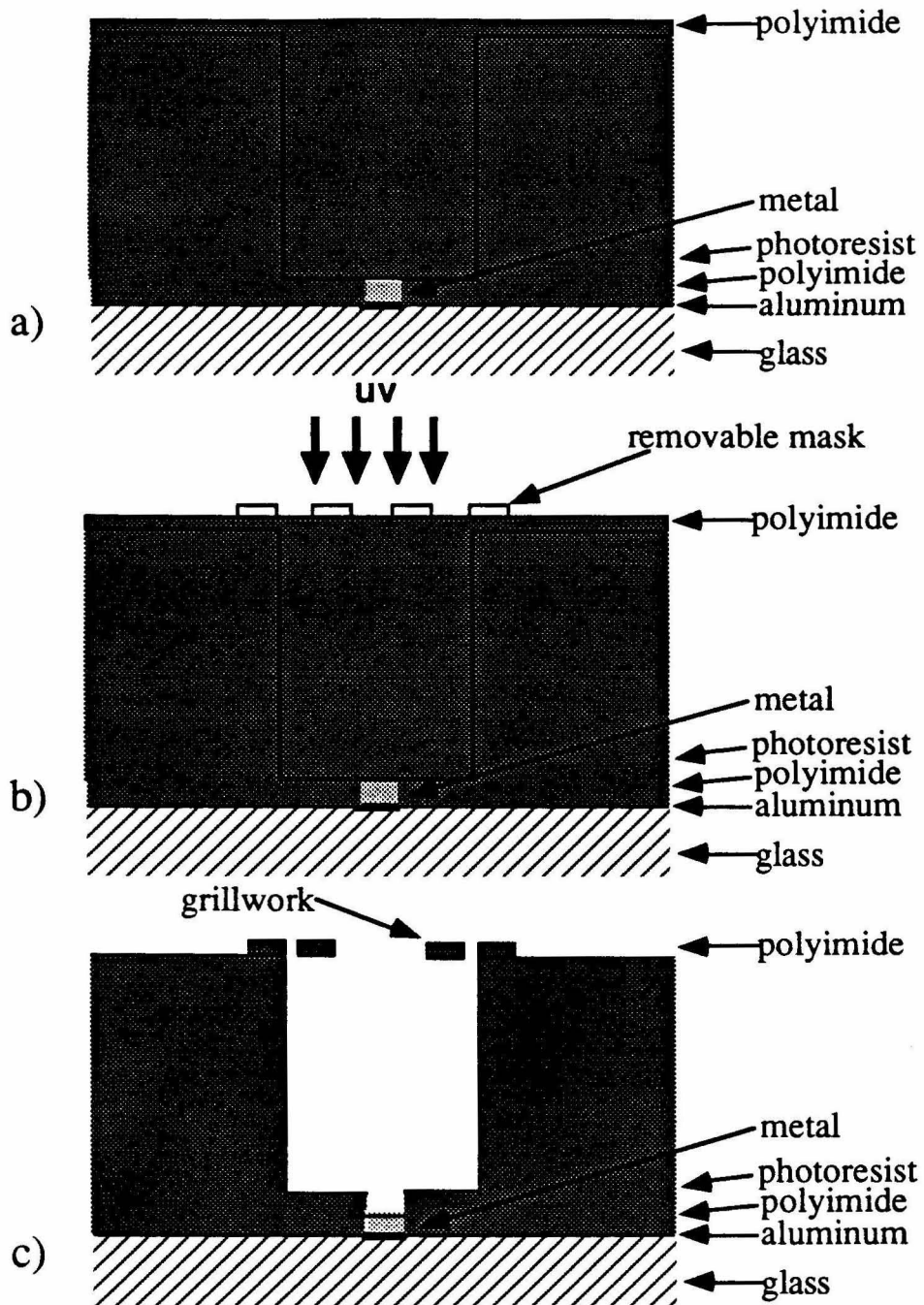


Figure 6.10 The grillwork is made out of a third layer of polyimide. a) Yet another layer of polyimide (Selectilux-50) is spun onto the coverslip. b) This layer is exposed lightly through a removable mask to form the grillwork. c) The unexposed polyimide is developed away; leaving a finished well.

To finish the fabrication I cure the polyimide overnight at 200°C.

6.3 Fabrication Techniques Developed Specifically for the Wells

I developed some of the techniques described in the preceding section specifically for the fabrication of the wells. These techniques, however, should be useful for many other micromachining tasks.

The first innovation was to allow the well electrodes to withstand extended periods of time in a harsh environment: tissue culture medium. To withstand months in saline, as the wells are designed to do, the adhesion between all the layers must be exceptional. The polyimide-to-glass bond is particularly weak. Without an adhesive agent, the polyimide will not remain attached to the glass. One excellent adhesive agent is available commercially from Hitachi. Unfortunately, this adhesion promoter must be baked at over 400°C for hours before use. Selectilux turns almost black (is no longer transparent) after being heated under these conditions. Because the commercial adhesion agent functions by breaking down to aluminum oxide when heated, a thin layer of evaporated aluminum seemed like a promising alternative adhesion promoter. In fact, I found that if I evaporated a 30 Å layer of oxidized aluminum on to the glass before adding the polyimide, the polyimide will withstand more than 3 hours in boiling water without detaching from the coverslip.

A second technique I developed for the fabrication of the wells was to fabricate the masks for the electrodes and wells as integral, sacrificial layers. The exposure was then done through the bottom of the coverslip. The bottom exposure not only insures that the polyimide at the surface of the coverslip is fully exposed, without overexposing the top surface, but also insures that the mask is in perfect contact with the polyimide. Bottom exposure of the insulation layer also has the advantage of affording automatic alignment to the lead pattern thus making the fabrication easier.

The third innovation enabled the unexposed polyimide to be cleaned out from the wells. Initially, cleaning out the wells proved troublesome at best. A partial solution to the problem was the use of the sacrificial mask layer and bottom exposure. The second half of the solution was using gold as the top surface of the mask. The gold repelled the polyimide to form a cleanly defined bottom to the wells. Without the inert gold surface at the bottom of the well, the polyimide never quite cleared off the electrode tip and the tip remained insulated from the bath.

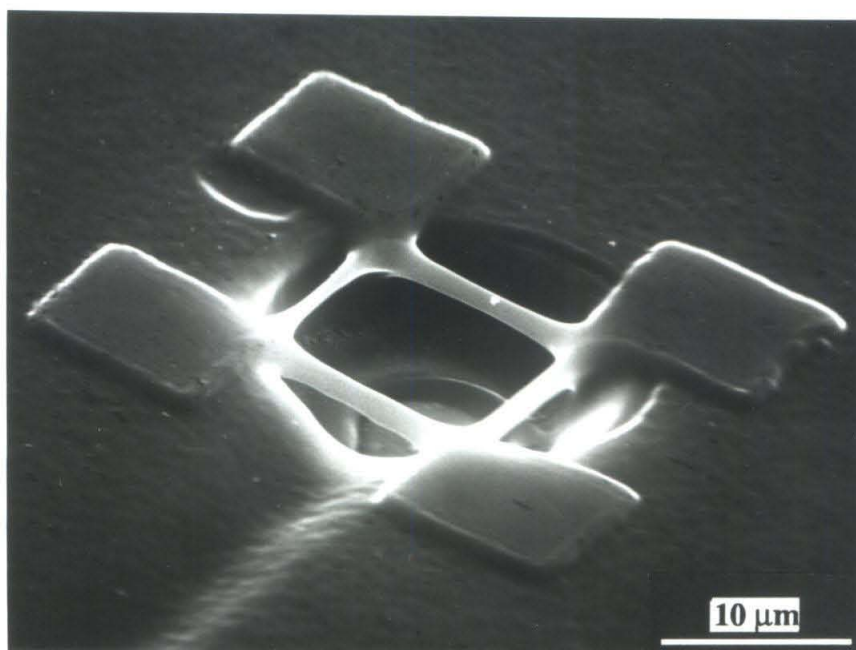


Figure 6.11 An electron micrograph grillwork made from a lightly exposed layer of polyimide. Although the bars are extremely thin the grillwork withstands considerable force as applied with a glass pipette.

Finally, it was essential to develop a means of developing a self-supporting grillwork (Figure 6.11). To do make the grillwork, I exposed the polyimide with only a minimal amount of UV light. Because the polyimide absorbs the UV light as it cures, the top of the polyimide is exposed to more light than the bottom. I used this differential

exposure to cure a thin lattice through which I removed the underlying polyimide by development. Remarkably, the exposed layer has enough structural integrity to support itself until baked and, after curing, is not fractured by the force of bending a thin glass pipette.

6.4 Preparation of the Wells for Experiments

After fabrication and curing, the wells still need substantial preparation before use. This preparation includes connecting the wells to the rest of the recording and stimulation circuitry, decreasing the impedance of the electrode, and making the wells attractive substrates for the neurons.

To connect the wells to the recording and stimulation circuitry, I used a previously designed printed circuit called the "Tim Board" (so named for its maker). I show a picture of the board in Figure 6.12. I made a number of modifications to the Tim Board in order to decrease noise and increase reliability. I will describe these modifications in Chapter 7. For the purposes of the discussion here, assume the Tim Board is simply a convenient printed circuit board for connecting the wells to the recording and stimulation electronics.

At the heart of the Tim Board is a $7/8$ by $1\ 1/2$ inch opening with 64 gold leads at the two long edges. These gold leads are connected via conducting zebra connectors to leads on a piece of printed circuit board that is in turn connected with silver paste to the contacts on the edge of a set of wells. Zebra connectors are strips of material that consist of a series of conducting and insulating layers laminated together to form conducting stripes when cut perpendicular to these layers. Electrical current can be carried by the conducting layers when compressed. Because of the arrangement of the materials, current can travel in only two dimensions. This makes zebra connectors useful for connecting a line of independent electrical connections. Because there are only 16 wells per dish, I shorted

three leads on the Tim Board together for each well electrode: this increased the reliability of these connections. Using this system, the wells can be reversibly connected to the Tim Board during an experiment.

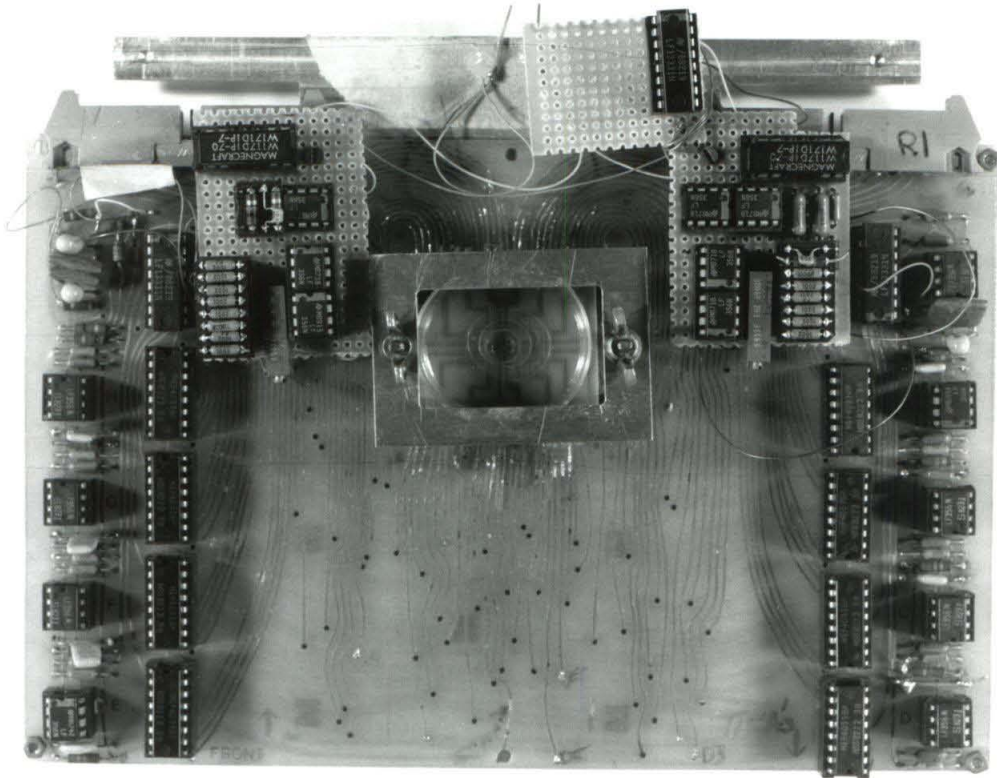


Figure 6.12 *Photograph of "Tim Board".*

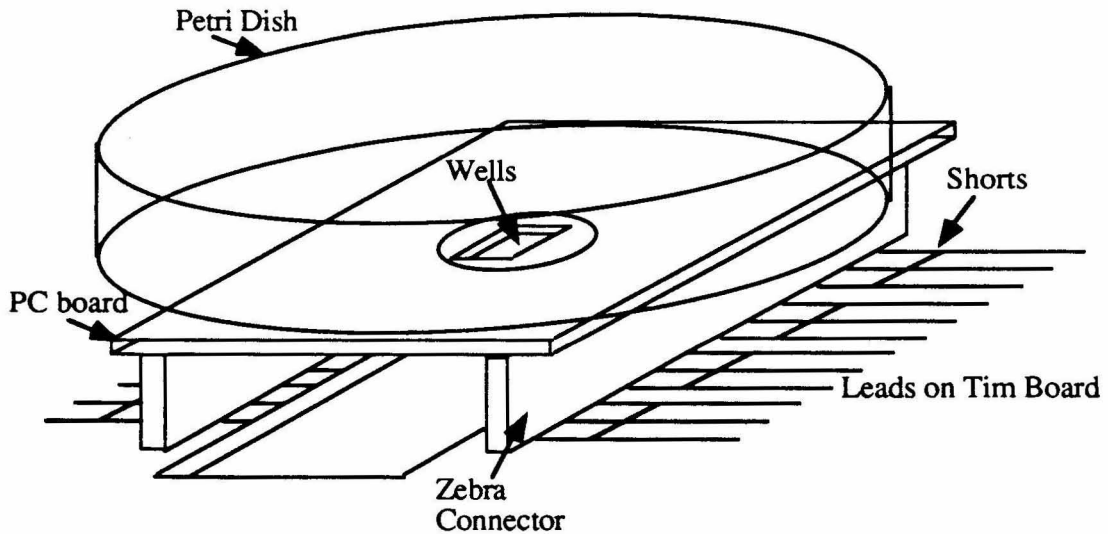


Figure 6.13 Schematic of the connection between the wells and the leads on the Tim Board.

I electrically connected the PC board to the well electrodes with a drop of silver paste at each contact and physically connected them with Sylgard (184 Dow Corning). I painted medical elastomer (Silastic MDX4-4210, Dow Corning) over the surface of the substrates from the contacts all the way into the inner well pattern. The Sylgard acted to both decrease the shunt capacitance to the bath and insure that there were no shorts to ground in the outer segments of the leads. The only other modification done to the wells at this point was to glue a petri dish to the top of the PC board using Sylgard. This petri dish held the cell culture media during experiments.

6.5 Platinization

I also prepared the wells for use by decreasing the impedance of the electrode tip. As discussed in Chapter 5, this enormous impedance, if not decreased, would increase the noise of the recording and limit the stimulation current severely. To decrease the

impedance of the electrode tips, I electroplated platinum black onto the surface of the gold electrodes. The platinum black is a porous structure which decreases the impedance of the electrode by increasing its surface area.

I generally measured the impedance of unplatinized well electrodes (approximately $50 \mu\text{m}^2$ surface area) at just above $4 \text{ M}\Omega$ at 1 KHz (the impedance of electrodes insulated from the bath was about $5 \text{ M}\Omega$). After proper application of the platinum, the impedance decreased to as low as $10 \text{ K}\Omega$ at 1 KHz as measured in the platinization solution, although typical impedances were about $40 \text{ K}\Omega$. In order to platinize the electrodes, I supplied 1.7 V across each of sixteen $10 \text{ M}\Omega$ resistors in series with the 16 electrodes (Figure 6.14) for 30 minutes in the presence of platinization solution (Platinum "AP" solution, replenisher, $4\text{g}/100 \text{ ml}$ from Technic Inc.).

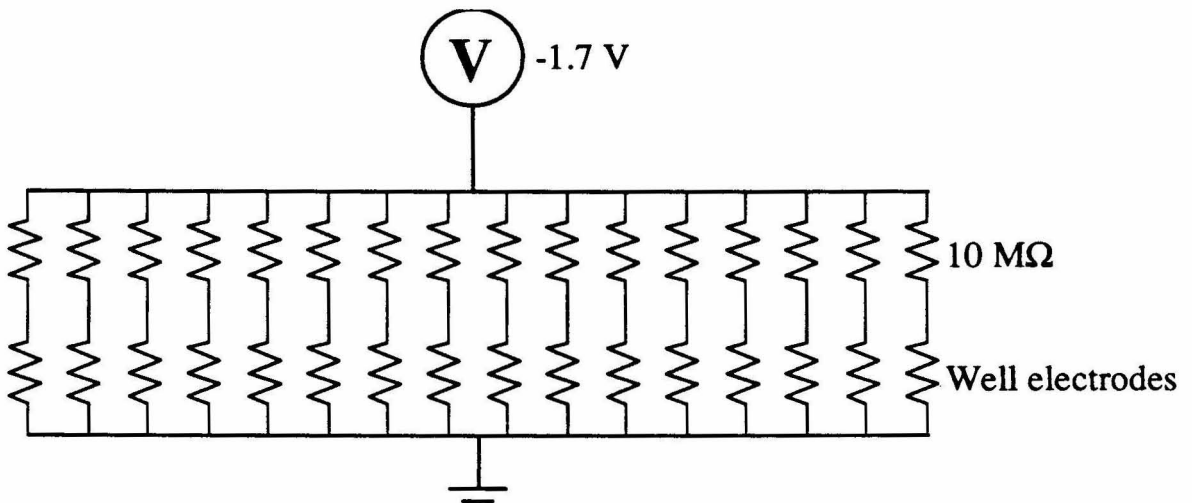


Figure 6.14 *The circuit for the platinization of the electrodes.*

Because platinizing solution typically contains a number of cytotoxic ingredients, including lead, I rinsed the wells extensively and allowed them to soak for at least one week in Dulbecco's PBS before use. After this washing, cells appear to be unaffected by the platinization. The impedance of the electrodes remained constant during this period.

The measured electrode impedance depended on the media in which it was measured. For instance, the impedance at 1 KHz in Dulbecco's PBS or the PBS with 1 mg/ml polylysine increased to around 110 K Ω and 250 K Ω , respectively. The addition of laminin did not appreciably alter the measured electrode impedance. The greatest increase in the electrode impedance, generally, occurred after I moved the cells into the wells. After moving the cells, the impedance would shoot up to about 1 M Ω . This increased impedance would be wonderful if it represented the decrease in the conductance of the full well as compared with the empty well. Unfortunately, the increase in impedance probably represents damage to the platinum layer since it returned to its original amplitude in only half of the wells after cleaning with a mixture of protease K and SDS. For the other electrodes, returning the electrodes to their previous "low" impedance (about 100 K Ω at 1 KHz) required replatinization of the wells. This phenomenon suggests that at least some of the increased impedance was due to damage during moving of the cells.

6.6 Protein Coating

After I decrease the electrode impedance by platinization, I still need to prepare the wells for cells. First, I wash the well in saline for up to one week to remove all residual lead or platinum that could potentially harm the cells. My standard washing protocol is given below:

- 1) Pull platinization solution from the dish
- 2) Rinse 3 times with 1% NaCl.
- 3) Rinse 3 times with Dulbecco's PBS
- 4) Allow to soak for at least one week
- 5) Rinse 2 times with Dulbecco's PBS

Second, I coat the surface of the wells with polylysine. The most important part of this step is to make sure that the polylysine solution fills the well. Surface tension will tend to prevent the well from filling with liquid during coating. To alleviate this problem, I wet

the wells first with dimethylsulfoxide (DMSO), rinse them with ethanol (without drying), then rinse them three times with water (without drying) before adding the protein-containing solution.

Unlike the experiments reported in Chapters 1-4, I did all of the well experiments on polylysine alone. I chose polylysine because it does not form a cell or clog the grillwork and because SCG neurons tend to wait 6 to 12 hours before sending out processes on polylysine. This delay allows the cells to settle and be moved into the wells before there is neurite outgrowth. After soaking overnight in 1 mg/ml polylysine in DPBS, I rinsed the wells three times in Dulbecco's PBS and dried them until use. I added media with or without cells to dry dishes, no laminin was added.

6.7 Plating Cells

I have grown two types of cells in the wells SCG and hippocampal neurons. I give the procedure for dissecting and preparing SCG neurons in Chapter 3. To plate the cells in well electrodes rather than in dishes, after trituration, I either plated the cells in 100 μ l drops (about 300 cells/ dish) directly on the dry well dishes or into short glass tubes that cover the wells in petri dishes filled with 2 ml of L15 (about 1000 cell/dish). Plating in drops tended to concentration the cells in the center of the well pattern: plating in tubes tended to concentration the cells at the periphery. Both plating methods were acceptable.

6.8 Moving Cells

After the cells are plated, they must be physically transferred into the wells. This is the key problem in using the wells for experiments. Moving the cells as described here is extremely tedious. The most successful way of moving the cells to date is to pull glass capillaries to a very fine flexible point, round the point and use the capillary to sweep the neurons to a well or to pick the neuron up with the capillary and move it to the well. Then

the neuron must be coaxed into the well. I can move cells into wells by gingerly dropping the cell over the well and pushing it in. If successful, I can distinguish the fine outline of the neuron in the well. The neurons are phase bright when alive and dark when dead. If a phase bright object is seen in the well after moving, there is about a 10 to 50% probability that a cell has survived transport. Often it is difficult to assess the brightness of the cell in the wells because even though the bottom of the well is clear glass covered by a thin translucent layer of polyimide, the electrode is not transparent. In addition, the grillwork and side walls of the well electrodes serve to decrease the visibility into the wells.

6.9 Survival in Wells

Although it is hard to move cells into the wells, once cells are moved into the wells they seem to grow normally. SCG neurons moved into a preliminary design made out of silicon without electrodes survived, trapped in the wells, for up to six weeks (Figures 6.15 and 6.16).

In polyimide wells with electrodes, I showed that SCG neurons could survive for at least two weeks. No cell ever pulled out of a well once it was trapped by an intact grillwork. Occasionally, the exact position of a cell was misjudged and a cell that was at first judged to be in the well was later found to be on top of its well. There was no unexplainable attrition of the cells in the wells. Three pictures of SCG neurons in polyimide wells with electrodes about 10 hours after plating are shown in Figure 6.17.

Hippocampal cells were also moved into wells and survived up to three days. No long term studies on their ability to survive were done.



Figure 6.15 A single SCG neurons trapped within a well. The cell's axons are visible on the surface of the substrate. The soma is not visible. The picture was taken three days after plating.

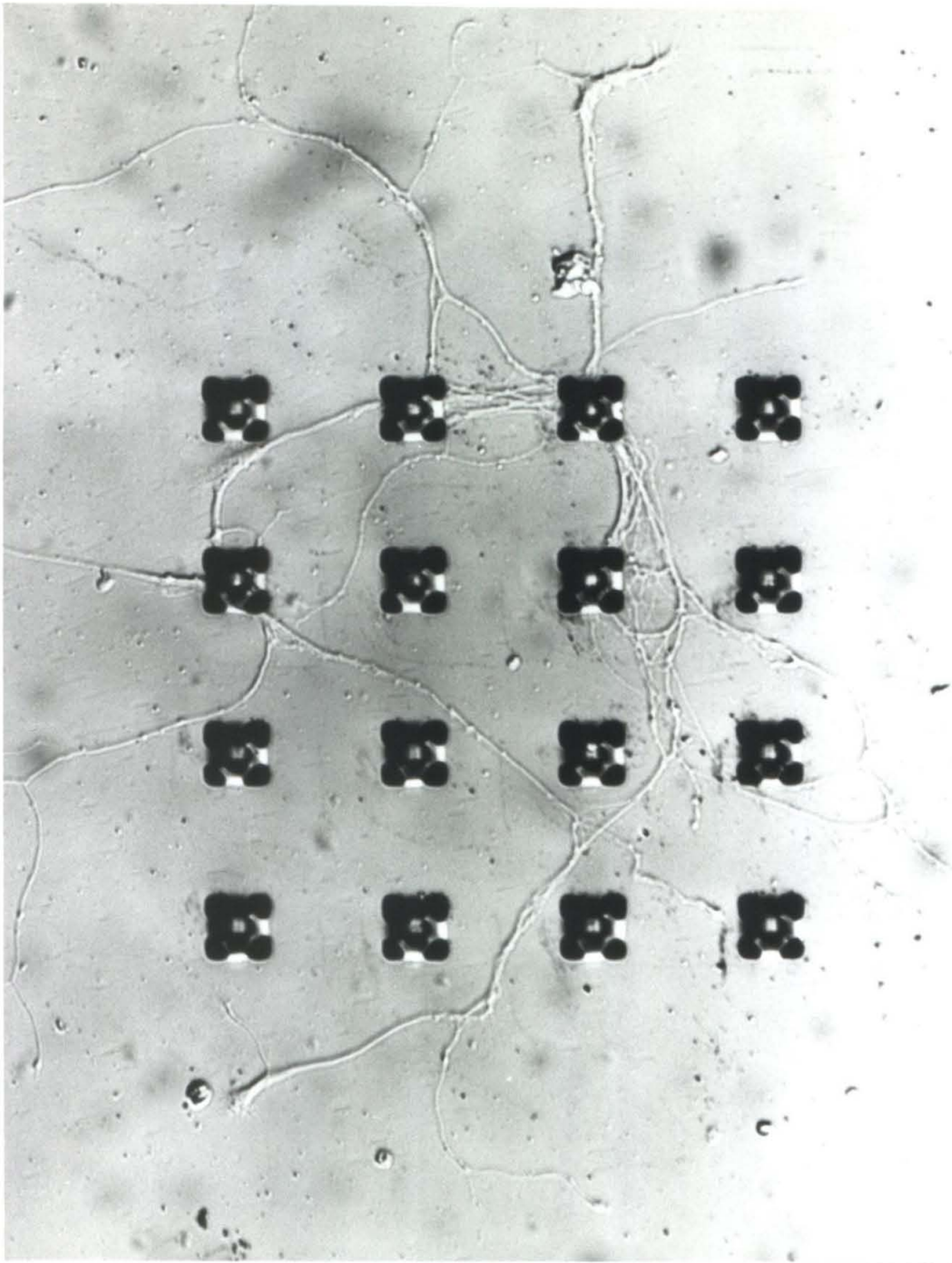


Figure 6.16 A four cell network of SCG neurons grown on a gold coated silicon substrate. The picture was taken three days after plating.

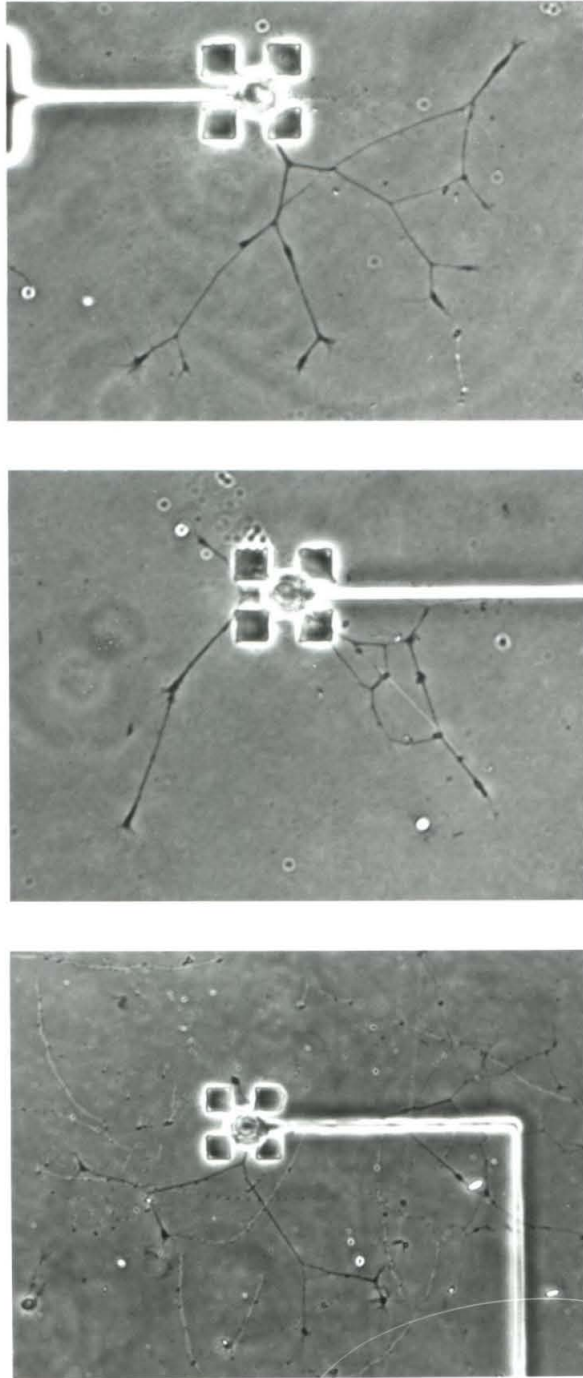


Figure 6.17 Pictures of three different SCG neurons growing out of polyimide wells with electrodes. The cells are shown about 10 hours after plating.

Chapter 7

Experimental Results

I designed the well electrode to facilitate the chronic simultaneous stimulation of and recording from numerous individual neurons concurrently. In this chapter, I will describe the hardware which I designed and built to allow simultaneous stimulation of and recording from identified neurons with the well electrodes and describe the limited success I achieved to date. I shall discuss some suggestions for improving the recording system.

7.1 Stimulation and Recording with Wells: the Electronics

To enable stimulation and recording with the wells, I built a fair quantity of electronics and connecting hardware. The wells are connected to the electronics through the Tim Board. For recording, the Tim Board also amplifies the difference between a recording electrode and the reference electrodes. To facilitate recording and stimulation with the wells, the Tim Board was modified in three ways. For robustness and since there are only 16 wells per dish, I tied three electrodes together for each connection to the PC board. To decrease pick-up in the stimulation signal I added a current source to the Tim Board. Finally, to enable disconnection of the current source from the electrodes at will I added a relay. The advantage of these latter two modification will become evident shortly.

The easiest way to discuss the electronics is to examine how a signal changes from input to output. A simplified schematic of the circuit that I built is shown in the top of Figure 7.1. The Tim Board receives (Figure 7.1a) and converts (Figure 7.1b) a stimulus voltage into a current. On each Tim Board here are two current sources: I connect each current source to one of two electrodes in each of four different families of electrodes. A relay connects the current sources to the electrodes only during stimulation (Figure 7.1c).

During recording, a differential amplifier compares the potential at the electrode and at a reference ground (Figure 7.1e). The differential signal is then filtered (Figure 7.1f), passed through a switch (Figure 7.1g) and further amplified (Figure 7.1h).

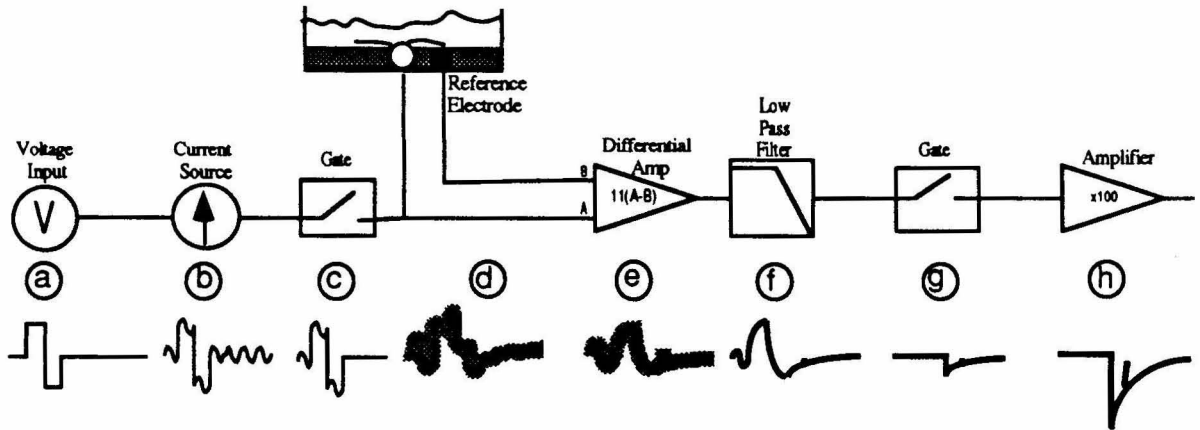


Figure 7.1 Schematic of the stimulation and recording electronics. The top line represents each of the major components in the system. The bottom line shows how the signal "looks" at each point in the circuit.

I designed the circuit to minimize noise and interference. At the bottom of Figure 7.1 is a rough sketch of how the signal looks at each step. Initially the stimulation voltage is a bipolar square pulse. A bipolar stimulus pulse is used for stimulation to minimize the magnitude of the residual electrode potential (see section 7.2.1).

I convert the stimulus voltage into the current need to create the depolarizing voltage (Figure 7.1b). The output of a current source must have a very high impedance so it can drive a high impedance electrode. The high impedance of the output increases the 60 Hz pick up. To minimize the pick up, I built the current source as close to the electrodes as possible, i.e., on the Tim Board. The components of the current source add significant 1/f noise to the signal, about 200 μV with a 1 M Ω load. Since the recorded signal may be as small as 25 μV , the 1/f noise would impede recording of evoked potentials if not removed. To enable recording, I remove the current source and associated noise from the circuit

during recording with a reed relay type switch. The reed relay is closed only during stimulation (Figure 7.1c).

After the relay, the current is injected through the electrode into a well. The large impedance of the electrode adds both Johnson noise and 60 Hz pick-up to the signal (Figure 7.1d). A differential amplifier compares the voltage at the well electrode with that of a reference electrode located in an empty well adjacent to the well electrode and amplifies the difference 11 times (Figure 7.1e). This comparison minimizes the effect of 60 Hz picked-up on the well electrode.

A three-pole RC low-pass filter filters the signal to decrease the bandwidth and limit the Johnson noise associated with the recorded signal. I designed the filter to cause a 50 percent attenuation of the recorded signal at 4 KHz. This design was a compromise between attenuating the action potential which has major frequency components between 1 and 5 KHz and limiting the Johnson noise (Figure 7.1f).

A reed relay switches the signal one more time (Figure 7.1g) to remove the large voltage transients that occur during stimulation. After removing the transients, the signal can be further amplified without saturating the amplifiers (Figure 7.1h). The circuit has much less than 10 μV noise overall as measured at the electrode with a 1 M Ω resistor substituted for an electrode. The 60 Hz pick-up is also less than 10 μV .

In Figure 7.2, I provide a complete schematic of the circuit described above.. The first four op amps represent the current source. The well electrodes are electroplated platinum on gold. To prevent any potential deplating from a D.C. potential build up on the electrodes, I have separated the current source from the electrode by a capacitor and grounded each electrode through a 10 M resistor. Op amps 5 and 6 compare the electrode's potential with that of a reference electrode in the bath and amplify the output 11 times. The three-pole low-pass filter has each pole at 15 KHz and attenuates the signal by 50% at 4

KHz. Op amp 7 isolates the output of the filter from the final amplifier by providing a high impedance input. Op amp 8 provides the final amplification shown, 100 times, but additional amplifiers can be added if needed.

7.2 Stimulation and recording with wells: success.

7.2.1 Stimulation

I was able to stimulate SCG neurons with the well electrodes. In Figure 7.3, I show two voltage traces recorded with an intracellular glass electrode in a SCG neuron, the neuron is stimulated by a bipolar current pulse from a well electrode. I performed the experiment one day after plating, at which time the SCG neurons have in general sprouted a few processes that are significantly over 100 μm in length. The traces show the voltage recorded when I had stimulated the neuron just above and just below threshold. The recorded potential behaves in an all-or-none manner typical of action potentials. The stimulus current pulse was 1 μA for 0.5 ms in each phase. Stimulus current induced changes in the cell and bath potentials is probably being picked-up by the recording potential in the first two lobes of the recorded trace. To test if this pick-up was likely to stimulate the cell, I attempted to stimulate the cell with a glass pipette using a stimulus pulse of the same magnitude and shape as the pick-up. This stimulus pulse did not fire the cell until the pulse's magnitude had been doubled.

7.2.2 Recording

I was also able to record action potentials evoked by an intracellular pipette with the well electrodes. I show two recorded traces from a well electrode at the top of Figure 7.4. At the bottom of the figure are two superimposed traces from the stimulating (intracellular) electrode. After subtracting the average 60 Hz interference, I redrew the middle trace in

Figure 7.5¹. The subtraction was done by measuring the height of the trace at 23 points during a cycle, over the three cycles before the stimulation, the stimulation cycle and the three cycles after the stimulation. The average height of each time point in the six non-stimulation cycles was subtracted from the height at that point during the stimulation cycle. Figure 7.6 shows the control where the height of the trace at each time point in each non-stimulation cycle is subtracted from the average height of that point in the other five non-

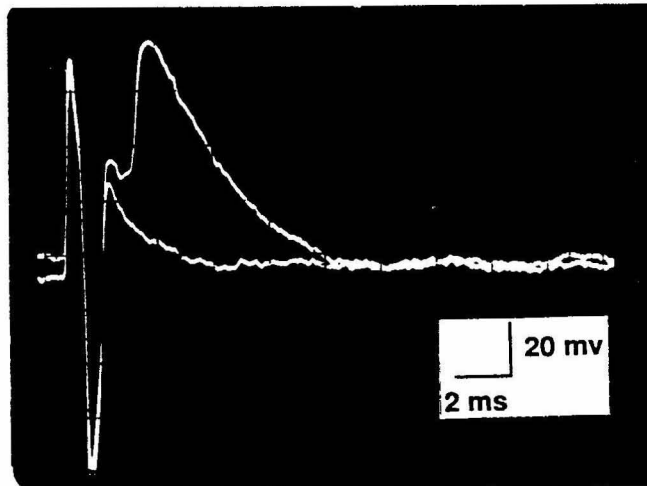


Figure 7.3 *Intracellular recording of an intracellular pipette in a SCG neuron being stimulated by a well electrode.* The top trace is just above threshold, and the bottom trace is just below threshold.

¹ The subtraction was done by measuring the height of the trace at 23 points during a cycle, over the 3 cycles before the stimulation, the stimulation cycle, and 3 cycles after the stimulation. To verify the uniformity of the non-stimulation cycles, the average height of the trace at each time point in the 6 non-stimulation cycles was subtracted from the height of the each time point in the other 5 non-stimulation cycles (Figure 7.6).

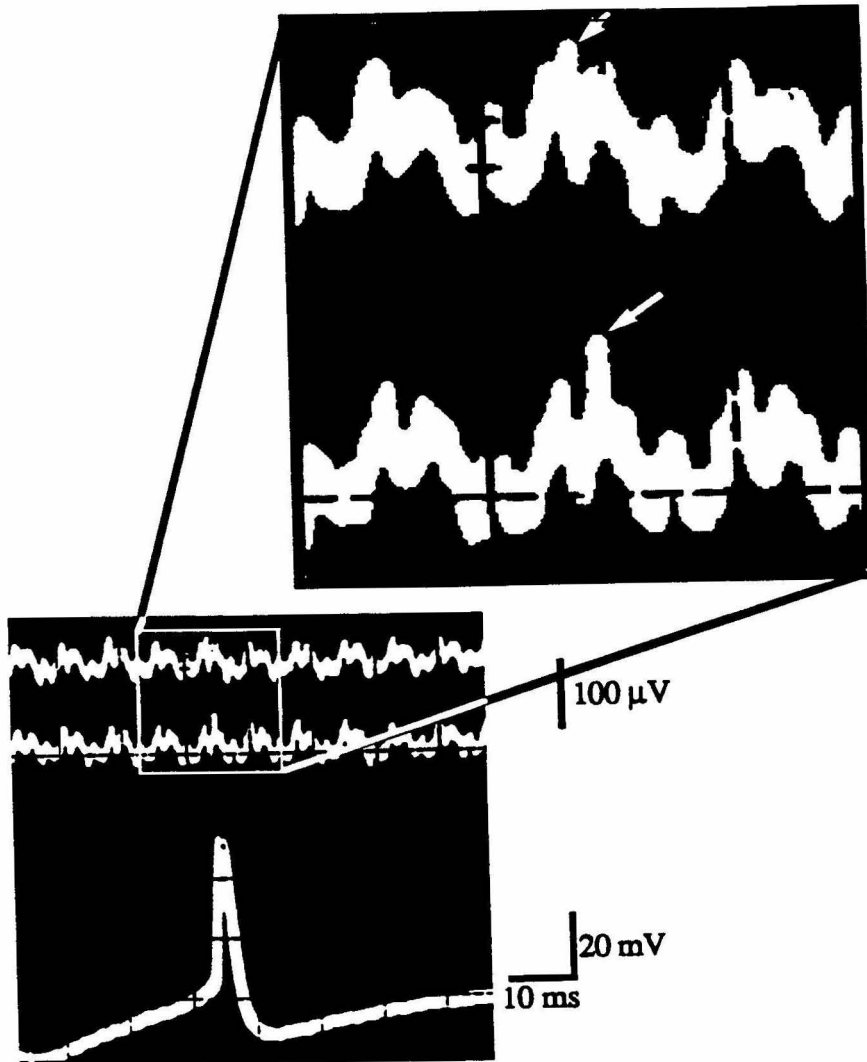


Figure 7.4 Recordings of an action potential with a well electrode evoked by an intracellular electrode. The recorded signal was processed as described above except for the substitution of a 3-pole low-pass filter that attenuates the signal by 50% at 1.4 KHz (not 4 KHz). A blow-up of the recorded action potentials is shown above.

stimulation cycles. For comparison, the equivalent calculation of the stimulus cycle with all six non-stimulation cycles is also plotted.

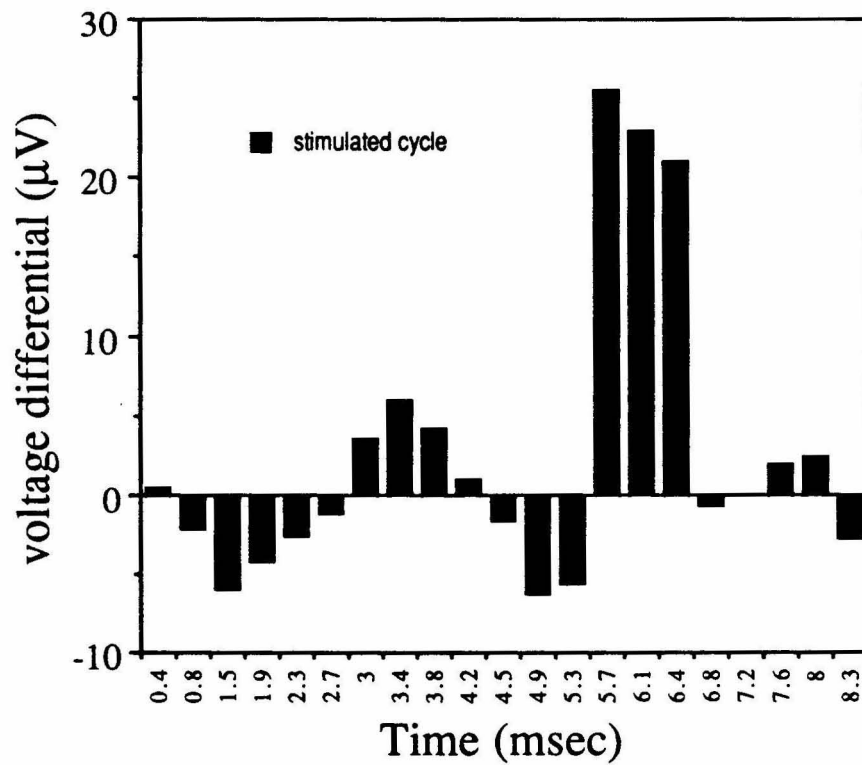


Figure 7.5 Well electrode recording of intracellularly evoked action potential with 60 Hz interference subtracted.

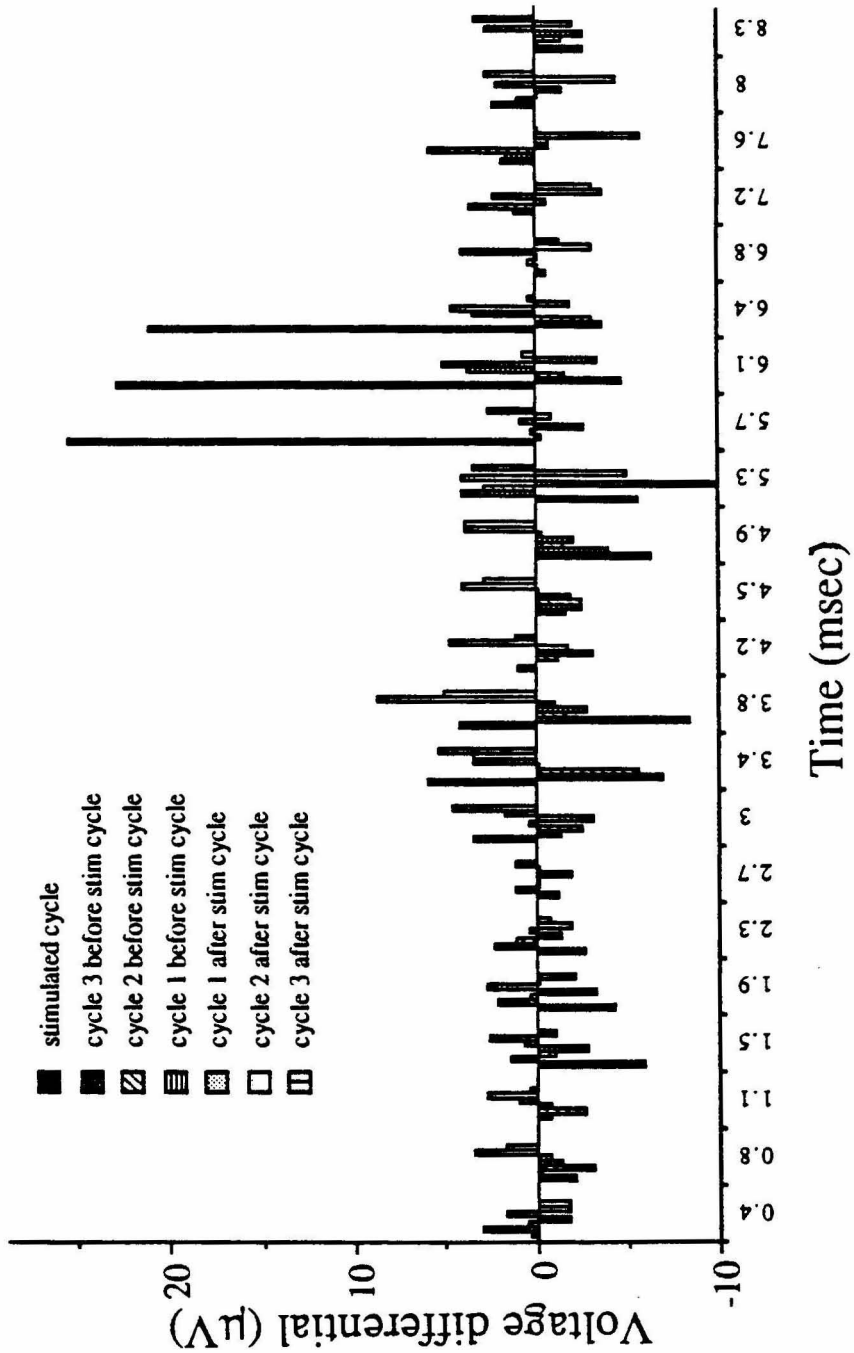


Figure 7.6 Comparison of the subtraction of 60 Hz interference for a trace of a well electrode recording an evoked action potential with that for the three preceding cycles and the three cycles that followed.

I made these recordings made with SCG neurons one day after they had been placed in wells. At this time the neurons had not yet grown to fill the wells; the cells were between 10 and 20 μm in diameter while the wells were 22 μm in diameter. The expected seal resistance of the well was very low, and so as expected the recorded signal was small. Although, older neurons should fill the wells and thus have a higher seal resistance, no measurements were made with more mature cells for two reasons. First, my thesis project, to look at the effect of electrical activity on neurite outgrowth required my studying the cells soon after plating; when the neurons were young. Second, as will be discussed in Section 7.2.3, the stimulus artifact associated with metal electrodes made simultaneous stimulation and recording with the well electrodes difficult. If a 16 bit A-D had been available, computer-based signal processing would have enabled me to continue this experiment. The unavailability of the computer-based signal processed inspired me to proceed with the experiments described in Chapters 1-4 instead of pursuing experimentation with the well electrodes.

7.2.3 Simultaneous Stimulation and Recording

I was not able to stimulate and record with the same electrode simultaneously because of the large, slow decay of the stimulation voltage. The residual stimulation voltage was large and slow to decay because the well electrodes are high impedance capacitive devices. Because the well electrodes are primarily capacitive, an applied current remains stuck on the electrode after the stimulus pulse ends. If a single phase pulse is used for stimulation, the electrode will have a large voltage left on it at the end of the stimulation pulse. This charge decays according to the time constant of the electrode. For our platinized electrodes this time constant is typically about 1 ms. To see a 100 μV evoked action potential when the stimulus pulse leaves 1 V on the electrode, about 80 ms would have to elapse. After 80 ms the voltage on the electrode will have discharged to less than 4

mV, (the point that 100 μ V could be seen on the oscilloscope). Unfortunately, an evoked action potential typically occurs about 4 ms or less after the end of stimulation.

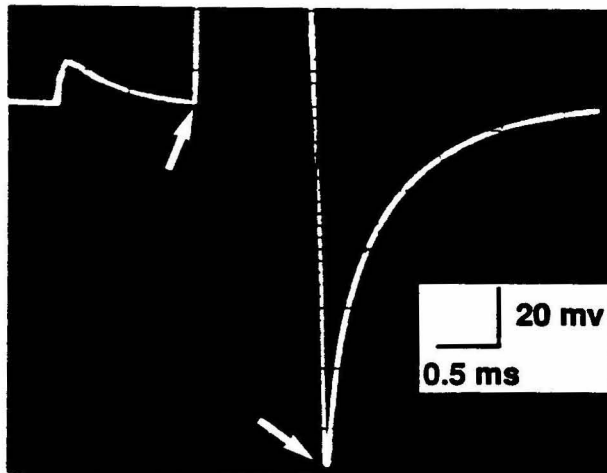


Figure 7.7 Typical voltage decay after a stimulation pulse has been evoked by a well electrode with a symmetric bipolar pulse. Arrows show start and end of stimulus pulse.

7.3 Solutions

7.3.1 Zero Residual Charge

Fortunately, there are many ways for me to reduce the residual charge on the electrode at the end of the stimulus pulse. I can stimulate with a biphasic pulse that leaves no net residual charge on the electrode at the end of the stimulation pulse. For instance, an 1 ms 1 μ A stimulating current pulse will leave 1 V on the electrode, but a symmetric 1 μ A, 0.5 ms biphasic stimulating pulse will leave only about 160 mV. I can further reduce this residual voltage with an asymmetric bipolar pulse.

Unfortunately, an asymmetric stimulation pulse can reduce but not completely eliminate the electrode potential at all times after stimulation. This limitation is due to a second, faster decaying component of the signal caused by the gating charge of the reed relay. The non-linear behavior of the electrode further complicates attempts to minimize the electrode potential. The electrode can not be modeled as an RC circuit. The non-linearity precluded me from completely canceling the gating charge and the stimulus decay with analog methods.

It is impossible to completely discharge the well electrodes at the time of the evoked action potential because of the non-linear behavior of the well electrodes. In Figure 7.8, I show five attempts at balancing a bipolar stimulating current to leave zero voltage on the electrode at the end of stimulation. The family of traces represents the effect of increasing or decreasing the magnitude of the second lobe of the bipolar stimulation pulse. For a given electrode, I can adjust the stimulation pulse to minimize but not eliminate the voltage on the electrode at a given time after the end of stimulation.

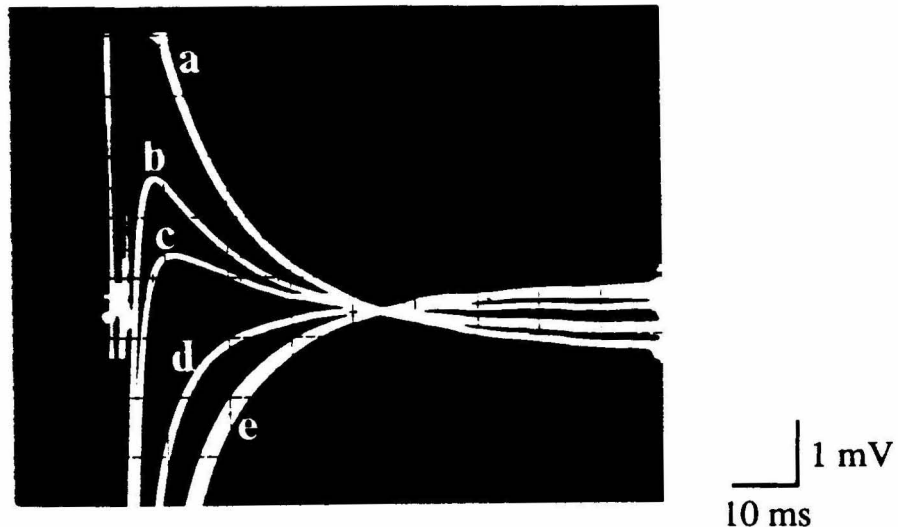


Figure 7.8 Attempts at leaving zero voltage on the electrode at the end of a bipolar stimulating pulse. The magnitude of the second half of the pulse increased from a to e.

7.3.2 Impractical Methods to Achieve Simultaneous Stimulation and Recording

To discriminate small action potentials in large capacitive decays I could use either analog or digital strategies. Analog strategies include filters, cut-offs and subtraction. Digital strategies also include filters, cut-offs and subtraction or they could involve more advanced signal processing such as deconvolving the digitized signal against the expected action potential waveform.

Filtering is the easiest strategy to implement. Unfortunately, the frequency components of the capacitive tail and the recorded action potential are similar. This similarity makes the elimination of the capacitive tail without eliminating the action potential nearly impossible with analog filters. I did not attempt to use digital deconvolution because I did not have access to a method of digitizing the signal with sufficient fidelity.

A second signal processing strategy is to monitor the electrode potential only when I expect the action potential to occur. This strategy allows me to amplify the signal after most of the stimulation artifact has decayed. I can thus use much higher gain amplifiers without saturating downstream processing components, such as amplifiers, oscilloscopes, or analog to digital (A to D) inputs. I use the same strategy to disconnect the noisy current source from the electrode during recording. I implement these disconnects with reed relays.

A third strategy, I attempted to use was to subtract the capacitive decay. A voltage decaying through one or more RC filters will easily mimic the RC decay of a potential on a linear electrode. To minimize the capacitive potential on an electrode, I could subtract this ideal RC filtered potential from the electrode potential. The well electrodes, however, can not be modeled by linear circuits since the capacitance decay is both time and electrode dependent. Therefore, it is cumbersome to match the decay of a given electrode with even three experimentally adjusted RC circuits.

7.3.3 Digital Subtraction :the Method of Choice

I could also do a subtraction after first digitizing the recorded signal. The digitized signal can be subtracted from either a simulated signal or another recorded signal. Subtracting a simulated signal is equivalent to subtracting an analog RC signal but the filter parameters can be calculated by the computer rather than by the experimenter. Alternatively, I would choose to subtract the signal from the previous stimulation pulse. The electrode decay should be similar between traces but the time between the stimulation and the action potential will vary. Both the positive action potential from the current trace and an inverted action potential from the previous trace will be seen.

The digitization of the signal can be done by importing the data into a computer with a 16 bit A to D converter. I was able to routinely minimize the magnitude of the capacitive transient to 50 to 150 mV any time greater than 1 ms after the end of a stimulus pulse using the electronics drawn in Figures 7.1 and 7.2. The A to D converter must have a input range of greater than 1 in 60,000 for the 20 μ V signal to be described by at least 3 bits on 150 mV capacitive artifact. Therefore, a 16 bit rather than a 12 bit A to D converter is both adequate and required.

7.4 Summary of Attempt to Record an Action Potential Elicited with a Well Electrode.

Well electrodes can stimulate and record from SCG neurons (Figures 7.3 and 7.4). Recording an action potential elicited with a well electrode is difficult because of the large capacitive stimulus artifact. There are two potential strategies for recording an evoked potential: increase the size of the signal or improve the recording system. My recorded signal represent the worst case (the smallest expected signals) since the cells were young

and did not fill the wells or even sit on the bottom yet. Allowing the cells to grow should increase the magnitude of the recorded signal.

The second strategy, improving the recording system, is best achieved by importing the data into a computer with a 16 bit A to D converter and subtracting each trace from the preceding trace. Suitable analog input devices are commercially available. In fact, an MIO16X ADC board has recently been acquired by the laboratory for the continuation of this project. The new ADC board will be used either as described above or with a modified digital subtraction scheme (Pine et al., 1991).

References

- Chien, C.B. (1990) Voltage-sensitive dye recording from networks of cultured neurons. Thesis from California Institute of Technology.
- Pine, J. (1980) Recording action potentials from cultured neurons with extracellular microcircuit electrodes. *J. Neurosci Meth.* 2:19-31.
- Pine, J., Tai, Y-C., Tatic, S., Kaiser, W.J., Kenny, T.W., Rochstad, H.K., Buzsaki, G., and Horvath, S. (1991) Cultured neuron probe. Quarterly Progress Report No. 4 Contract No. NO1-NS-0-2383.

Chapter 8

The Future for Well Electrodes

We designed and built the well electrodes to allow long-term connections between neurons and electrodes which could be used to both stimulate and record from an entire small network of neurons for upwards of one month. The devices are sized to snugly fit individual SCG neurons about one week after plating, but still allow the transport of the freshly plated cell into the well. The electrodes themselves are gold electroplated with platinum black. We made the rest of the wells from layers of polyimide on a glass coverslip. The wells are very durable. They are able to survive repeated use and storage in a saline environment up to at least six months. Neonatal rat SCG neurons once maneuvered into a well will survive in the well for six weeks or longer. We could use individual electrodes for both recording from and stimulating a neuron, though additional hardware is needed to record an action potential evoked by the recording electrode. The wells promise to allow a researcher to study the same set of neurons continuously or repeatedly for more than a month.

A few problems impede the continued use of the well electrodes. The two largest impediments are the inability to record an action potential elicited by the stimulating electrode, and the difficulty attached to maneuvering cells into the wells. As discussed in Chapter 7, the recent acquisition of a 16 bit A to D converter and associated hardware and software should solve the former problem. The second problem is more intractable.

After extensive experimentation, we were able to move SCG neurons into wells with a modicum of success. On the best days 50% of the cells moved into wells on a single dish (out of four to six dishes attempted) would survive moving and remain trapped. On that dish typically I had moved eight to ten cells (four to five cells survived). On the other dishes, often, not a single cell survived in a well. On other days, few if any cells

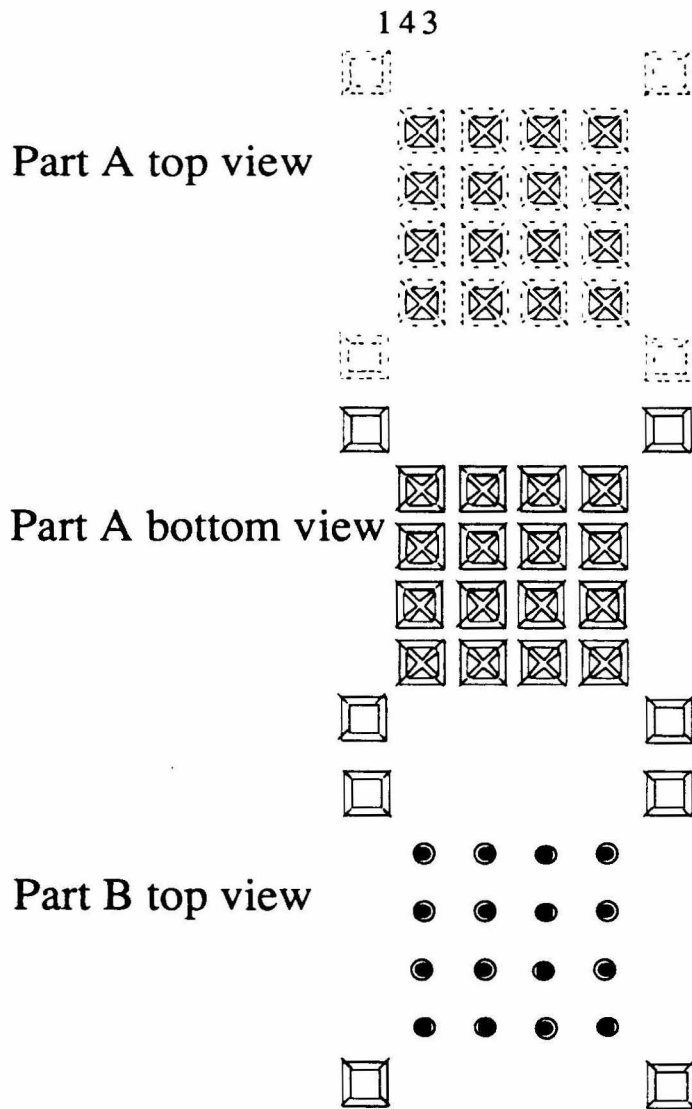
would survive the manipulation. This rate of success is unacceptable. I view the extreme difficulty of moving cells into wells as the single largest impediment to working with the wells.

8.1 Solutions: Easy Loading Designs

To overcome the difficulty of moving cells into wells, I propose two new designs. The first design is a two piece gluable well assembly and the second design has a sliding and locking grillwork over the top of the wells. Both of these designs have the neurons entering the well before the overlying grillwork is added. Since the grillwork will be missing, the open area through which the cell must enter is 22 μm diameter or 380 μm^2 opening versus the current 10-15 μm square or 225 μm^2 opening. I believe that this enlargement would minimize the difficulty of moving cells into wells since I found that it is easier to fill larger wells (30 μm square with 18 μm diameter top openings). I also saw wells fall and stick to the bottom of uncovered wells. With the well designs described below, I can hopefully avoid moving individual cells into wells altogether or minimized to movement to a simple sweeping motion. Because can easily be moved into open wells, open wells should represent a significant advantage over the present design. This improvement will need to precede widespread acceptance of the wells.

8.1.1 Two-Piece Wells

I illustrate one method for building closable wells in Figure 8.1. Each well is a large open divot in a silicon substrate. The grillwork is located at and forms the bottom of each divot. If the substrate is silicon and the grillwork is either silicon dioxide or silicon



Crossection of the assembled probe
Part A is on top.

Figure 8.1 *Two piece construction of well electrodes.* Part A contains the well and the grillwork. Part B contains the electrodes and leads. The two pieces are brought together and glued with a UV setting paste. The paste can be applied to a false well so that the glue can be exposed through the transparent grillwork layer at the surface of the wells. The cross section shows the two pieces after they have been glued together, a neuron fills one of the wells.

oxynitride, the grillwork should serve as both the etch stop and bottom of the well. The second piece or cover will both trap the cells and include the electrodes. Separating the electrodes and the wells into two different structures will allow each to be both more intricate and simpler to fabricate. For instance, I illustrate one possible cup-shaped electrode configuration in Figure 8.1. Each of the pieces will be simpler to manufacture than the current well electrodes. After fabrication the neurons will be plated into the wells and the two pieces will be glued together. Little or no moving of individual neurons should be necessary.

8.1.2 Ratcheted Wells

I illustrate a second possible method for building the closable wells in Figure 8.2. In this configuration, the researcher will lock the grillwork over each well after it has been filled with a cell. At the start of the experiment, the grillwork is next to but not on top of the wells. After the wells have been filled the grillwork is slid over the top of the well. A ratcheted mechanism in the guide prevents the grillwork from returning to their original positions.

These wells like those shown in Figure 8.1 would be made from silicon rather than glass and polyimide. The grillwork will be manufactured using sacrificial layer technology similar to the devices described by (Delapierre, 1989).

145

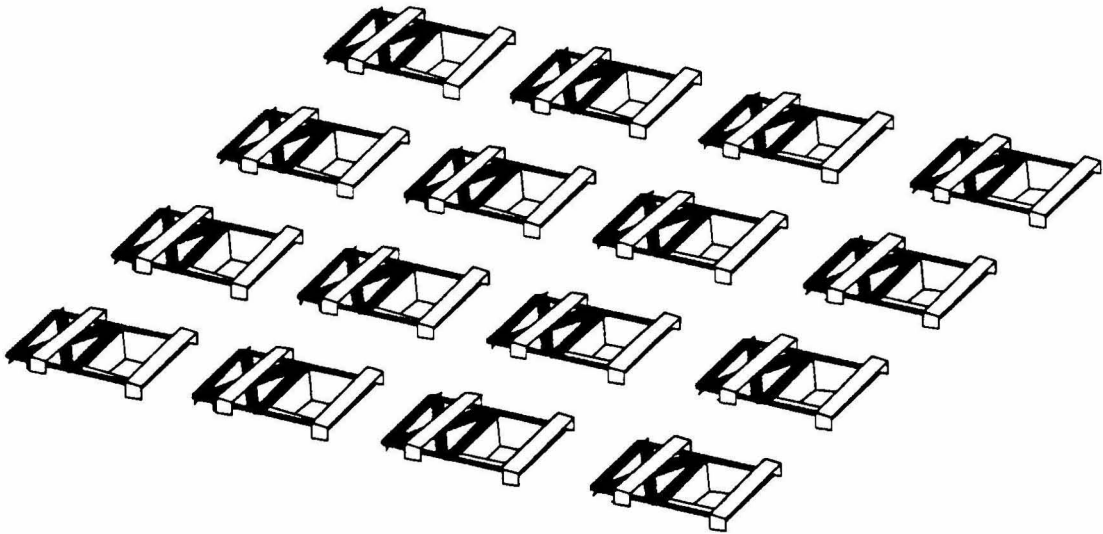


Figure 8.2 *Easy loading wells with ratchets.* Cells are plated on to the dish covered with 16 wells when the wells are in the open (as shown) position. After cells are placed in the wells, the grillwork assembly is gently pushed over the wells to seal the cells in place. The electrodes (not shown) are located at the bottom of the wells.

8.2 Neural Probes

Both of the above designs could also be drawn as probes (Figures 8.3 and 8.4). The well electrodes are envisioned to eventually be used in vivo as prostheses. As a prosthetic, the electrodes will connect the stimuli with the transducer neurons trapped within the wells. These transducer neurons, in turn, will grow out and connect to the target neurons within the brain. Because neurons are actually an integral part of the device, we expect the connections between the device and the brain to be synaptic rather than extracellular. Because of the synaptic connections, the device should have greater selectivity in its connection with the brain than extracellular devices. We will choose transducer neurons on the basis of their expected synaptic specificity.



Figure 8.3 *Two-piece wells on a probe.* Cross section through an assembled two piece probe.

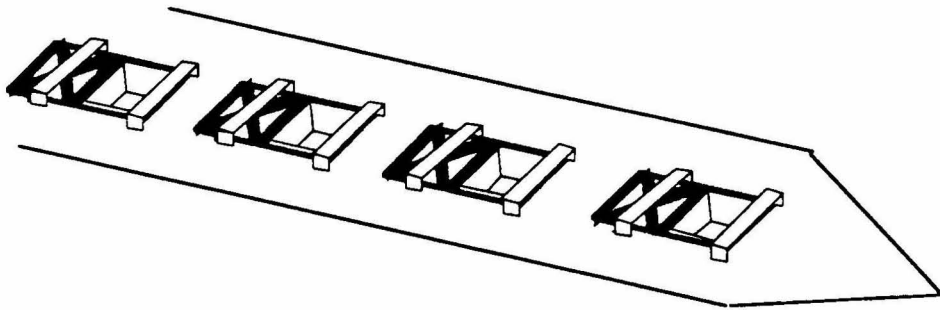


Figure 8.4 *Racheted wells on a probe.*

8.3 Summary

The neuronal wells hold a tremendous promise for enabling researchers to stimulate and record from neurons chronically or repetitively. With the electronics built to date, the wells can stimulate and record action potentials from neurons. Some additional basic signal processing will enable the wells to record and stimulate neurons concurrently. The greatest problem associated with using the wells currently is that it is difficult to move cells into the wells. The designs proposed in this chapter should mitigate this problem. Once we address these two problems, the wells should prove valuable both in culture and as a neuronal prosthetic for developmental studies, behavioral monitoring, and possibly as a treatment for some pathologies.

References

Delapierre, G. (1989) Micro-machining: A survey of the most commonly used processes. *Sensors and Actuators* 17:123-138.

Appendix A

Step by step instructions to microfabricate the well electrodes.

- 1) Clean 25mm square glass coverslips:
 - sonicate ten minutes in TCE
 - sonicate ten minutes in acetone
 - sonicate five minutes in ethanol
 - rinse three times in distilled water
 - blow off with nitrogen and bake for five minutes at 200 °C to dry

- 2) Make the lead pattern by lift off:
 - spin on 1350J positive photoresist at 4000 RPM for 30 sec.
 - soft bake at 85 °C for 25 minutes
 - expose resist for ten seconds at 11.2 mW/cm²
 - soak in chlorobenzene for ten minutes
 - blow dry and bake at 125 °C for five minutes
 - develop for three and a half minutes in 50% AZ developer
 - evaporate 70 Å Cr, 1000 Å Au, and 70 Å Cr on to the surface
 - complete liftoff by sonicating in acetone for five to ten minutes
 - rinse in ethanol
 - rinse three times in dH₂O
 - blow dry and bake for five minutes at 200 °C to dry

- 3) Make the adhesion layer
 - evaporate 30 Å of aluminum on to the surface

- 4) Make the contacts
 - spin on Selectilux 50 at 2500 RPM for 20 seconds
 - smooth edge bead at room temperature for five minutes
 - bake at 85 °C for 20 minutes uncovered
 - expose through the back for 25 seconds at 11 mW/cm²
 - expose through a protector mask for 25 seconds at 11 mW/cm²
 - develop by hand in a bath for 20 seconds
 - bake for 10 minutes at 200 °C

- 5) Make mask for back exposure of wells
 - prepare lift-off by spinning on 1350J at 4000 RPM for 30 seconds
 - bake for 25 minutes at 85 °C
 - expose for 15 seconds at 11 mW/cm²
 - soak 10 minutes in chlorobenzene
 - blow dry with nitrogen
 - bake five minutes at 125 °C
 - develop in 50% AZ developer for four minutes
 - evaporate 200 Å Cr and 1000 Å Au
 - sonicate in acetone for about ten minutes
 - rinse in ethanol
 - rinse three times in distilled water
 - bake at 200 °C for five minutes

- 6) Make the wells
 - spin on Selectilux 200 at 2200 RPM for 20 seconds
 - smooth edge bead 20 minutes at room temperature
 - bake at 85 °C for 30 minutes in an open petri dish
 - back expose 135 seconds at about 12 mW/cm²
 - develop by gently waving in developer for sixty seconds
 - bake ten minutes at 200 °C

- 7) Optional: Define top of well more carefully:
 - spin on Selectilux 50 for 20 seconds at 5000 RPM
 - let sit five minutes at room temperature
 - bake ten minutes at 85 °C in an open petri dish
 - expose with "top cell well mask" for 30 seconds at 12 mW/cm²
 - develop by hand for 15 seconds
 - bake to partially cure for ten minutes at 200 °C

- 8) Remove Au and Cr in bottom of the well
 - protect the exposed outer leads by pointing on 1350J
 - bake ten minutes at 135 °C
 - soak water in gold etch for two minutes
 - check the bottom of the well, it should look translucent
 - remove photoresist by sonicating with acetone
 - rinse in ethanol
 - rinse in dH₂O
 - etch with chrome etchant for three minutes
 - rinse in 2% H₂SO₄
 - rinse three times in distilled water

9) Make the grillwork

spin on Selectilux 50 at 5000 RPM for 20 seconds

let sit five minutes at room temperature

bake for ten minutes at 85 °C in an open dish

expose through the well mask for 11.5 seconds at about 12 mW/cm²

develop for just fifteen seconds

bake overnight at 200 °C to cure the wells

Appendix B

Reconstitution of Signaling in Bacterial Chemotaxis

Alan J. Wolfe, M. Patricia Conley, Tina J. Kramer, and Howard C. Berg

Journal of Bacteriology, May 1987, p.1878-1885.

Reconstitution of Signaling in Bacterial Chemotaxis

ALAN J. WOLFE,[†] M. PATRICIA CONLEY,[†] TINA J. KRAMER, AND HOWARD C. BERG^{†*}

Division of Biology, California Institute of Technology, Pasadena, California 91125

Received 10 November 1986/Accepted 22 January 1987

Strains missing several genes required for chemotaxis toward amino acids, peptides, and certain sugars were tethered and their rotational behavior was analyzed. Null strains (called gutted) were deleted for genes that code for the transducers Tsr, Tar, Tap, and Trg and for the cytoplasmic proteins CheA, CheW, CheR, CheB, CheY, and CheZ. Motor switch components were wild type, *flaAII(cheC)*, or *flaBII(cheV)*. Gutted cells with wild-type motors spun exclusively counterclockwise, while those with mutant motors changed their directions of rotation. CheY reduced the bias (the fraction of time that cells spun counterclockwise) in either case. CheZ offset the effect of CheY to an extent that varied with switch allele but did not change the bias when tested alone. Transducers also increased the bias in the presence of CheY but not when tested alone. However, cells containing transducers and CheY failed to respond to attractants or repellents normally detected in the periplasm. This sensitivity was restored by addition of CheA and CheW. Thus, CheY both enhances clockwise rotation and couples the transducers to the flagella. CheZ acts, at the level of the motor, as a CheY antagonist. CheA or CheW or both are required to complete the signal pathway. A model is presented that explains these results and is consistent with other data found in the literature.

Sensory transduction in bacterial chemotaxis involves receipt of information about the external environment, passage of this information across the cytoplasmic membrane, generation of signals that converge on the flagellar motors, and activation of mechanisms that permit adaptation. The concentrations of certain chemicals are sensed by transmembrane receptors, also called transducers or methyl-accepting chemotaxis proteins (1, 11, 39; for a review, see reference 10). Four transducers are known, one sensitive to aspartate, maltose, and certain repellents (Tar), a second sensitive to serine and certain other repellents (Tsr), a third sensitive to galactose and ribose (Trg), and a fourth sensitive to dipeptides (Tap [17]). Changes in receptor occupancy, through a series of intermediate events that we hope to understand, alter the probability that the flagella spin clockwise (CW) or counterclockwise (CCW). If they spin CW, the cells move erratically with little net displacement (they tumble); if they spin CCW, the cells swim smoothly (they run) (15, 16). If a run happens to carry the cell up a spatial gradient of an attractant (e.g., of aspartate), the probability of CW rotation decreases and the probability of CCW rotation increases (4, 5), extending the run. This enables the cell to move toward a more favorable environment (3).

How is sensory information transferred from the receptors to the flagella? From measurements of signal propagation in filamentous cells, Segall et al. (31) showed that there is an internal signal but that its range is short, only a few micrometers. To explain this limited range, they suggested that the signal is a small protein or ligand that is inactivated as it diffuses through the cytoplasm. CheY was considered to be the most likely candidate (see also reference 27). According to this hypothesis, CheY is activated at the transducers at a rate that is depressed by the binding of attractant. Active CheY enhances CW rotation. A second protein, CheZ, inactivates CheY as it diffuses through the cytoplasm. This hypothesis was consistent with the following facts: (i) strains

defective in *cheY* have a large bias (tend to rotate their flagella CCW [21, 22]); (ii) cell envelope preparations have a large bias (27); (iii) strains lacking transducers have a large bias (29); (iv) addition of attractant increases the bias (15); (v) strains defective in *cheZ* have a small bias (tend to rotate their flagella CW [25]); (vi) strains defective in *cheZ* have a slow response time (4) and a long signal decay length (31); and (vii) analyses of second-site revertants show that CheY and CheZ interact with components of the flagella motor (with FlaAII and FlaBII [26]).

Recent work has directly implicated CheY in the signaling process. Clegg and Koshland (8) overproduced CheY in a strain deleted for the transducers Tar and Tap and all the chemotaxis genes known to code for cytoplasmic products: *cheA*, *cheW*, *cheR*, *cheB*, *cheY*, and *cheZ* (strain RP1091 [24]). In the absence of CheY, the flagella spun CCW; in its presence, they spun CW and could not be switched back by the addition of serine, an attractant that acts through one of the remaining transducers, Tsr. Ravid et al. (28) added various amounts of purified CheY to the medium used to prepare envelopes from cells wild type for chemotaxis. The more they added, the larger the fraction of reconstituted envelopes that spun their flagella CW. However, once a flagellum spun CW, it did so indefinitely. The reconstituted envelopes failed to respond to chemotactic stimuli.

The work described here follows a similar strategy. We constructed a strain that we call "gutted" that is deleted for the four known transducers, as well as for *cheA*, *cheW*, *cheR*, *cheB*, *cheY*, and *cheZ*. We added back subsets of these genes to the gutted strain, or to strains less extensively deleted, via multicopy plasmids or lambda hybrids. We also effected variable control with inducible promoters. We tethered these cells and measured the fraction of time that they spin CCW and their response to certain attractants and repellents. We conclude that CheY is a diffusible signal; its activity is modulated by the transducers and it interacts with the motors. CheZ counteracts the effects of CheY, but it does not appear to be a CCW signal. The transducer and CheY alone are not capable of transmitting information

* Corresponding author.

[†] Present address: Department of Cellular and Developmental Biology, Harvard University, Cambridge, MA 02138.

TABLE 1. Bacterial strains used for constructions

Strain	Relevant genotype	Source or reference and comments
CP177	$\Delta(trg)100::zbd::Tn5$	G. L. Hazelbauer; <i>zbd::Tn5</i> approx. 50% linked to $\Delta(trg)100$
D158 <i>recA</i>	$\Delta(cheY)m60-21$ <i>recA</i>	F. W. Dahlquist
RP1091	$\Delta(cheA-cheZ)2209$	24
RP1131	<i>trg::Tn10</i>	J. S. Parkinson
RP1616	$\Delta(cheZ)6725$	J. S. Parkinson
RP2893	$\Delta(tap-cheZ)2206$	24
RP3000	$\Delta(cheY-cheZ)m43-13$ <i>scyA2 supD metF159(Am)</i>	26; <i>scyA2</i> = <i>flaAII</i> allele
RP3001	$\Delta(cheY-cheZ)m43-13$ <i>scyA3 supD metF159(Am)</i>	26; <i>scyA3</i> = <i>flaAII</i> allele
RP3068	$\Delta(cheY-cheZ)m43-13$ <i>scyB10 supD metF159(Am)</i>	26; <i>scyB10</i> = <i>flaBII</i> allele
RP4979	$\Delta(cheY)m43-10$	J. S. Parkinson
RP5046	$\Delta(cheA-cheB)2229$	24
RP5714	$\Delta(tsr)7021$ <i>mal</i> (λ') <i>eda-50</i>	J. S. Parkinson
RP5838	$\Delta(tar-tap)5201$ $\Delta(tsr)7021$	J. S. Parkinson
RP5854	$\Delta(tar-tap)5201$	J. S. Parkinson

originating in the periplasm. This requires the addition of CheA or CheW or both.

MATERIALS AND METHODS

Chemicals. Restriction enzymes and T4 DNA ligase were obtained from New England BioLabs. Synthetic amino acids were used for chemotaxis assays (12): sodium L-aspartate was purchased from ICN Pharmaceuticals Inc.; L-serine and L-leucine were purchased from K & K Laboratories, Inc. Ampicillin, tetracycline hydrochloride, and kanamycin sulfate were purchased from Sigma Chemical Co. L-Arabinose was purchased from Fisher Scientific Co. Tryptone and agar were from Difco Laboratories. Other chemicals were reagent grade.

Bacterial strains, plasmids, and bacteriophages. All strains were derivatives of *Escherichia coli* K-12 and are listed in Tables 1 and 2. Generalized transductions involved the use of phage P1kc (33). To verify all constructions, complementation was performed as described by Parkinson, except that the strains tested were not lysogenic for λ (22; see method I). A set of λ *che22* mutants that carry missense mutations in each of the chemotaxis genes of interest (generously supplied by J. S. Parkinson) were used for this purpose.

λ gt4-*tar101* was described previously (14). All plasmids

were derivatives of pBR322 and are listed in Table 3. Transformants were constructed as described by Silhavy et al. (33) and are listed in Table 4.

The plasmid pBB1 expresses CheZ under the control of the tryptophan promoter of *Serratia marcescens*. It was constructed by ligation of the *PvuII* fragment of pRL22 (18), which carries most of the *cheZ* gene, to the *PvuII* site of the plasmid pRL22*ΔcheYΔpvuII*. The latter plasmid contains an approximately 50-base-pair deletion centered about the *SalI* site of *cheY* and thus does not express a functional chemotaxis gene product. Expression of CheZ by pBB1 was verified via complementation with a strain deleted for *cheZ* (RP1616).

CheY assay. Estimates were made of the amount of CheY produced in strains containing the plasmid pRL22*ΔpvuII* (Table 3), in which transcription of *cheY* was promoted by *prp*, e.g., HCB328 (Table 4), and in strains containing *cheY* in single copy, in which transcription was promoted by *pmocha*, e.g., HCB350 (Table 2), as compared with the wild type, in which transcription was promoted by *pmeche*, e.g., RP437 (22). Cells were grown in tryptone broth (1 liter), containing an antibiotic when appropriate, and harvested at mid-exponential phase. The following steps were carried out at 4°C. Cells were washed three times in 10 ml of 10 mM

TABLE 2. Bacterial strains constructed for this study

Strain ^a	Relevant genotype	Chemotaxis genes present ^b	P1 construction (parents: relevant selection/screen)
HCB314	$\Delta(tsr)7021$ $\Delta(cheA-cheZ)2209$ <i>mal</i> (λ')	<i>trg</i>	RP1091 × RP5714: <i>Eda</i> ⁻ / <i>Che</i> ⁻
HCB315	$\Delta(tsr)7021$ $\Delta(cheA-cheZ)2209$ <i>mal</i> ⁻ (λ')	<i>trg</i>	RP5838 × HCB314: <i>Mal</i> ⁻ / λ'
HCB316	$\Delta(tsr)7021$ $\Delta(tar-tap)5201$	<i>trg cheAWRBYZ</i>	RP5854 × HCB317: <i>Eda</i> ⁻ / <i>Che</i> ⁻
HCB317	$\Delta(tsr)7021$ <i>mal</i> ⁻ (λ')	<i>trg tar tap cheAWRBYZ</i>	RP5838 × RP5714: <i>Mal</i> ⁻ / λ'
HCB326	$\Delta(tsr)7021$ $\Delta(cheA-cheZ)2209$ <i>trg::Tn10</i>	None	RP1131 × HCB315: <i>Tc</i> ^r
HCB339	$\Delta(tsr)7021$ $\Delta(tar-tap)5201$ <i>trg::Tn10</i>	<i>cheAWRBYZ</i>	RP1131 × HCB316: <i>Tc</i> ^r
HCB349	$\Delta(tsr)7021$ $\Delta(tap-cheZ)2206$	<i>trg tar cheAW</i>	RP2893 × HCB317: <i>Eda</i> ⁻ / <i>Che</i> ⁻
HCB350	$\Delta(tsr)7021$ $\Delta(cheA-cheB)2229$	<i>trg cheYZ</i>	RP5046 × HCB317: <i>Eda</i> ⁻ / <i>Che</i> ⁻
HCB429	$\Delta(tsr)7021$ $\Delta(tar-tap)5201$ $\Delta(tar)100$ <i>zbd::Tn5</i>	<i>cheAWRBYZ</i>	CP177 × HCB339: <i>Kn</i> ^r / <i>Tc</i> ^r
HCB433	$\Delta(tsr)7021$ $\Delta(trg)100$ <i>zbd::Tn5</i>	<i>tar tap cheAWRBYZ</i>	CP177 × HCB317: <i>Kn</i> ^r /galactose-blind
HCB437	$\Delta(tsr)7021$ $\Delta(trg)100$ <i>zbd::Tn5 $\Delta(cheA-cheZ)2209$ <i>metF159(Am)</i></i>	None	RP1091 × HCB433: <i>Eda</i> ⁻ / <i>Che</i> ⁻ and <i>Kn</i> ^r
HCB482	$\Delta(tsr)7021$ $\Delta(trg)100$ <i>zbd::Tn5 $\Delta(cheA-cheZ)2209$ <i>scyA2 supD metF159(Am)</i></i>	<i>flaAII</i> (<i>scyA2</i>)	RP3000 × HCB437: <i>Met</i> ⁻ /tumbly
HCB483	As HCB482 except <i>flaAII</i> (<i>scyA3</i>)	<i>flaAII</i> (<i>scyA3</i>)	RP3001 × HCB437: <i>Met</i> ⁻ /tumbly
HCB484	As HCB482 except <i>flaBII</i> (<i>scyB10</i>)	<i>flaAII</i> (<i>scyB10</i>)	RP3068 × HCB437: <i>Met</i> ⁻ /tumbly
HCB527	$\Delta(tsr)7021$ $\Delta(tap-cheZ)2206$ <i>flaAII</i> (<i>scyA2</i>)	<i>trg tar flaAII</i> (<i>scyA2</i>) <i>cheAW</i>	RP3000 × HCB349: <i>Met</i> ⁻ /tumbly

^a The initials used to identify the strains constructed in this laboratory have been changed from HB to HCB.

^b Out of the set *tsr*, *trg*, *tap*, *cheAWRBYZ*, unless otherwise noted.

TABLE 3. Plasmids

Plasmid	Relevant genotype ^a	Source and comments
pRL22	<i>pirp-cheYZ</i>	18
pRL22 Δ <i>pvuII</i>	<i>pirp-cheY</i>	P. Matsumura
pRL22 Δ <i>cheY</i> Δ <i>pvuII</i>	<i>pirp-Δ(cheY)</i>	P. Matsumura
pBB1	<i>pirp-Δ(cheY)</i> <i>cheZ</i>	This study
pJH120	<i>para-cheY</i>	F. W. Dahlquist; inducible by arabinose
pAK101RI	<i>tar</i>	14

^a *pirp* refers to the tryptophan promoter of *S. marcescens*; *para* refers to the regulatory region of the arabinose operon of *E. coli* B; *tar* is promoted by its native promoter.

MgSO₄, resuspended in 10 ml of the same medium, treated for 10 min with lysozyme (10 μ g/ml), and repeatedly sonicated: large cell fragments were removed by centrifugation at ca. 8,000 \times g for 5 min, and smaller material was removed by centrifugation at ca. 300,000 \times g for 1 h. Samples of supernatant fractions were run on 15% polyacrylamide gels in the presence of sodium dodecyl sulfate, stained with Coomassie blue, and scanned with a densitometer (LKB 2202 run at 633 nm). The integrated optical densities of the CheY peaks for strains HCB328 and HCB350 (less the background owing to a small amount of other protein observed for the gutted strain HCB326) were about 3.8 and 0.7 times larger, respectively, than that for strain RP437.

Swarm plates. Cells (5 μ l of a stationary culture) were inoculated at the center of a plate containing tryptone broth in 0.3% agar. Antibiotics and L-arabinose were added when appropriate. The plates were incubated at 30°C in a moist environment.

Tethered cells. Cells were grown in tryptone broth at 30°C. When strains contained plasmids, inocula were taken from stocks stored in 10% dimethyl sulfoxide at -70°C, and the

broth was supplemented with the appropriate antibiotic. When strains did not contain plasmids, inocula also were taken from saturated cultures; the behavior of the cells was the same in either case. In experiments involving induction, cultures were grown to saturation in the absence of arabinose and then diluted 1:100 into fresh broth containing the desired concentration of L-arabinose; both media contained ampicillin. All cultures were harvested at mid-exponential phase, washed, and tethered as described by Block et al. (4), except that the motility buffer was 10 mM potassium phosphate (pH 7)–67 mM NaCl–10 mM sodium lactate–0.1 mM disodium EDTA–0.001 mM L-methionine. Neither antibiotics nor arabinose was added to the motility buffer.

Data acquisition and analysis. The cover slip to which cells were tethered was mounted on a flow cell (2) on the stage of a phase-contrast microscope. The behavior of the cells was recorded at room temperature before and after shifts to motility buffer containing attractants or repellents. The data were recorded on videotape and analyzed by computer, as described elsewhere (2a). This system allowed us to detect essentially every transition between CW and CCW states and to carry out a complete statistical analysis. Estimates of bias (the fraction of time that a cell spins CCW, i.e., that it turns its flagella CCW) and of reversal rate (the number of CW-to-CCW and CCW-to-CW transitions per second) for a given culture were based on averages of data spanning about 180 s for each of 10 to 34 cells.

RESULTS

The null phenotype. The gutted strains (HCB326 [Fig. 1] and HCB437 [Table 5]) rotated exclusively CCW. In both strains the bias was 1.0 and the reversal rate was zero. No reversals were detected in 20 cells monitored for periods averaging 180 s. No reversals occurred in response to

TABLE 4. Bacterial strains containing plasmids or phage or both

Strain	Parent ^a	Plasmid or phage ^b	Chemotaxis genes present ^c
D158 <i>recA</i> (pJH120)	D158 <i>recA</i>	pJH120	<i>trg tsr tar tap cheAWRBZ para-cheY</i>
HCB328	HCB326	pRL22 Δ <i>pvuII</i>	<i>pirp-cheY</i>
HCB330	HCB315	pRL22 Δ <i>pvuII</i>	<i>trg pirp-cheY</i>
HCB332	HCB315	λ gt4- <i>tar101</i>	<i>trg tar</i>
HCB334	HCB332	pRL22 Δ <i>pvuII</i>	<i>trg tar pirp-cheY</i>
HCB338	RP1091	pRL22 Δ <i>pvuII</i>	<i>trg tsr pirp-cheY</i>
HCB351	HCB350	pRL22 Δ <i>pvuII</i>	<i>trg cheYZ pirp-cheY</i>
HCB449	HCB437	pRL22	<i>pirp-cheYZ</i>
HCB450	HCB437	pRL22 Δ <i>pvuII</i>	<i>pirp-cheY</i>
HCB465	HCB437	pJH120	<i>para-cheY</i>
HCB475	HCB465	λ gt4- <i>tar101</i>	<i>tar para-cheY</i>
HCB488	HCB483	pRL22	<i>pirp-cheYZ</i>
HCB490	HCB482	pRL22 Δ <i>pvuII</i>	<i>flaAII(scvA2) pirp-cheY</i>
HCB491	HCB483	pRL22 Δ <i>pvuII</i>	<i>flaAII(scvA3) pirp-cheY</i>
HCB492	HCB484	pRL22 Δ <i>pvuII</i>	<i>flaBII(scvB10) pirp-cheY</i>
HCB493	HCB482	pBB1	<i>flaAII(scvA2) pirp-cheZ</i>
HCB494	HCB483	pBB1	<i>flaAII(scvA3) pirp-cheZ</i>
HCB496	HCB482	pRL22 Δ <i>cheY</i> Δ <i>pvuII</i>	<i>flaAII(scvA2)</i>
HCB497	HCB483	pRL22 Δ <i>cheY</i> Δ <i>pvuII</i>	<i>flaAII(scvA3)</i>
HCB499	HCB482	pAK101RI	<i>flaAII(scvA2) tar</i>
HCB500	HCB483	pAK101RI	<i>flaAII(scvA3) tar</i>
HCB501	HCB484	pAK101RI	<i>flaAII(scvB10) tar</i>
HCB525	HCB349	pJH120	<i>trg tar cheAW para-cheY</i>
HCB526	HCB429	λ gt4- <i>tar101</i>	<i>tar cheAWRBYZ</i>
HCB529	HCB527	pJH120	<i>flaAII(scvA2) trg tar cheAW para-cheY</i>

^a See column 1 or Table 2.

^b See Table 3.

^c See Table 2, footnote b.

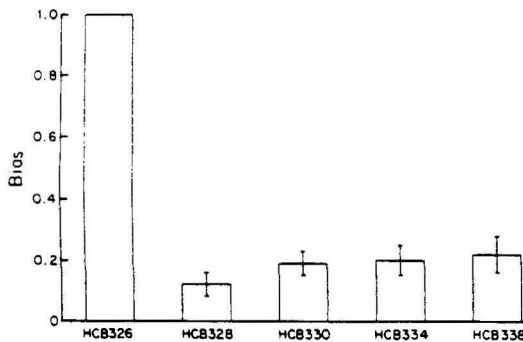


FIG. 1. The bias of a gutted strain (HCB326), that of the same strain containing a plasmid in which CheY is expressed via the tryptophan promoter of *S. marcescens* (HCB328), and those of strains containing this plasmid but not deleted for *irg* (HCB330), *irg* and *tar* (HCB334), or *irg* and *tsr* (HCB338). The error bars represent the standard error of the mean for the cell population.

repellents (1 mM Ni²⁺, 10 mM L-leucine, shifts from pH 7 to 6, or 10 mM sodium acetate at pH 6).

CheY. CheY was required for CW rotation in both the wild type and gutted background. Strain RP4979, deleted only for *cheY*, exhibited the null phenotype: its bias was 1.0, its reversal rate was zero, and it did not respond to repellents (Table 5). CW rotation was restored to the gutted strain upon addition of a multicopy plasmid in which *cheY* was under the control of the tryptophan promoter (Fig. 1, HCB328; Table 5, HCB450). These cells spent most, but not all, of their time spinning CW. Unlike the situation for reconstituted cell envelopes (28), reversals still occurred. In general, CheY decreased the CW-to-CCW transition rates (lengthened tumbles) and increased the CCW-to-CW transition rates (shortened runs), as noted in the last two columns of Table 5. Both HCB328 and HCB450 failed to respond to attractant (100 μ M aspartate) or repellent (1 mM Ni²⁺). A small decrease in bias was observed following shifts from pH 7 to 6 and upon addition of 10 mM sodium acetate at pH 6. However, this decrease was delayed, developing gradually over a few minutes.

Expression of CheY over a wide range was obtained by using a plasmid (pJH120) in which *cheY* is under the control of the arabinose promoter. The bias and reversal rate of the resultant strain (HCB465) are plotted as a function of arabinose concentration in Fig. 2A and B. As the concentration of arabinose increased, the bias and reversal rate approached the values obtained with strain HCB450. As before, CW intervals lengthened and CCW intervals short-

ened (data not shown). In the absence of arabinose, the cells spun exclusively CCW but responded to the addition of 10 mM sodium acetate at pH 6, indicating that some CheY must have been present. Additional evidence for the presence of CheY in cells grown without arabinose was obtained by using strain D158*recA*(pJH120), which contains the same plasmid and which is deleted only for *cheY*. These cells, when grown in swarm plates in the absence of arabinose, produced well-formed chemotactic rings approximately 80% as large as those found with a wild-type control (HCB526; data not shown).

Transducers and CheY. To test the effect of transducer upon the behavior of CheY-containing cells, the plasmid pRL22 Δ *pvuII* was transformed into strains which carried single copies of the transducer genes *irg*, *trg* and *tar*, or *irg* and *tsr*, to yield strains HCB330, HCB334, and HCB338, respectively. All three strains had a bias greater than that exhibited by HCB328 (Fig. 1). This difference was small but appeared to be related to the amount of transducer present. To verify this effect, a λ gt4-*tar101* lysogen of strain HCB465 was constructed (strain HCB475). The bias and reversal rate of HCB475 are plotted as a function of arabinose concentration in Fig. 2A and B. The presence of Tar resulted in an increase in bias and a decrease in reversal rate (compare strains HCB465 and HCB475). While the standard errors of the means for the aggregate data were relatively large (not shown), the mean bias of HCB475 cells was always greater than that of HCB465 cells tethered on the same day. The difference between these means was generally larger than the sum of their standard errors. All of the above strains decreased their bias when the pH was shifted from 7 to 6 or when 10 mM acetate was added at pH 6 (data not shown). As before, this change in bias developed gradually.

Tar. To rule out the possibility that the shifts in bias effected by Tar were due to an interaction of Tar and the motor not involving CheY, we repeated some of the above experiments in gutted strains that contained either the *flaAII(cheC)* allele *scyA2* or *scyA3* or the *flaBII(cheV)* allele *scyB10*. These alleles were isolated as second-site mutations from different pseudorevertants of a single strain defective in *cheY* (26). They are thought to be cause defects in components of the motor that control its direction of rotation (so-called switch components). Even in the gutted background (HCB482, HCB483, and HCB484; Table 6), these alleles enabled the cells to spin alternately CW and CCW and thus permitted us to test for CCW shifts in the absence of CheY. CheY significantly decreased the bias in all three constructs (HCB490, HCB491, and HCB492; Table 6). This is not surprising, given that the pseudorevertants retain some chemotactic activity in the wild type background (26). That activity, and the bias in the wild type and *ptrp-cheY* backgrounds, fall in the same order: *scyA3* > *scyA2* > *scyB10*. In the absence of CheY, Tar (carried by pAK101RI)

TABLE 5. Behavior of reconstituted strains with wild-type flagellar motors^a

Strain	Chemotaxis genes present ^a	Bias	Reversal rate (s ⁻¹)	k_c (s ⁻¹)	k_{cc} (s ⁻¹)
HCB437	None	1	0	>180	<.01
RP4979	All but <i>cheY</i>	1	0	>180	<.01
HCB450	<i>ptrp-cheY</i>	0.17 \pm 0.14	1.27 \pm 0.96	1.29 \pm 1.11	46.8 \pm 25.6
HCB449	<i>ptrp-cheYZ</i>	>0.99 \pm 0.00	0.04 \pm 0.01	167.4 \pm 8.7	0.02 \pm 0.01
HCB351	<i>irg cheYZ ptrp-cheY</i>	0.98 \pm 0.01	0.25 \pm 0.12	134.4 \pm 17.8	0.15 \pm 0.08

^a Bias = fraction of time spinning CCW; k_c = CW-to-CCW transition rate; k_{cc} = CCW-to-CW transition rate; reversal rate = number of CW-to-CCW and CCW-to-CW transitions per second = $2k_c k_{cc} / (k_c + k_{cc})$. The numbers given are the means and standard errors of the means for the cell population.

^b See Table 2, footnote b.

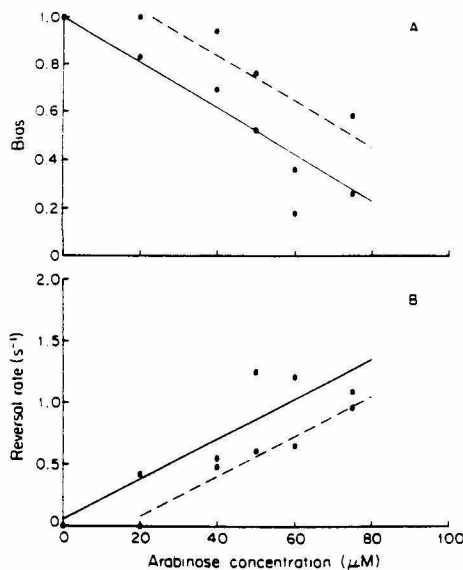


FIG. 2. The bias (A) and reversal rate (B) of a gutted strain expressing CheY (HCB465; ●, —) or a gutted strain expressing Tar and CheY (HCB475; ○, ----) as a function of the concentration of the inducer for *para-cheY*, L-arabinose. The two strains were identical, except that the second is a λ gt4-*tar101* lysogen (Table 4). Each point represents the mean of one to four experiments, each involving 8 to 24 cells. The lines were drawn by eye.

did not alter the behavior of the strains containing *scyA3* or *scyB10* (HCB500 and HCB501, respectively). The presence of Tar in the *scyA2* background did appear to have a significant effect upon behavior (HCB499; Table 6), but this effect proved to be independent of Tar, since a plasmid that expressed no functional chemotaxis gene product (pRL22 Δ *cheY* Δ *pvuII*) also generated a similar shift in this background (HCB496). Therefore, the CCW shift produced by Tar in strains wild type for *flaAII* and *flaBII* cannot be accounted for by a direct interaction between the transducer and the flagellar motors.

CheZ. In plasmid pRL22, both *cheY* and *cheZ* are expressed by the tryptophan promoter. When this plasmid was transformed into the gutted strain, the resultant strain (HCB449) exhibited a large bias. Of the 25 cells examined, only 2 were able to spin CW; the bias averaged over the cell population was >0.99 , and the reversal rate was 0.04 s^{-1} (Table 5). Thus, CheZ counteracts the effect of CheY. Note that this is true even when the expression of CheY greatly exceeds that of CheZ (HCB351; Table 5).

Strain RP1616, whose only defect is a *cheZ* deletion (Table 1), responded to the attractants aspartate and serine. Thus, CheZ is not required for a CCW response. Furthermore, CheZ, introduced via plasmid pBB1, did not change the bias or the reversal rate in the *scyA3* background (HCB494; Table 6). Although the presence of CheZ appeared to shift the bias CCW in the *scyA2* background (HCB493; Table 6), the control plasmid (pRL22 Δ *cheY* Δ *pvuII*) also exhibited a similar effect (HCB496; Table 6). Thus, CheZ does not act alone

to increase the bias. We conclude that CheZ is not a CCW signal.

When pRL22 was transformed into the *scyA3* background, yielding strain HCB488, the bias was intermediate between that of the null strain, HCB483, and that of the CheY-containing strain, HCB491, while the reversal rate was higher than that of either of these two strains (Table 6). If CheZ acts on CheY only in the cytoplasm, its effects should not depend on the phenotype of the motor; thus, the rotational behavior of HCB488 should mimic that of its gutted parent, HCB483. The sharp increase in reversal rate shows that this is not the case and suggests that CheZ exerts an effect on CheY at the flagellar motors.

Transducer, CheY, CheA, and CheW. No response to the attractant aspartate or the repellent Ni^{2+} was observed in the reconstituted strain that produces CheY and the transducer Tar (HCB475; Table 7). However, a strain that produces CheA, CheW, CheY, and the transducers Tar and Trg (HCB525) did respond to both aspartate and Ni^{2+} (Table 7). It also responded to shifts from pH 7 to 6 and to the addition of 10 mM acetate at pH 6. These responses were inverted, as expected for strains carrying only the Tar transducer (14, 19). All of the responses occurred at a rate expected for *cheZ* mutants (4), and the cells failed to adapt, as expected for *cheR cheB* mutants (4). Despite these differences, it is clear that CheA and CheW restored sensitivity to changes in concentration occurring at the level of the periplasm.

A strain (HCB349) that produces CheA, CheW, Tar, and Trg but not CheY rotated only CCW and did not respond to the repellent Ni^{2+} (Table 7). The *scyA2* allele, when added to this background, enabled the cells to spin alternately CW and CCW and thus permitted us to test for responses to both attractants and repellents. The resultant strain (HCB527) still did not respond to either aspartate or Ni^{2+} . However, when CheY was added back via plasmid pJH120, the responses were restored (HCB529; Table 7).

The presence of CheA and CheW dramatically decreased the bias of a strain containing transducer and CheY (compare HCB475 and HCB525; Table 7). This effect was not significantly diminished by the presence of the *scyA2* allele (compare HCB527 and HCB529; Table 7). However, when

TABLE 6. Behavior of reconstituted strains with flagellar motors defective in FlaAII (CheC) or FlaBII (CheV)^a

Strain	Allele	Chemotaxis genes present ^b	Bias	Reversal rate (s^{-1})
HCB482	<i>scyA2</i>	None	0.56 ± 0.06	3.74 ± 0.45
HCB499	<i>scyA2</i>	<i>tar^c</i>	0.80 ± 0.03	3.52 ± 0.28
HCB496	<i>scyA2</i>	<i>ptrp-Δ(cheY)</i>	0.75 ± 0.05	2.60 ± 0.34
HCB493	<i>scyA2</i>	<i>ptrp-Δ(cheY) cheZ</i>	0.82 ± 0.03	2.81 ± 0.32
HCB490	<i>scyA2</i>	<i>ptrp-cheY</i>	0.10 ± 0.05	0.51 ± 0.29
HCB483	<i>scyA3</i>	None	0.84 ± 0.02	2.82 ± 0.24
HCB500	<i>scyA3</i>	<i>tar^c</i>	0.80 ± 0.02	3.37 ± 0.42
HCB497	<i>scyA3</i>	<i>ptrp-Δ(cheY)</i>	0.83 ± 0.02	3.54 ± 0.40
HCB494	<i>scyA3</i>	<i>ptrp-Δ(cheY) cheZ</i>	0.89 ± 0.01	3.06 ± 0.35
HCB491	<i>scyA3</i>	<i>ptrp-cheY</i>	0.27 ± 0.08	0.95 ± 0.25
HCB488	<i>scyA3</i>	<i>ptrp-cheYZ</i>	0.57 ± 0.07	4.25 ± 0.51
HCB484	<i>scyB10</i>	None	0.53 ± 0.08	2.35 ± 0.29
HCB501	<i>scyB10</i>	<i>tar^c</i>	0.60 ± 0.06	2.57 ± 0.50
HCB492	<i>scyB10</i>	<i>ptrp-cheY</i>	0.02 ± 0.01	0.20 ± 0.17

^a See Table 5, footnote a.

^b See Table 2, footnote b.

^c *tar* was carried in multicopy by plasmid pAK101RI.

TABLE 7. Behavior of reconstituted strains in the presence of transducers and the *cheY* or *cheAW* gene products or both^a

Strain	Allele	Chemotaxis gene present ^b	Concn of arabinose (μ M)	Bias	Reversal rate (s^{-1})	Response to following change ^c :			
						Aspartate (0 to 2.5 μ M)	NiCl ₂ (0 to 0.1 mM)	pH 7 to pH 6	Acetate (pH 6) (0 to 10 mM)
HCB475	<i>scyA</i> ⁻	<i>tar para-cheY</i>	20	1	0	NR	NR	-	-
HCB349	<i>scyA</i> ⁻	<i>cheAW tar trg</i>	0	1	0	NR	NR	NR	NR
HCB525	<i>scyA</i> ⁺	<i>cheAW tar trg para-cheY</i>	0	0.01 \pm 0.00	0.12 \pm 0.03	+	-	+	+
HCB527	<i>scyA2</i>	<i>cheAW tar trg</i>	0	0.91 \pm 0.04	1.11 \pm 0.52	NR	NR	NR	NR
HCB529	<i>scyA2</i>	<i>cheAW tar trg para-cheY</i>	0	0.08 \pm 0.04	0.69 \pm 0.35	+	-	-	+

^a See Table 5, footnote a.

^b See Table 2, footnote b.

^c NR, No response; +, an increase in bias; -, a decrease in bias. The - responses in strain HCB475 developed over a few minutes.

CheY was absent. CheA and CheW had no effect upon bias (HCB349; Table 7). Thus, CheA or CheW or both appear to modulate the effectiveness of CheY. Whether this occurs in the absence of transducer is not known.

DISCUSSION

In summary, we constructed strains of *E. coli* deleted for genes that code for the known transducers Tar, Tsr, Trg, and Tap and the known cytoplasmic *che* gene products CheA, CheW, CheR, CheB, CheY, and CheZ. These strains possessed functional flagellar motors, with either wild type or mutant switch components, so that they could be tethered and their rotational behavior could be analyzed. One or more of the missing components were added back, and changes in rotational bias and sensitivity to attractants and repellents were noted. We established the following facts. (i) In the absence of transducers and cytoplasmic *che* gene products, wild type motors rotate exclusively CCW, while motors containing defective FlaAII or FlaBII components continue to change their directions of rotation. (ii) CheY decreases the bias in either case by lengthening CW intervals and shortening CCW intervals. (iii) The magnitude of the shift observed with wild type motors increases with the concentration of CheY and is greater at lower external and internal pH. (iv) The magnitude of this shift is reduced by transducers; however, transducers do not affect the bias in the absence of CheY. (v) The effect of CheY is offset by CheZ, even when *cheZ* is expressed at a relatively low level; however, CheZ does not affect the bias in the absence of CheY. (vi) Cells containing transducers and CheY fail to respond to attractants or repellents known to interact with periplasmic transducer domains. (vii) This sensitivity is restored by CheA and CheW; however, these components do not affect the bias in the absence of CheY. Whether CheA can restore this sensitivity in the absence of CheW, or whether CheW can do so in the absence of CheA, is not yet known.

We conclude that CheY interacts with both the transducers and with the flagellar motors. Thus, it appears to play a central role in coupling one to the other. Given the small size of the shift in bias as a result of the action of transducers and the lack of genetic evidence indicating a direct interaction between transducers and CheY (in particular, that pseudorevertants of *cheD* have not been found in CheY [23]), this interaction might well be indirect. However, since there are allele-specific pseudorevertants of *cheY* in *flaAII* and *flaBII* (26) and since CheY can change the direction of flagellar rotation in cell envelopes depleted of other cytoplas-

mic components (28), the interaction between CheY and the motor must be direct.

CheZ acts as a CheY antagonist. It does not appear to shift flagellar bias in the absence of CheY. Given that its effect on CheY activity differs depending upon the structure of the switch components and that allele-specific pseudorevertants of *cheZ* also occur in *flaAII* and *flaBII* (26), CheZ appears to exert its antagonism at the flagellar motors. However, our evidence does not rule out the possibility that CheZ also acts in the cytoplasm. Note that the filamentous cells studied previously (31) contained many flagellar motors, only a few of which carried external markers, so that CheZ could have shortened the signal decay length by acting either at the flagellar motors or in the cytoplasm or both.

CheA or CheW or both are required to complete the signal pathway. Cells containing transducers, CheA, CheW, and CheY respond to attractants and repellents. CheR, CheB, and CheZ are not necessary. Strain constructions are under way that will allow us to determine whether CheA or CheW act alone or whether both are required.

A model for the signal pathway is given in Fig. 3. It includes a molecule of low molecular weight and its precursor, as explained below. The model is meant to be provocative: we hope that it will stimulate the design of significant experiments.

Since CheY acts as a tumble generator, it is easier to describe the response of the system to the addition of repellent (or removal of attractant) than it is to the addition of attractant. The steps in the pathway are as follows (with numbers corresponding to those in Fig. 3). (Step 1) An increase in the concentration of repellent changes the configuration of the transducer. (Step 2) This increases the rate of catalytic conversion of the precursor to the low-molecular-weight molecule. This catalysis requires CheA or CheW or both. In addition, the production of these molecules requires ATP. Some molecules (or functional analogs) are present endogenously, even in a gutted strain. (Step 3) The molecule behaves as an activated intermediate: it decays, e.g., by hydrolysis, back to the precursor or to some other inert product. (Step 4) The molecule activates CheY; it also activates CheB (not shown). (Step 5) Activated CheY binds to the switch components of the motor and enhances CW rotation. (Step 6) CheZ inactivates CheY at the motor, releasing the precursor or some other inert product. CheZ might also inactivate CheY in the cytoplasm. To explain the CCW shift effected by transducers in the presence of CheY (Fig. 1 and 2), we assume that the transducer, acting alone, weakly hydrolyzes the molecule; see the discussion of *cheD* mutants given below. The rate of this hydrolysis is not

- chemotaxis. *J. Bacteriol.* **144**:1048-1060.
12. Hedblom, M. L., and J. Adler. 1983. Chemotactic response of *Escherichia coli* to chemically synthesized amino acids. *J. Bacteriol.* **155**:1463-1466.
 13. Kehry, M. R., T. G. Doak, and F. W. Dahlquist. 1985. Aberrant regulation of methyltransferase activity in *cheD* mutants of *Escherichia coli*. *J. Bacteriol.* **161**:105-112.
 14. Krikos, A., M. P. Conley, A. Boyd, H. C. Berg, and M. I. Simon. 1985. Chimeric chemosensory transducers of *Escherichia coli*. *Proc. Natl. Acad. Sci. USA* **82**:1326-1330.
 15. Larsen, S. H., R. W. Reader, E. N. Kort, W.-W. Tao, and J. Adler. 1974. Change in direction of flagellar rotation is the basis of the chemotactic response in *Escherichia coli*. *Nature (London)* **249**:74-77.
 16. Macnab, R., and M. K. Ornston. 1977. Normal-to-curly flagellar transitions and their role in bacterial tumbling. Stabilization of an alternative quaternary structure by mechanical force. *J. Mol. Biol.* **112**:1-30.
 17. Manson, M. D., V. Blank, G. Brade, and C. F. Higgins. 1986. Peptide chemotaxis in *E. coli* involves the Tap signal transducer and the dipeptide permease. *Nature (London)* **321**:253-256.
 18. Matsumura, P., J. J. Rydel, R. Linzmeier, and D. Vacante. 1984. Overexpression and sequence of the *Escherichia coli cheY* gene and biochemical activities of the CheY protein. *J. Bacteriol.* **160**:36-41.
 19. Muskavitch, M. A., E. N. Kort, M. S. Springer, M. F. Goy, and J. Adler. 1978. Attraction by repellents: an error in sensory information processing by bacterial mutants. *Science* **201**:63-65.
 20. Mutoh, N., K. Oosawa, and M. I. Simon. 1986. Characterization of *Escherichia coli* chemotaxis receptor mutants with null phenotypes. *J. Bacteriol.* **167**:992-998.
 21. Parkinson, J. S. 1976. *cheA*, *cheB*, and *cheC* genes of *Escherichia coli* and their role in chemotaxis. *J. Bacteriol.* **126**:758-770.
 22. Parkinson, J. S. 1978. Complementation analysis and deletion mapping of *Escherichia coli* mutants defective in chemotaxis. *J. Bacteriol.* **135**:45-53.
 23. Parkinson, J. S. 1981. Genetics of bacterial chemotaxis. *Symp. Soc. Gen. Microbiol.* **31**:265-290.
 24. Parkinson, J. S., and S. E. Houts. 1982. Isolation and behavior of *Escherichia coli* deletion mutants lacking chemotaxis functions. *J. Bacteriol.* **151**:106-113.
 25. Parkinson, J. S., and S. R. Parker. 1979. Interaction of the *cheC* and *cheZ* gene products is required for chemotactic behavior in *Escherichia coli*. *Proc. Natl. Acad. Sci. USA* **76**:2390-2394.
 26. Parkinson, J. S., S. R. Parker, P. B. Talbert, and S. E. Houts. 1983. Interactions between chemotaxis genes and flagellar genes in *Escherichia coli*. *J. Bacteriol.* **155**:265-274.
 27. Ravid, S., and M. Eisenbach. 1984. Direction of flagellar rotation in bacterial cell envelopes. *J. Bacteriol.* **158**:222-230.
 28. Ravid, S., P. Matsumura, and M. Eisenbach. 1986. Restoration of flagellar clockwise rotation in bacterial envelopes by insertion of the chemotaxis protein, CheY. *Proc. Natl. Acad. Sci. USA* **83**:7157-7161.
 29. Reader, R. W., W.-W. Tao, M. S. Springer, M. F. Goy, and J. Adler. 1979. Pleiotropic aspartate taxis and serine taxis mutants of *Escherichia coli*. *J. Gen. Microbiol.* **111**:363-374.
 30. Segall, J. E., S. M. Block, and H. C. Berg. 1986. Temporal comparisons in bacterial chemotaxis. *Proc. Natl. Acad. Sci. USA* **83**:8987-8991.
 31. Segall, J. E., A. Ishihara, and H. C. Berg. 1985. Chemotactic signaling in filamentous cells of *Escherichia coli*. *J. Bacteriol.* **161**:51-59.
 32. Shioi, J.-I., R. J. Galloway, M. Niwano, R. E. Chinneck, and B. L. Taylor. 1982. Requirement of ATP in bacterial chemotaxis. *J. Biol. Chem.* **257**:7969-7975.
 33. Silhavy, T. J., M. L. Berman, and L. W. Enquist. 1984. Experiments with gene fusions. Cold Spring Harbor Laboratory, Cold Spring Harbor, N.Y.
 34. Simms, S. A., M. G. Keene, and J. Stock. 1985. Multiple forms of the CheB methyltransferase in bacterial chemosensing. *J. Biol. Chem.* **260**:10161-10168.
 35. Smith, R. A., and J. S. Parkinson. 1980. Overlapping genes at the *cheA* locus of *Escherichia coli*. *Proc. Natl. Acad. Sci. USA* **77**:5370-5374.
 36. Springer, M. S., and B. Zanotari. 1984. Sensory transduction in *Escherichia coli*: regulation of the demethylation rate by the CheA protein. *Proc. Natl. Acad. Sci. USA* **81**:5061-5065.
 37. Stock, A., D. E. Koshland, Jr., and J. Stock. 1985. Homologies between the *Salmonella typhimurium* CheY protein and proteins involved in the regulation of chemotaxis, membrane protein synthesis, and sporulation. *Proc. Natl. Acad. Sci. USA* **82**:7989-7993.
 38. Taylor, B. L., R. C. Tribhuvan, E. H. Rowsell, J. M. Smith, and J. Shioi. 1985. Role of ATP and cyclic nucleotides in bacterial chemotaxis, p. 63-71. *In* M. Eisenbach and M. Balaban (ed.), *Sensing and response in microorganisms*. Elsevier Science Publishers, Amsterdam.
 39. Wang, E. A., and D. E. Koshland, Jr. 1980. Receptor structure in the bacterial sensing system. *Proc. Natl. Acad. Sci. USA* **77**:7157-7161.